RELEASE OF NANOCLAY AND SURFACTANT FROM POLYMER-CLAY NANOCOMPOSITE SYSTEMS

By

YINING XIA

A DISSERTATION

Submitted to
Michigan State University
in partial fulfillment of the requirements
for the degree of

Packaging – Doctor of Philosophy

2014

ABSTRACT

RELEASE OF NANOCLAY AND SURFACTANT FROM POLYMER-CLAY NANOCOMPOSITE SYSTEMS

By

Yining Xia

In the past decade, applications of nanocomposites consisting of polymers and engineered nanoparticles have been significantly expanded, causing increasing concern about the release of nanoparticles and their by-products which may impact human health and the environment. This research aims to evaluate the release of nanoclay and surfactant (organo-modifier of nanoclay) from nanocomposites into food simulants.

A graphite furnace atomic absorption spectrometry (GFAAS) method was developed for rapid measurement of organo-modified montmorillonite (O-MMT) concentration in water-ethanol solutions with Si and Al as markers of the nanoclay. Special precautions were taken to ensure the stability of O-MMT in water-ethanol solutions. A solution with an ethanol concentration higher than 70 % (v/v) was preferred to obtain a good dispersion of O-MMT in the sonicated solutions, while the dispersion in water was improved by the addition of an organic surfactant. The correlation between Si and Al concentrations and O-MMT concentrations in solution gave the composition of O-MMT which was in agreement with the results obtained by an X-ray fluorescence spectrometry (XRF) method.

A liquid chromatography tandem mass spectrometry (LC-MS/MS) method was developed to measure the surfactant released from O-MMT into food simulants. Two types of O-MMT containing different quaternary alkylammonium surfactants were used. The release of surfactant from O-MMT was evaluated as a function of temperature, sonication and simulant type. There was more surfactant released at a higher temperature than at a lower one. More

surfactant was released when sonication was applied to the nanoclay suspension. A substantial amount of surfactant was released into ethanol, while much less was released into the water/ethanol mixture (1:1, v/v) or pure water. The affinity between the solvent and the surfactant was discussed based on solubility parameters and correlated with the surfactant release into different solvents.

Release assessment of O-MMT nanoclay and surfactant was performed on two types of polymer-clay nanocomposites: polypropylene (PP) and polyamide 6 (PA6) with O-MMT. The release experiment was carried out in accordance with ASTM D4754-11 with the nanocomposite films exposed to ethanol as a fatty-food simulant at 22, 40 and 70 °C. A GFAAS method was developed to measure the release of nanoclay. Both nanocomposites released small amounts of nanoclay particles (μg L^{-1} level) into ethanol. There were more nanoclay particles released from PP-clay films than PA6-clay films. There was no difference in the amount of nanoclay released from PP-clay films with different film thicknesses, revealing that the release mainly occurred at the film surface. A LC-MS/MS method was developed to identify and quantify the surfactant released into ethanol from the two nanocomposite systems. A substantial amount of surfactant in ethanol (mg L^{-1} level) was detected, indicating changes in the nanoclay structure within the nanocomposite while exposed to the solvent. Finally, Fick's diffusion equation was applied to describe the surfactant release. The diffusion coefficients were on a scale of 10^{-13} to 10^{-12} cm^2 s^{-1} for the surfactant release from PP-clay films, and 10^{-13} to 10^{-10} cm^2 s^{-1} for the surfactant release from PA6-clay films.

不积跬步，无以至千里；
不积小流，无以成江海。

A journey of thousands of miles may not be achieved through accumulation of each single step, just as the enormous ocean may not be formed by gathering every brook or stream.

—Xun Zi

ACKNOWLEDGEMENTS

Upon completion of my Ph.D., I would like to express my deepest and sincere gratitude to those who helped me in my research during the past three years. The way toward a Ph.D. degree is full of difficulties and challenges, but also filled with happiness and cheerfulness because of your warm support.

The greatest appreciation should be expressed to my advisor, Associate Professor Maria Rubino, for her invaluable instructions on my research and tireless guidance on my writing. I greatly appreciate the kind help and valuable suggestions from my committee members: Associate Professor Rafael Auras, Professor Susan Selke and Professor Krishnamurthy Jayaraman. I also appreciate the financial aid from the Center for Packaging Innovation and Sustainability at MSU and the assistantship from the MSU Food Safety Group to support my research project.

I would like to express my personal appreciation to Dr. Carlos Diaz for his great collaboration at the beginning of my research; Dr. Kathy Severin for her assistance and allowing access to the GFAAS; Lijun Chen for her assistance on the LC-MS/MS; Dr. Wei Zhang for his assistance on the Malvern instrument; Dr. Tyrone Rooney for the composition analysis of nanoclay by XRF; Dr. Ajay Kathuria for the measurement of nanoclay surface area; Jin Zhang and Yan Shi for their help on MATLAB.

I am thankful to the faculty and staff of the School of Packaging; and to my classmates and friends at school and also outside school for their help.

Finally, I would like to send my deep gratitude to my farther Dr. Jingyuan Xia and my mother Shumin Wang who always support me and prey for my success toward graduation.

TABLE OF CONTENTS

LIST OF TABLES

LIST OF FIGURES

CHAPTER 1: Introduction

1.1 Background

Packaging plays an important role for consumer goods as it provides containment of the product, affords protection of the product from the outer environment, and gives the detailed information of the product [Selke *et al.* 2004]. A variety of materials are used for packaging purposes including metal, glass, paper, wood and plastic. Compared to other materials, plastic, as a specific category of polymer, is a relatively new material and extensively used in packaging. Plastics possess some advantages that have made them promising materials for packaging applications, such as easy to shape, low in cost, almost chemically inert, lightweight, superior sealing ability, and relatively good barrier properties [Coles *et al.* 2003].

The plastic (polymer) properties can be further improved by adding the engineered nanoparticles (ENPs) at small loadings. For example, the use of nanoscale metals enhances antimicrobial activity and UV resistance of polymers [Han & Yu 2006; Radheshkumar & Munstedt 2006]; the incorporation of carbon nanotubes improves thermal, mechanical and electrical properties of polymers [Kashiwagi *et al.* 2004; Bal & Samal 2007]; and the addition of nanoclays increases barrier properties and heat stability of polymers [Pereira de Abreu *et al.* 2007; Rathi & Dahiya 2012].

The consumption of nanoparticle-containing polymers (nanocomposites) is growing rapidly with global sales of over US$1.2 billion in 2013 rising to an estimated US$4.2 billion by 2019 [BCC Research 2014]. Among the ENPs, nanoclays such as organo-modified montmorillonite (O-MMT) are extensively used in nanocomposites for their commercial availability, low cost, high stability, and relatively simple processing. Nanocomposites with

O-MMT as nanofiller account for over half of the total nanocomposite consumption with the primary application in packaging materials [Patel *et al.* 2006; BCC Research 2014]. MMT is obtained from layered silicate minerals with a hydrophilic nature. It can be organically modified by attaching organic cationic surfactants (*e.g.*, alkylammonium cations) onto its surface, to improve the compatibility with the polymer and achieve good dispersion in the polymer [De A. Prado *et al.* 2005].

Nanoclays are added in several polymer matrices including polypropylene and low density polyethylene to improve the barrier (*e.g.*, to water vapor and gases such as oxygen and carbon dioxide) and mechanical properties [Pereira de Abreu *et al.* 2007; Choudalakis & Gotsis 2009]. Therefore, thinner films with addition of nanoclay can be produced having similar mechanical strength and barrier properties as thicker films without nanoclay in order to reduce the solid waste. For novel bio-based plastics such as polylactic acid and thermoplastic starch, the incorporation of nanoclay has extended the application range of these materials by overcoming their performance limitations (*e.g.*, low barrier to moisture, low heat-deflection temperature) [Sinha Ray & Okamoto 2003; Lagaron & Lopez-Rubio 2011].

1.2 Motivation

The wide use of nanocomposites has raised concern about the release of nanoparticles and their by-products into different media and as a consequence promoting possible exposure to biological systems and the environment. Nanoparticles could reach biological systems through different routes. One route of exposure could be via nanocomposites used as a food packaging material in contact with food [Chaudhry *et al.* 2008; Silvestre *et al.* 2011], where nanoparticles are released from the packaging material into the food. Other routes of exposure could be via

nanocomposites either manufactured in the work place or buried in landfills, where nanoparticles are released into the surrounding environments (atmosphere, leachate, runoff, water streams, etc.) and reach plants, wildlife or humans [Gottschalk & Nowack 2011; Raynor *et al.* 2012]. Once the nanoparticles enter biological systems, they may interact with the living tissues or cells, causing undesired health effects.

Toxicological studies showed that nanoclays, due to their small size, large surface area and high reactivity, have the potential to cause adverse effects such as cytotoxic effects [Lordan *et al.* 2011; Baek *et al.* 2012] and genotoxic effects [Sharma *et al.* 2010; Houtman *et al.* 2014]. The potential risks of surfactants (organo-modifiers of nanoclay) have also been investigated and the results showed that some surfactants and their degradation products are harmful to ecosystems, animals and humans [Talmage 1994; Sonnenschein & Soto 1998; Venhus & Mehrvar 2004; Ying 2006; Routledge & Sumpter 2009].

The US Food and Drug Administration (FDA) and the European Food Safety Authority (EFSA) are aware of nanocomposites used in food packaging applications and are making efforts to regulate such materials [EFSA 2009; FDA 2013]. The National Research Council has recently released a report [NRC 2013] regarding the environmental, health and safety aspects of engineered nanomaterials. However, the potential risks of nanoparticles to human health and the environment are not well understood, as there is a lack of ability to detect and characterize nanoparticles in different media as well as to evaluate the exposure level to nanoparticles [Thomas *et al.* 2006; EFSA 2011; Szakal *et al.* 2014]. So far, release assessment of nanoclay from nanocomposites is scarce, and no attention has been given to surfactant release from the nanocomposites. Gaining knowledge on the transport of these components from nanocomposites when exposed to different conditions is critical to the evaluation of exposure dose and related

risk assessment.

1.3 Goal and Objectives

The overall goal of this research is to evaluate the release of nanoclay and surfactant from polymer-clay nanocomposite systems into food simulants. Specific objectives are addressed to achieve the goal:

(1) Develop an instrumental method for the quantification of nanoclay released into food simulants;

(2) Develop an instrumental method for the identification and quantification of surfactant released into food simulants;

(3) Investigate interactions among the nanoclay, the polymer and the food simulant, and correlate with the release process;

(4) Implement mathematical models to describe the release process.

BIBLIOGRAPHY

BIBLIOGRAPHY

Baek, M.; Lee, J.A.; Choi, S.J. Toxicological effects of a cationic clay, montmorillonite *in vitro* and *in vivo*. *Mol. Cell Toxicol.* **2012**, 8, 95-101.

Bal, S.; Samal, S.S. Carbon nanotube reinforced polymer composites - A state of the art. *Bull. Mater. Sci.* **2007**, 30, 379-386.

BCC Research. Global Markets for Nanocomposites, Nanoparticles, Nanoclays, and Nanotubes. BCC Research LLC, Wellesley, MA, USA, 2014. Available from: http://www.bccresearch.com/market-research/nanotechnology/nanocomposites-market-nan021f.html

Chaudhry, Q.; Scotter, M.; Blackburn, J.; Ross, B.; Boxall, A.; Castle, L.; Aitken, R.; Watkins, R. Applications and implications of nanotechnologies for the food sector. *Food Addit. Contam*. **2008**, 25, 241-258.

Choudalakis, G.; Gotsis, A.D. Permeability of polymer/clay nanocomposites: a review. *Eur. Polym. J.* **2009**, 48, 967-984.

Coles, R.; McDowell, D.; Kirwan, M. Food Packaging Technology. CRC Press: Boca Raton, FL, 2003.

De A. Prado, L.A.S.; Karthikeyan, C.S.; Schulte, K.; Nunes, S.P.; De Torriani, I.L. Organic modification of layered silicates: structural and thermal charaterizations. *J. Non-cryst. Solids* **2005**, 351, 970-975.

[EFSA] European Food Safety Authority. The Potential Risks Arising from Nanoscience and Nanotechnologies on Food and Feed Safety. *EFSA J.* **2009**, 958, 1-39. Available from: http://www.efsa.europa.eu/en/efsajournal/doc/958.pdf

[EFSA] European Food Safety Authority. Guidance on the risk assessment of the application of nanoscience and nanotechnologies in the food and feed chain. *EFSA J.* **2011**, 9, 2140 [36 pp]. Available from: http://www.efsa.europa.eu/en/efsajournal/doc/2140.pdf

[FDA] Food and Drug Administration. FDA Nanotechnology Regulatory Science Research Plan, 2013. Available from: http://www.fda.gov/ScienceResearch/SpecialTopics/Nanotechnology/ucm273325.htm

Gottschalk, F.; Nowack, B. The release of engineered nanomaterials to the environment. *J. Environ. Monit.* **2011**, 13, 1145-1155.

Han, K.Q.; Yu, M.H. Study of the preparation and properties of fabrics of a PET/TiO_2 nanocomposite prepared by in situ polycondensation. *J. Appl. Polym. Sci.* **2006**, 100, 1588-1593.

Houtman, J.; Maisanaba, S.; Puerto, M.; Gutierrez-Praena, D.; Jorda, M.; Aucejo, S.; Jos, A. Toxicity assessment of organomodified clays used in food contact materials on human target cell lines. *Appl. Clay Sci.* **2014**, 90, 150-158.

Kashiwagi, T.; Grulke, E.; Hilding, J.; Groth, K.; Harris, R.; Butler, K.; Shields, J.; Kharchenko, S.; Douglas, J. Thermal and flammability properties of polypropylene/carbon nanotube nanocomposites. *Polymer* **2004**, 45, 4227-4239.

Lagaron, J.M.; Lopez-Rubio, A. Nanotechnology for bioplastics: opportunities, challenges and strategies. *Trends Food Sci. Tech.* **2011**, 22, 611-617.

Lordan, S.; Kennedy, J.E.; Higginbotham, C.L. Cytotoxic effects induced by unmodified and organically modified nanoclays in the human hepatic HepG2 cell line. *J. Appl. Toxicol.* **2011**, 31, 27-35.

[NRC] National Research Council. Research Progress on Environmental, Health, and Safety Aspects of Engineered Nanomaterials. National Academy Press, Washington DC, USA, 2013. Available from: http://www.nap.edu/catalog.php?record_id=18475

Patel, H.A.; Somani, R.S.; Bajaj, H.C.; Jasra, R.V. Nanoclays for polymer nanocomposites, paints, inks, greases and cosmetics formulations, drug delivery vehicle and waste water treatment. *Bull. Mater. Sci.* **2006**, 29: 133-145.

Pereira de Abreu, D.A.; Paseiro Losada, P.; Angulo, I.; Cruz, J.M. Development of new polyolefin films with nanoclays for application in food packaging. *Eur. Polym. J.* **2007**, 43, 2229-2243.

Radheshkumar, C.; Munstedt, H. Antimicrobial polymers from polypropylene/silver composites-Ag^+ release measured by anode stripping voltammetry. *React. Funct. Polym.* **2006**, 66, 780-788.

Rathi, S.; Dahiya, J.B. Polyamide 66/nanoclay composite: synthesis, thermal and flammability properties. *Adv. Mater. Lett.* **2012**, 3: 381-387.

Raynor, P.C.; Cebula, J.I.; Spanqenberger, J.S.; Olson, B.A.; Dasch, J.M.; D'Arcy, J.B. Assessing potential nanoparticles release during nanocomposite shredding using direct-reading instruments. *J. Occup. Environ. Hyg.* **2012**, 9, 1-13.

Routledge, E.J.; Sumpter, J.P. Estrogenic activity of surfactants and some of their degradation products assessed using a recombinant yeast screen. *Environ. Toxicol. Chem.* **2009**, 15, 241-248.

Selke, S.; Culter, J.; Hernandez, R. Plastic packaging: Properties, processing, applications, and regulations. Hanser Pub.: Munich, Germany, 2004.

Sharma, A.K.; Schimidt, B.; Frandsen, H.; Jacobsen, N.R.; Larsen, E.H.; Binderup, M.L. Genotoxicity of unmodified and organo-modified montmorillonite. *Mutat. Res.* **2010**, 700, 18-25.

Sinha Ray, S.; Okamoto, M. Polymer/layered silicate nanocomposites: a review from preparation to processing. *Prog. Polym. Sci.* **2003**, 28, 1539-1641.

Sonnenschein, C.; Soto, A.M. An updated review of environmental estrogen and androgen mimics and antagonists. *J. Steroid Biochem. Mol. Biol.* **1998**, 65, 143-150.

Szakal, C.; Roberts, S. M.; Westerhoff, P.; Bartholomaeus, A.; Buck, N.; Illuminato, I.; Canady, R.; Rogers, M. Measurement of nanomaterials in foods: Integrative consideration of challenges and future prospects. *ACS Nano* **2014**, *8*, 3128-3135.

Talmage, S.S. Environmental and Human safety of major surfactants: alcohol ethoxylates and alkylphenol ethoxylates. CRE Press: Boca Raton, FL, USA, 1994.

Thomas, T.; Thomas, K.; Sadrieh, N.; Savage, N.; Adair, P.; Bronaugh, R. Research strategies for safety evaluation of nanomaterials, Part VII: Evaluating consumer exposures to nanoscale materials. *Toxicol. Sci.* **2006**, 91, 14-19.

Venhus, S.H.; Mehrvar, M. Health effects, environmental impacts, and photochemical degradation of selected surfactants in water. *Int. J. Photoenergy* **2004**, 6, 115-125.

Ying, G.G. Fate, behavior and effects of surfactants and their degradation products in the environment. *Environ. Int.* **2006**, 32, 417-431.

CHAPTER 2: Literature Review

This chapter starts with a brief review of nanoclays, including their structure and properties, organo-modification, applications in polymer nanocomposites, potential risks and regulatory issues. Special focuse is placed on the transport of nanoclay and surfactant within food packaging systems, and recommendations for migration tests of these components. Finally, instrumental methodologies regarding the detection and characterization of nanoclay are introduced.

2.1 Structure and properties of nanoclay

Clays are naturally occurring layered silicate minerals with variation in composition depending on their source [Uddin 2008]. The clays used for the preparation of nanoclays mainly belong to the smectite family, also known as 2:1 phyllosilicates (Figure 2.1). Smectite clays have a layered structure with a layer thickness of about 1 nm and a lateral dimension that varies from tens of nanometers to several microns depending on the particular clay. The crystal structure of each clay layer consists of an octahedral sheet containing either alumina (Al^{3+}) or magnesia (Mg^{2+}) located between two tetrahedral sheets containing silica (Si^{4+}) [Sinha Ray & Okamoto 2003]. The clay layers are held together by van der Waals forces with a gap between the layers known as the clay gallery containing exchangeable cations (*e.g.*, Na^{+} or K^{+}) to balance the negative charge created by isomorphic substitution within the clay layers (*e.g.*, Si^{4+} by Al^{3+}, Al^{3+} by Mg^{2+} or Fe^{2+}, Mg^{2+} by Li^{+}). Nanoclays have very large surface areas, up to hundreds of $m^2\ g^{-1}$. They are also characterized by the cation exchange capacity (CEC) with a unit of mequiv $100^{-1}g^{-1}$. CEC is a reflection of the charge on nanoclay surface and varies widely from one type

of nanoclay to another.

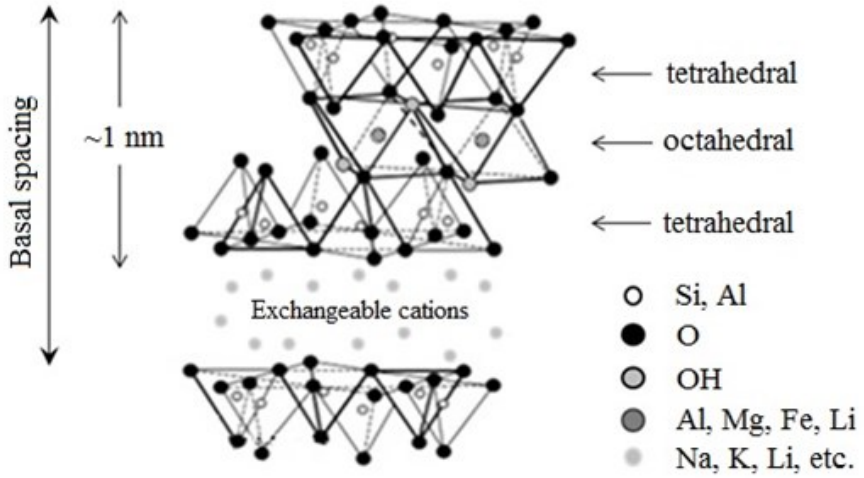

Figure 2.1 Schematic diagram of the structure of 2:1 phyllosilicates, reproduced from [Sinha Ray & Okamoto 2003].

The nanoclay used in this research is montmorillonite (MMT) which belongs to the smectite family with a general molecular formula of $\{M_y (Al_{(4-y)}Mg_y) Si_4O_{10}(OH)_2 \cdot nH_2O$, M=Na, K or Ca} [De A. Prado *et al.* 2005]. The crystal structure of MMT consists of two silica tetrahedral sheets fused to an edge-shared alumina octahedral sheet [Xie *et al.* 2001]. The natural-existing MMT is in the form of tactoids which are the stacking of parallel clay platelets with about 1 nm interlayer space. Each platelet has a thickness of about 1 nm and a diameter of 20-200 nm [Ajayan *et al.* 2003]. MMT has a large surface area of 750 $m^2 g^{-1}$ [Hussain *et al.* 2006] and a high CEC of 110 mequiv 100^{-1} g^{-1} [Sinha Ray & Okamoto, 2003].

The large surface area and surface charge make nanoclays an ideal sorbent for both small and big molecules. Water molecules are adsorbed to both external and internal nanoclay surfaces causing swelling of the clay layers [Cases *et al.* 1992; Zheng *et al.* 2011]. The adsorption is

mainly affected by the size and charge of cations in the clay gallery as well as the charge on the silica sheets [Newman 1987; Whitley & Smith 2004; Bergaya *et al.* 2006]. The adsorption of heavy metals by nanoclays makes them useful for wastewater treatment [Kaya & Oren 2005; Veli & Alyuz 2007; Ijagbemi *et al.* 2009]. The adsorption is initiated by either a coordination reaction at the specific surface sites or electrostatic interaction between the adsorbing ions and the nanoclay surface [Bayens & Bradbury 1997; Bradbury & Bayens 1999; Ikhsan *et al.* 2005]. The adsorption of gas molecules (*e.g.*, O_2, CO_2, or N_2) through van der Waals forces enables the determination of nanoclay surface area [Allen 2004]. Besides small molecules, large molecules like proteins can be adsorbed by nanoclays, leading to the changes in the nanoclay surface as well as the structure and activity of the adsorbed proteins [Gysell 2011; Nitva *et al.* 2012]. In biological systems, the interaction between nanoclay and protein has the potential to induce adverse health effects.

2.2 Organo-modification of nanoclay

Pristine nanoclays are hydrophilic so they can be swelled by water molecules through the hydration of interlayer cations [Hensen & Smit 2002]. When embedded into polymers to form nanocomposites, the pristine nanoclays are miscible only with hydrophilic polymers such as polyethylene oxide (PEO) [Aranda & Ruiz-Hitzky 1992] and polyvinyl alcohol (PVA) [Strawhecker & Manias 2000]. However, most of the engineered polymers are non-hydrophilic and aggregation of nanoclay particles occurs in these polymers, resulting in separation into discrete phases analogous to those normally observed in polymer blends. To improve the compatibility between the nanoclay and the polymer, the hydrophilic nanoclay needs to be converted to an organophilic one. To achieve this, organo-modification of nanoclay is carried out

by attaching organic groups onto the nanoclay surface through two approaches: silylation or ion exchange [De A. Prado *et al.* 2005].

Silylation is performed by covalent grafting of organo-functional silanes onto the nanoclay surface [Okutomo *et al.* 1999]. The functionalized silanes usually contain an organic component with a terminal methacryloyl group. Depending on the number of terminal methacryloyl group, silanes are classified as mono-, di- or trifunctionalized. The grafting reaction takes place between the reactive methacryloyl group of silane and the silanol group (Si-OH) on the nanoclay surface (mainly on the edge) (Figure 2.2). As a result, the clay gallery is expanded after grafting the ogranosilane groups. An improved dispersion of nanoclay particles after silylation was reported in many polymers such as epoxy resin [Di Gianni *et al.* 2008], polyacrylate [Ianchis *et al.* 2011], polyurethane-acrylic hybrid [Subramani *et al.* 2007] and polystyrene-butyl acrylate hybrid [Herrera *et al.* 2004].

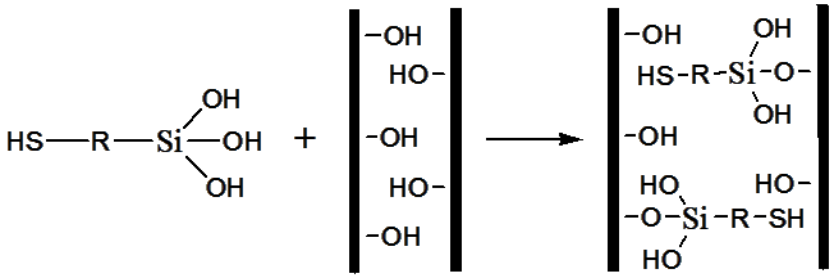

Figure 2.2 Schematic representation of the grafting reaction of trifunctional silane on the nanoclay surface, adapted from [Diaz *et al.* 2013]. The clay layers are expressed by the straight dark lines.

Ion exchange is conducted by replacing the interlayer cations with organic cationic surfactants in an aqueous solution. The surfactants used are mainly primary, secondary, tertiary

and quatenary alkylammonium or alkylphosphonium cations. The driving force for the ion exchange reaction is attributed to two aspects: (a) the hydration of interlayer cations in the aqueous solution leading to the swelling of nanoclay, and (b) the tendency of the hydrophobic surfactants to be repelled by the aqueous solution and collected on the nanoclay surface. The longer are the organic tails of the surfactant, the stronger is the repelling force from the aqueous solution [Yariv 2002]. After ion exchange, the clay gallery is expanded due to the insertion of surfactants. The arrangement of surfactants in the clay gallery depends on the packing density, temperature and alkyl chain length. The ideal arrangements of surfactants (with mono or bilayers) are either parallel to or radiating away from the clay layers (Figure 2.3), while such arrangements are seldom achieved. It is possible for various arrangements to coexist due to the transition of alkyl chains between liquid-like and solid-like states depending on the chain length and temperature [Vaia *et al.* 1994]. The presence of surfactants lowers the surface energy of nanoclay and improves the wetting characteristics with the polymer, leading to a better dispersion of nanoclay particles in the polymer. In addition, the ion exchange approach can be combined with silylation to further improve the compatibility of nanoclay with the polymer [Manias 2001; Ianchis *et al.* 2012; Cadambi & Ghassemieh 2013].

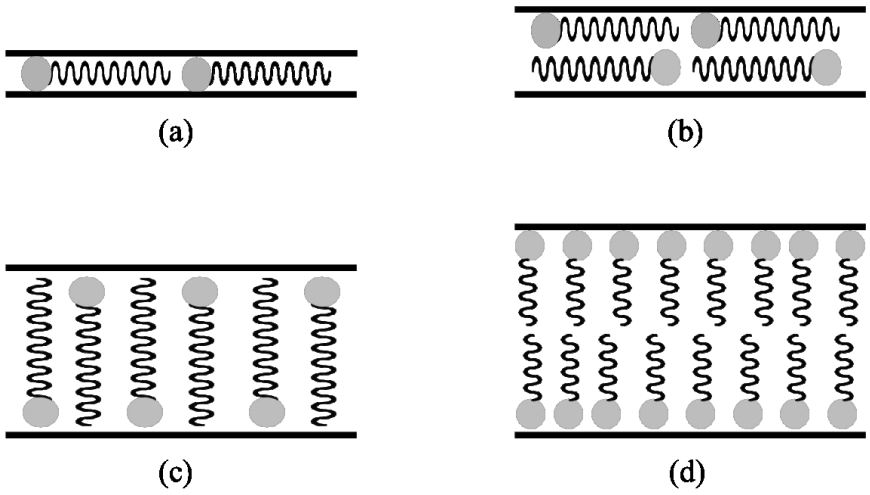

Figure 2.3 Schematic diagram of the idealized arrangements of alkylammonium cations between the clay layers: (a) parallel monolayer, (b) parallel bilayer, (c) radiated monolayer, and (d) radiated bilayer, adapted from [Vaia *et al.* 1994].The clay layers are expressed by the straight dark lines.

2.3 Applications of nanoclay

Nanoclays have broad applications such as rheological modifiers for paints, inks and greases; drug delivery systems for controlled release of medical agents; and industrial wastewater treatment [Patel *et al.* 2006]. One important application of nanoclays is their use as reinforcement nanofiller in the polymer for the preparation of nanocomposite. The first commercialized polymer-clay nanocomposite (Nylon 6/MMT) was produced by Toyota Company in the 1980's and used in automotive parts such as timing belt coating [Okada *et al.* 1990; Osaka & Usuki 1995]. Since then, the use of nanoclay has been expanded to many other commercialized polymers (Table 2.1). The demand for polymer-clay nanocomposites has grown rapidly achieving a market size of over 1 billion pounds by 2009 with applications mainly in packaging, automotive, coating, and building and construction [Patel *et al.* 2006].

Table 2.1 Examples of commercially exfoliated nanocomposite systems.

Polymer	Clay type	Surfactant	Compatibilizer	Ref.
PET	Cloisite®15A	Dimethyl-dihydrogenated tallow ammonium	None	[Frounchi & Dourbash 2009]
PP	Nanomer®I.31PS	Onium	PP-g-MA	[Chen *et al.* 2004]
HDPE	Na^+ type MMT	Octadecylamine	PE-g-MA	[Lee *et al.* 2005]
LDPE	Nanomer® I.30P	Octadecylamine	PE-g-MA	[Morawiec *et al.* 2005]
Nylon	Nanomer® I.34TCN	Methyl-dihydroxyethyl hydrogenated tallow ammonium	None	[Shen *et al.* 2004]
PLA	Cloisite®30B	Methyl bis-2-hydroxyethyl tallow ammonium	None	[Krishnamachari *et al.* 2009]
PS	Cloisite®15A	Dimethyl-dihydrogenated tallow ammonium	None	[Kaci *et al.* 2010]
PVC	Cloisite®93A	Methyl-dihydrogenated tallow ammonium	None	[Saad & Dimitry 2012]

Note: Cloisite® and Nanomer® are trade names of nanoclays supplied by Southern Clay Products and Nanocor, respectively.

2.3.1 Preparation of polymer-clay nanocomposite

Intercalation of polymer chains between the clay layers is a well-established approach for the preparation of polymer-clay nanocomposite. Three methods had been developed depending on the starting materials and processing techniques: in situ intercalative polymerization, solution-induced intercalation and melt intercalation [Sinha Ray & Okamoto 2003; Patel *et al.* 2006].

2.3.1.1 In situ intercalative polymerization method

In this method, monomers along with catalysts or initiators are inserted between the clay layers. The clay layers are further expanded into the polymer matrix through polymerization (Figure 2.4). This method enables the exfoliation of nanoclay particles in the polymer, and therefore it has been applied to a wide range of polymers such as nylon 6 [Kojima *et al.* 1993], polycaprolactone (PCL) [Messersmith & Giannelis 1993], polyethylene terephthalate (PET) [Ke *et al.* 1999], polyolefin [Tudor *et al.* 1996; Bergman *et al.* 1999], polymethyl methacrylate (PMMA) and polystyrene (PS) [Okamoto *et al.* 2000; Okamoto *et al.* 2001].

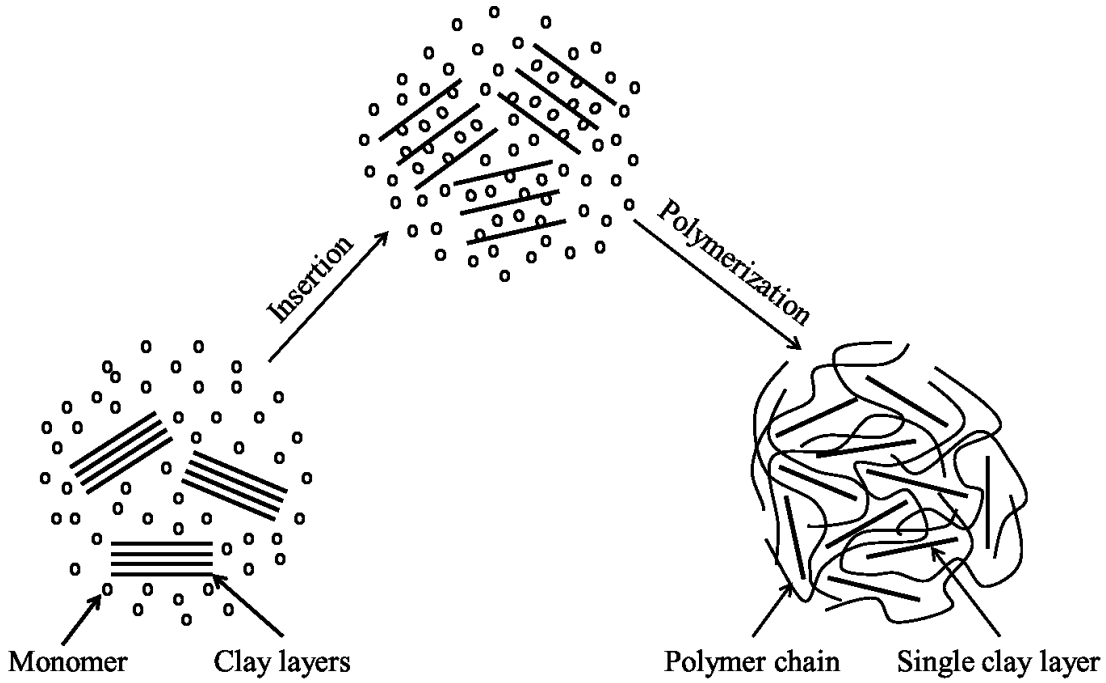

Figure 2.4 Schematic illustration of nanocomposite preparation by in situ intercalative polymerization.

2.3.1.2 Solution-induced intercalation method

This method involves solvents to swell and disperse nanoclay particles into a polymer solution, followed by the intercalation of polymer chains into the clay gallery (Figure 2.5). Water-soluble polymers like PEO [Aranda & Ruiz-Hitzky 1992], PVA [Pandey *et al.* 2010] and polyethylene vinyl alcohol (PEVA) [Zhao *et al.* 1989] are suitable for this method. However, this method can also be applied to polymers that are soluble in non-aqueous systems. For example, chloroform was used to prepare PCL-clay nanocomposite [Jimenez *et al.* 1997] and polylactide (PLA)-clay nanocomposite [Ogata *et al.* 1997]. Polyethylene (PE)-clay nanocomposite was prepared by using xylene and benzonitrile as the solvent [Jeon *et al.* 1998], while toluene was selected as the solvent for the preparation of polyurethane (PU)-clay nanocomposite [Widya & Macosko 2005].

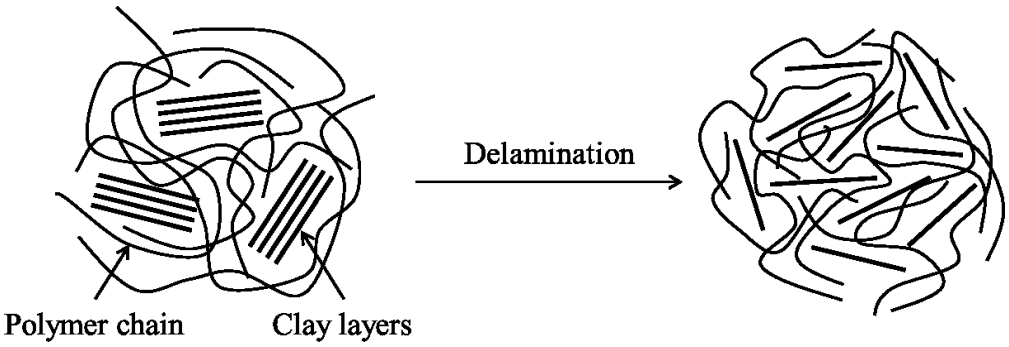

Figure 2.5 Schematic illustration of nanocomposite preparation by solution-induced intercalation.

2.3.1.3 Melt intercalation method

This method provides the intercalation and exfoliation of nanoclay particles in polymer matrices with shear at the melting stage (Figure 2.6). Melt intercalation is a popular approach for the preparation of polymer-clay nanocomposite since it has several advantages over the other methods. First, melt intercalation is more environment-friendly and generates less waste as there is no need for the use of solvent. Since melt intercalation avoids the use of solvent, it can be applied to many polymers that may not be suitable for the other approaches due to the solvent restrictions on those polymers. Moreover, melt intercalation is compatible with current industrial processing techniques such as extrusion and injection molding. This method was first applied in the preparation of PS-clay nanocomposite [Vaia *et al.* 1993], and then expanded to other polymers such as polyolefin [Pereira de Abreu *et al.* 2007; Sarkar *et al.* 2008], nylon 6 [Fornes *et al.* 2001], PLA [Sinha Ray *et al.* 2002], PET [Davis *et al.* 2002], and polyvinyl chloride (PVC) [Awad *et al.* 2009].

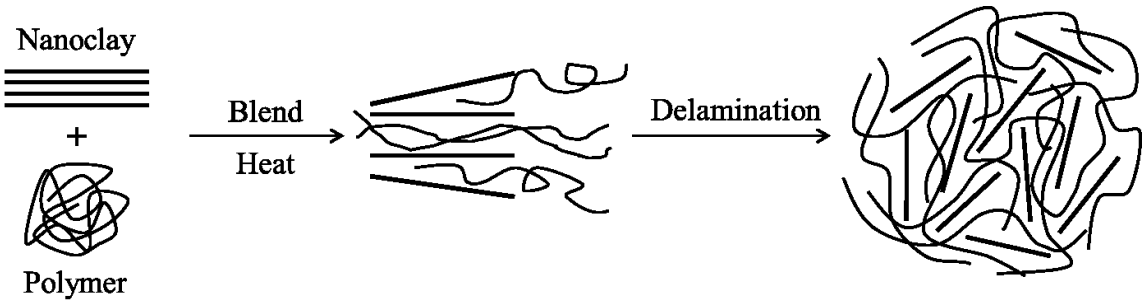

Figure 2.6 Schematic illustration of nanocomposite preparation by melt intercalation.

2.3.2 Morphology of polymer-clay nanocomposite

Polymer-clay nanocomposites can be divided into three general types depending on the differences in their morphology, as shown in Figure 2.7. In an intercalated nanocomposite, the clay gallery is inserted by a few layers of polymer chains; however the clay structure still occurs in a crystallographically regular fashion with an average distance between the clay layers, regardless of the amount of nanoclay added into the polymer. The intercalated-and-flocculated nanocomposite is similar to the intercalated one, while the clay layers are sometimes flocculated due to the hydroxylated edge to edge interaction. In an exfoliated nanocomposite, the clay layers are fully separated and randomly dispersed in the continuous polymer matrix with an average distance depending on the nanoclay content. Therefore, the average interlayer distance will no longer be determined.

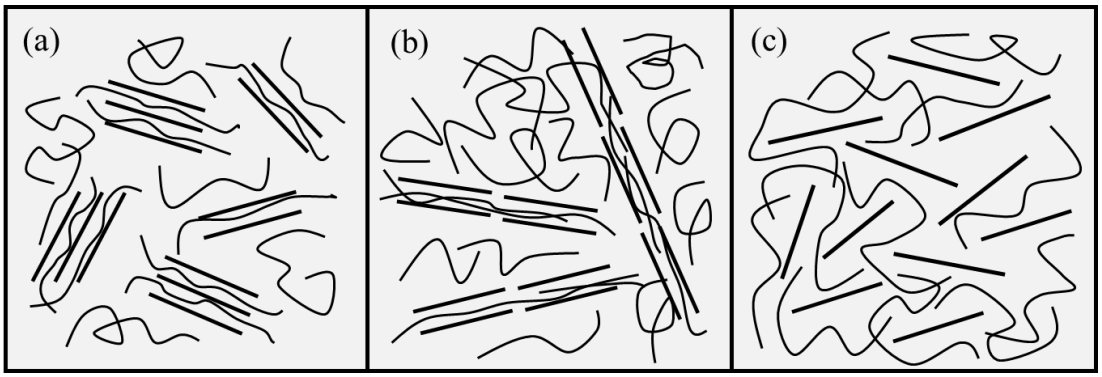

Figure 2.7 Schematic diagram of three different structures of polymer-clay nanocomposite: (a) intercalation, (b) intercalation-and-flocculation, and (c) exfoliation, adapted from [Sinha Ray & Okamoto 2003].

2.3.3 Benefits of polymer-clay naocomposite

In recent years, polymer-clay nanocomposite has become a subject of intensive research, development and commercialization. Compared to the neat polymer or conventional composite (*e.g.*, micrometer reinforcement), polymer with addition of nanoclays at small loadings (3-6 wt%) exibits remarkable improvement in material properties including mechanical, thermal, and barrier properties [Patel *et al.* 2006].

2.3.3.1 Mechanical properties

An improvement in mechanical properties is usually observed after embedding nanoclays into the polymer. The improvement is mainly attributed to the interaction between the nanoclay and the polymer. One such interaction could be via hydrogen bonding at the interface between the nanoclay and the polymer (Figure 2.8) [Liu *et al.* 2006]. Strong polymer-clay interaction facilitates the dispersion of nanoclay particles within the polymer matrix. Otherwise, aggregation of nanoclay particles occurs when the interaction is thermodynamically unfavorable, contributing

to the decreased mechanical properties. In this situation, a compatibilizer is added to improve the polymer-clay interaction. An example is the use of maleic anhydride-graft-polypropylene (MAPP) in the preparation of PP-clay nanocomposite [Reichert *et al.* 2000; Chaudhary & Jayaraman 2011], where the nanoclay particles are conjugated to MAPP and dispersed in the polymer matrix during polymer processing.

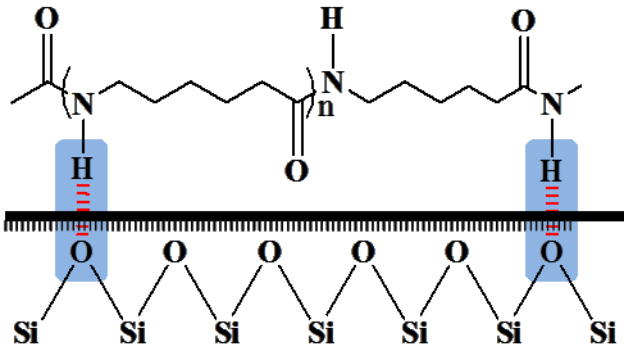

Figure 2.8 Schematic illustration of the formation of hydrogen bonds in Nylon 6-clay nanocomposite, adapted from [Sinha Ray & Okamoto 2003].

2.3.3.2 Thermal properties

Polymers, when exposed to a flow of heat, exhibit weight loss after a certain temperature called thermal decomposition temperature (T_d). The weight loss is casued by the formation of volatile components during decomposition and measured by thermogravimetric analysis (TGA). The thermal stability of polymers can be enhanced by adding nanoclay which acts as a superior heat insulator [Noh *et al.* 1999] and mass transport barrier [Zanetti *et al.* 2001]. The barrier effect of nanoclay is owing to two aspects. First, the presence of nanoclay particles retards the oxygen/air diffusion from the gas phase into the polymer matrix, and therefore reduces the polymer oxidation. Second, the presence of nanoclay particles hinders the release of volatile

components from the polymer, especially when there is char formation at the polymer surface due to the aggregation of nanoclay particles during thermal decomposition [Zhu *et al.* 2001, Liu *et al.* 2003]. The improved thermal stability was first reported in the study of PMMA-clay nanocomposite [Blumstein 1965]. TGA result showed that the nanocomposite had a 40-50 °C higher T_d compared to the neat PMMA. Similar phenomenon was also found in other polymers such as epoxy resins [Pashaei *et al.* 2010], PP [Golebiewski & Galeski 2007], PS [Praseetha *et al.* 2012] and nylon [Rathi & Dahiya 2012].

2.3.3.3 Barrier properties

Mass transfer of small molecules such as gases in a polymer-clay nanocomposite is similar to that in a semi-crystalline polymer. The nanoclay particles are considered as non-permeable regions dispersed in a permeable polymer matrix. The dispersed non-permeable regions lengthen the diffusion path of small molecules in the polymer. This phonomenon is known as tortuosity (Figure 2.9) which is the main mechanism for the improvement of barrier properties [Nielsen 1967]. The improvement of gas barrier is indicated by the decrease of gas permeability which has been found in many polymers such as PE [Passaglia *et al.* 2008; Carrera *et al.* 2013], PP [Pereira de Abreu *et al.* 2007], PS [Nazarenko *et al.* 2007], PET [Sanchez-Garcia *et al.* 2007], PLA [Maiti *et al.* 2002], and nylon [Picard *et al.* 2007].

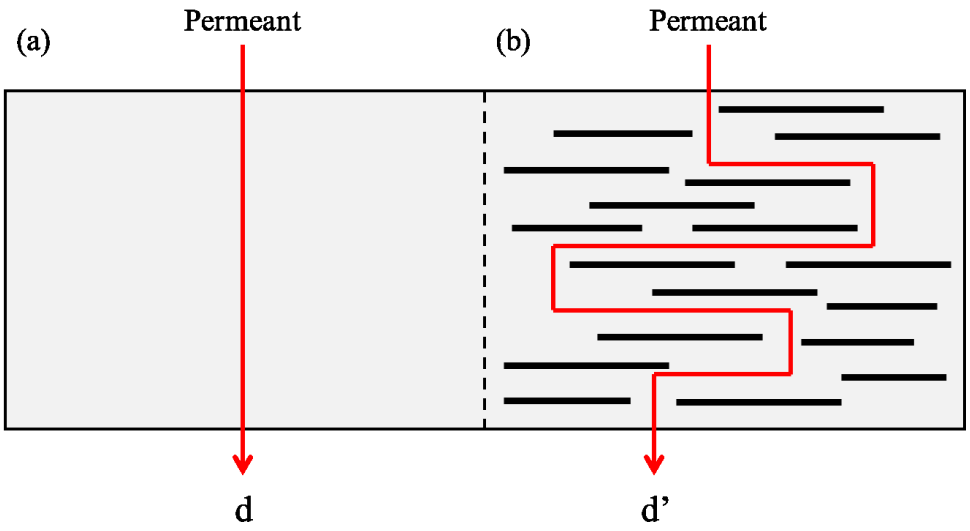

Figure 2.9 Schematic illustration of the tortuous pathway in the polymer-clay nanocomposite. (a) In the neat polymer, the diffusion direction of the permeant is perpendicular to the polymer surface. (b) In the nanocomposite, the permeant must travel around the non-permeable nanoclay particles, causing an increase in the diffusion length.

2.4 Public concerns and regulatory issues on nanoclay

The wide spread of nanocomposites has raised concerns regarding the release of nanoparticles and their by-products which may threaten human health due to the exposure to those components. [Lin *et al.* 2010; Lowry *et al.* 2012; von der Kammer *et al.* 2012; Westerhoff & Nowack 2013]. Many efforts have been made on the understanding of interactions between nanoparticles and biological systems, and the possible ways that nanoparticles might be toxic. Efforts have also been made toward the improvement of rules and regulations on the use of nanocomposites, in order to ensure food safety as well as protect human health.

2.4.1 Potential risks of nanoclay

The potential risks of nanoclay are affected by the physicochemical characteristics of nanoclay including particle size, shape, composition, surface property, and reactivity with biological systems [Chau *et al.* 2007; Uddin 2008]. Among those factors, particle size plays an important role in the toxicity of nanoclay. Natural clays are in the form of clusters with the size in the micrometer range so that their toxicity may not be a concern. When the particle size drops to the nanometer range, toxic properties are exhibited and generally enhanced as the particle size is further reduced [Lauterwasser 2005]. Surface property is another important factor that determines the nanoclay toxicity. Nanoclay particles, due to their high surface area and ion exchange capacity, have the potential to interact with the surrounding environments. In biological systems, adverse health effects may be generated due to the structure and activity change of proteins adsorbed by nanoclay particles or the ion exchange between nanoclay particles and the environment around cells [Gysell 2011; Baek *et al.* 2012].

Toxicity of nanoclay occurs through different routes of exposure including inhalation, dermal absorption and oral ingestion. With these routes, nanoclay particles enter the human body, reach organs through blood circulation and cause tissue damage [Chau *et al.* 2007; Uddin 2008]. Cytotoxic effects of nanoclay have been investigated in various model cells such as human hepatic cells [Lordan *et al.* 2011], human epithelial cells [Verma *et al.* 2012] and human normal intestinal cells [Baek *et al.* 2012]. It was found that the nanoclay particles caused inhibition of cell proliferation and damage to cell membrane. Furthermore, the shape and surface area of nanoclay particles may impact cell viability; platelet-like particles were more cytotoxic than tubu-like ones.

The potential risks of surfactant, as the organo-modifier of nanoclay, have also been investigated; the results showed that some surfactants are toxic to ecosystems, animals and

humans [Talmage 1994; Venhus & Mehrvar 2004; Ying 2006]. The degradation products of phynol-containing surfactants are considered as endocrine disrupting chemicals that may cause adverse health effects on wildlife or humans [Sonnenschein & Soto 1998; Routledge & Sumpter 2009]. Cytotoxic effects of surfactant vary with the surfactant structure [Inacio *et al.* 2011]. Surfactant with phenyl or pyridinium group in its hydrophobic tail is more toxic than that with just alkyl chain. Surfactant with shorter hydrophobic carbon chains is more toxic than that with longer ones, although no linear relationship is evident between the toxicity and carbon chain length.

2.4.2 Regulatory perspectives on the use of nanoclay

In the US, the use of food contact materials (FCMs) is regulated by the Food and Drug Administration (FDA) under the Code of Federal Regulations (CFR): 21 CFR 174 - 21 CFR 190. There are strict rules for FCMs regarding the release of additives from packaging materials into food. Although many nanocomposites for food packaging applications are in the process of commercialization, regulations on the use of such materials are scarce due to the lack of information on the exposure evaluation and risk assessment of nanoparticles. Currently, clay minerals are generally recognized as safe according to FDA 21 CFR 184. This consideration is based on the *in vitro* studies indicating that clay minerals normally exhibit cytotoxic effects only after exposure to a high dose (*e.g.*, thousands of ppm), while human exposure to such dose is unlikely to happen [Li *et al.* 2010; Baek *et al.* 2012]. However, seldom have *in vivo* studies been carried out with low dose and prolonged exposure, which is critical for the risk assessment. Regulatory agencies such as the FDA and the European Food Safety Authority (EFSA) are in the process of developing guidelines for the use of nanoparticles in food packaging systems [EFSA

2009; FDA 2013]. With more experimental data available on the nanoclay toxicity, especially the low dose effects caused by the accumulation of nanoclay particles in organs, new regulations regarding the use of nanoclay in nanocomposite as FCMs might be needed in the future.

2.5 Transport of nanoclay within food packaging systems

Study on the fate and transport of engineered nanoparticles (ENPs) within different biosystems and environments has been received increasing interest [Lin *et al.* 2010; Lowry *et al.* 2012; von der Kammer *et al.* 2012; Westerhoff & Nowack 2013]. A migration process is usually associated with the transport of nanoparticles and their by-products within packaging systems, which describes the release of nanoparticles from a packaging material (*e.g.*, nanocomposite) into the surrounding environment (*e.g.*, food). Nanoclay particles and surfactants have the potential to release from nanocomposites in contact with food. The driving force is the concentration difference of these components between the nanocomposite and the food, so that spontaneous release from a high concentration side (nanocomposite) to a low concentration side (food) occurs in order to balance such difference. However, the release process of nanoclay particles and surfactants may be different due to their size difference and specific chemistry.

2.5.1 Release of surfactant - theories and modeling

Surfactants are considered as small molecules and their release from a packaging material into food follows the migration behavior of small molecules that can be described by the Fick's second law [Crank 1975]:

$$\frac{\partial C}{\partial t} = D\frac{\partial^2 C}{\partial x^2} \tag{2.1}$$

where C is the migrant concentration in the polymer; x is the diffusion distance; t is the diffusion time; and D is the diffusion coefficient of the migrant in the polymer. The direction of diffusion is perpendicular to the polymer surface.

Fick's second law of diffusion is useful to describe the release process in food packaging systems. This second order differential equation can be resolved to express the amount of migrant released from the polymer into food as a function of time t [Brandsch *et al.* 2002]:

$$\frac{M_{F,t}}{M_{F,\infty}} = 1 - \sum_{n=1}^{\infty} \frac{2\alpha(1+\alpha)}{1+\alpha+\alpha^2 q_n^2} exp\left(-\frac{Dq_n^2}{L^2}t\right) \tag{2.2}$$

with

$$\alpha = \frac{1}{K_{P,F}} \frac{V_F}{V_P} \tag{2.3}$$

where $M_{F,t}$ is the amount of migrant in food at time t, $M_{F,\infty}$ is the amount of migrant in food at equilibrium, L is the film thickness, V_P is the volume of the polymer, V_F is the volume of the food, q_n is the positive roots of equation $tan\, q_n = -\alpha q_n$, and $K_{P,F}$ is the partition coefficient of migrant in the polymer/food system and can be calculated from the ratio of migrant concentration in the polymer ($C_{P,\infty}$) and food ($C_{F,\infty}$):

$$K_{P,F} = \frac{C_{P,\infty}}{C_{F,\infty}} \tag{2.4}$$

To get a more reliable result on the theoretical migration with Equation 2.2, a very large number of positive roots of equation $tan\, q_n = -\alpha q_n$ are required. To avoid the heavy work of calculation, Equation 2.2 can be reduced to [Chung *et al.* 2002]:

$$\frac{M_{F,t}}{M_{F,\infty}} = (1+\alpha)[1 - \exp(\omega)\, erfc(\omega^{0.5})] \tag{2.5}$$

with

$$\omega = \frac{Dt}{\alpha^2 L^2} \tag{2.6}$$

In the case that the volume of food simulant is much larger than the polymer and the migration is mainly diffusion controlled ($V_F \gg V_P$ and/or $K_{P,F} < 1$), a simplified equation can be used to determine the diffusion coefficient [Hamdani *et al.* 1997]:

$$\frac{M_{F,t}}{M_{F,\infty}} = 1 - \frac{8}{\pi^2} \sum_{n=1}^{\infty} \frac{1}{(2n+1)^2} exp\left[-\frac{(2n+1)^2}{4L^2} D\pi^2 t\right] \tag{2.7}$$

Equations 2.2, 2.5 and 2.7 are applied to describe the release of migrant from packaging films either in one-sided or two-sided contact with food, while half film thickness (L/2) is used in the case of two-sided contact. To enable the application of these diffusion equations, some assumptions are made [Helmroth *et al.* 2002]: (a) initially homogeneous distribution of the migrant throughout the film; (b) even thickness of the film; (c) absence of migrant in food at the beginning of migration; and (d) no obvious swelling of the film caused by food.

2.5.2 Release of nanoclay - theories and mechanisms

The Fick's diffusion theories used to describe the migration of small molecules like surfactants may not be suitable for large nanoparticles like nanoclay. Simon *et al.* investigated the migration of nanoparticles from polymeric packaging into food from a physicochemical point of view [Simon *et al.* 2008]. Three factors were taken into account: particle size, distance from the polymer surface, and viscosity of the polymer. The authors demonstrated that the migration of nanoparticles would be likely to happen when the particles are small in size (with radius in the order of magnitude of 1 nm) and close to the polymer surface. Meanwhile, the polymer should be low in viscosity and not interact with nanoparticles. A mathematic model was established to describe the release process based on Stokes-Einstein equation [Atkins 1998]:

$$D = \frac{K_B T}{6\pi\eta r} \tag{2.8}$$

where D is the diffusion coefficient of nanoparticle in the polymer, T is the temperature, K_B is the Boltzmann constant (1.3807×10^{-23} J K^{-1}), r is the hydrodynamic particle radius, and η is the dynamic viscosity of the polymer at a given temperature which can be expressed as:

$$\eta(T) = \eta(T_g) \exp\left[-\frac{C_1(T - T_g)}{C_2 + T - T_g}\right] \tag{2.9}$$

where C_1 and C_2 are empirical parameters. For a wide range of polymers, the values C_1 = 17.44 K and C_2 = 51.6 K are used. Equation 2.8 provides a useful tool to describe the migration of nanoparticles from polymers in theory, but the model lacks support from any experimental data.

Migration of nanoclay particles was observed in studies of the flame retardancy properties of polymer-clay nanocomposites [Lewin 2002; Zanetti *et al.* 2002; Tang *et al.* 2004; Lewin 2006]. Char formation at the polymer surface under pyrolysis or annealing above the melting point of the polymer suggested the migration of nanoclay particles toward the surface and the subsequent aggregation at the surface. There are two different mechanisms associated with the migration of nanoclay particles in the polymer melt. The first mechanism is the formation of gas and bubbles during the decomposition of surfactant and compatibilizer, which propel the nanoclay particles to the polymer surface [Lewin 2006; Tang & Lewin 2008]. The second mechanism is that during annealing, the surface energy of nanoclay is lower than that of the polymer, leading to the segregation of nanoclay particles from the polymer matrix and subsequent accumulation towards the polymer surface. The migrated nanoclay particles are those exfoliated in the polymer matrix and the clay clusters are unlikely to move because of their large size [Tang *et al.* 2006; Zammarano *et al.* 2006]. The annealing process above the melting point

of the polymer could help the exfoliation of nanoclay particles, since the diffusion of oxygen into the polymer induces polymer oxidation which in turn facilitates the intercalation of polymer chains into the clay gallery [Pastore *et al.* 2004; Hao *et al.* 2006].

When the temperature drops far below the melting point of the polymer, the migration of nanoclay particles is hardly to happen. Only a few studies have addressed the relesase of nanoclay from nanocomposite into the solvent; it was found that nearly no nanoclay particle was released [Avella *et al.* 2005; Schmidt *et al.* 2009; Mauricio-Iglesias *et al.* 2010]. These findings were in general agreement with Simon's theory that large nanoparticles are difficult to migrate from the polymer [Simon *et al.* 2008]. However, in another study, release of nanoclay particles (layered double hydroxide platelets) from PLA was observed and attributed indirectly to the change of polymer molecular weight during film processing [Schmidt *et al.* 2011].

2.5.3 Factors impacting the nanoclay release

Release process in the packaging system is controlled by both thermodynamics and kinetics, or partition and diffusion, respectively [Gilbert *et al.* 1980; Karayanni *et al.* 1987; Koszinowski & Piringer 1987]. Partition (thermodynamics process) of the migrant between the polymer and food (or solvent) at equilibrium of migration is affected by the interaction of the migrant with the two phases. Diffusion (kinetics process) is a more important factor that provides information on the migration velocity. Diffusion of nanoparticles in the polymer could be influenced by: (a) interaction between the polymer and the solvent; (b) interaction between the nanoparticle and the solvent; and (c) interaction between the nanoparticle and the polymer. Therefore, evaluating the interactions among different factors (nanoclay, polymer and solvent) would be helpful to understand the release process of nanoclay.

2.5.3.1 Polymer-solvent interaction

One parameter describing the interaction between two phases is affinity, which is estimated by the solubility parameter δ [Scott & Hilderbrand 1962]. The principle for the use of solubility parameter is "like dissolves like", which means two liquids with similar δ values are miscible with each other. This principle can be extended to the miscibility between solid and liquid or solid and solid. In order to precisely define the degree of likeness in a given system, the solubility parameter is divided into three components which are known as Hansen solubility parameters (HSPs) [Hansen 1999] and designated as δ_D, δ_P and δ_H, referring to dispersion, polar and hydrogen bonding parameters, respectively. The interaction between the polymer and the solvent can be described by the relative energy difference (RED) of the polymer-solvent system [Hansen 1999]:

$$RED = \frac{R_a}{R_0} \tag{2.10}$$

where R_0 is the interaction radius of the polymer, R_a is the distance of the solvent from the center of the polymer solubility sphere and expressed as:

$$R_a = \sqrt{4(\delta_{D1} - \delta_{D2})^2 + (\delta_{P1} - \delta_{P2})^2 + (\delta_{H1} - \delta_{H2})^2} \tag{2.11}$$

The second subscript 1 and 2 represent the solvent and the polymer, respectively. If $R_a < R_0$ or $RED < 1$, the polymer is soluble in the solvent; if $R_a = R_0$ or $RED = 1$, the polymer is swelled by the solvent or partially dissolved in the solvent; and if $R_a > R_0$ or $RED > 1$, the polymer is not soluble in the solvent.

2.5.3.2 Solvent-nanoclay interaction

When the polymer is in contact with a solvent, the solvent molecules are able to penetrate the polymer matrix and interact with nanoclay particles inside. Similar to the polymer-solvent

interaction, a good solvent-nanoclay interaction is expected if nanoclay particles are swelled by the solvent due to the adsorption of solvent molecules into the clay gallery. Burgentzle *et al.* adopted a free swelling factor (the ratio of clay volume after swelling to the volume of dry clay powder) to express the interaction between the organo-modified nanoclay and the solvent [Burgentzle *et al.* 2004]. The factor was influenced by the type of solvent and the type of surfactant within the nanoclay. Ho & Glinka investigated the effect of solvent solubility parameter on the dispersion of nanoclay particles in suspension [Ho & Glinka 2003]. Three categories of nanoclay dispersion were observed: precipitation, tactoids and fully exfoliation, revealing different solvent-nanoclay interactions. The solvent dispersion parameter significantly affected the precipitation of nanoclay particles, whereas the polar and hydrogen bonding parameters dominated the formation of tactoids and exfoliation of nanoclay particles.

2.5.3.3 Polymer-nanoclay interaction

The nanocomposite morphology can be used to express the interaction between the polymer and the nanoclay. A weak interaction is indicated by the aggregation/agglomeration of nanoclay particles in the polymer, resulting in microcomposites rather than nanocomposites. On the other hand, a good interaction causes the intercalation of polymer chains into the clay gallery and the further exfoliation of nanoclay particles. In this case, the extent of interaction between the polymer and the nanoclay could be correlated with the degree of exfoliation [Alexandre & Dubois 2000; Shiraz *et al.* 2013]. Polymer-nanoclay interaction also affects the distribution of nanoclay particles in an immiscible polymer blend with different polarity in its constituents. Nanoclay particles are likely to move to the polar phase of the polymer blend where better polymer-nanoclay interaction is achieved [Chow *et al.* 2005; Zhu *et al.* 2008]. It should be

noticed that the balance between the polymer and the nanoclay is affected by solvent exposure. Modification of the polymer matrix as well as the nanoclay due to the penetration of solvent molecules may lead to the rearrangement of nanoclay particles, and therefore the probable movement of nanoclay particles within the polymer matrix [Acharya *et al.* 2004].

2.6 Migration test

In order to ensure food safety, migration test is carried out to determine the amount of migrant released from a packaging material into food. In the US, rules for migration test are set by the FDA under 21 CFR 170.39 (Threshold of regulation for substances used in food-contact articles). Some standards like ASTM standards [ASTM D4757-11, ASTM D1239-07] are also available as guidelines for migration test. The migration experiment is usually carried out under finely controlled laboratory conditions and designed to: (a) simplify the experimental operations, and (b) simulate the migration in real case. Some recommendations for the design of migration experiments [FDA 2007] are listed below in three parts.

2.6.1 Design of migration cell

A food container such as a water bottle can be directly used as the migration cell. However, a specifically designed migration cell should be considered when: (a) the surface area of the food container is not large enough to provide sufficient extractives (migrant) for analysis; or (b) a soft film was used as the packaging material. A specimen of known surface area and a food simulant of known volume are required for the use of a migration cell. The specimen can be either one-sided or two-sided contact with a food simulant. For the latter case, a two-sided migration cell is adopted [Snyder & Breder 1985] with two essential features: (a) separation of

polymer films or sheets by inserting spacers (*e.g.*, glass beads) to allow the free flow of food simulant around each film or sheet; and (b) minimization of headspace with gas-tight or liquid-tight seals. In case that a two-sided migration cell is not suitable for the migration test (*e.g.*, when a multilayer film is used), other cell designs such as a one-sided migration cell could be used [Limm & Holifield 1995].

2.6.2 Selection of food simulant

The extraction of migrant from food is difficult and time consuming due to the complexity of food matrices [Simon & Joner 2008]. Thus, migration test is usually performed by using food-simulating liquids to avoid the complicated extraction process. Food simulants recommended by the FDA are: water for aqueous foods, 3% acetic acid for acid foods, 10 to 50% ethanol for low and high alcoholic foods, food oil (*e.g.*, olive oil, HB307, or Miglyol 812) for fatty foods. When oil is used as a food simulant, an extra step is needed to extract the migrant into a solvent that is suitable for instrumental analysis. To avoid this step, some aqueous-based solvents are used as alternatives for fatty-food simulants. Absolute or 95 % ethanol is an effective fatty-food simulant for polyolefins, and 50% ethanol is used as a fatty-food simulant for rigid PVC, PS and rubber-modified PS [Piringer *et al.* 1992]. The simulant volume-to-specimen surface area ratio should match the value in actual food packaging, for instance, a ratio of 10 ml in^{-2} is acceptable.

2.6.3 Temperature and exposure time

The FDA has recommended short-term accelerated testing to reflect the migration in real applications. For room temperature applications, a temperature of 40 ºC for 10 d is applied,

which is approximately equivalent to the migration for 6 months under room temperature. For refrigerated or frozen food applications, a test temperature of 20 ºC is used. Other temperatures and exposure times may also be used to match the conditions of different applications. Portions of the testing solution should be analyzed during the migration test. At least four samplings should be taken with variant time intervals. Analysis of a control is also recommended.

2.7 Detection and characterization of nanoclay

The migration test requires the detection of nanoclay to estimate the exposure dose. Meanwhile, there is a need to characterize nanoclay since the potential risks of nanoclay highly depend on its physicochemical characteristics. To address the nanoclay detection and characterization, instrumental analysis is carried out with two aspects in consideration. First, the techniques applied should be sensitive enough to enable the measurement at an ultra-low nanoclay concentration. Second, the analysis conducted under laboratory conditions should be a good reflection of the real environmental status [Tiede *et al.* 2008].

2.7.1 Detection

Detection of nanoclay is normally conducted by two instrumental techniques: atomic absorption spectrometry (AAS) and inductively coupled plasma mass spectrometry (ICP-MS) [Avella *et al.* 2005; Schmidt *et al.* 2009; Mauricio-Iglesias *et al.* 2010; Schmidt *et al.* 2011]. Both techniques provide direct measurement of element concentration but not particle concentration such as number or mass concentration.

2.7.1.1 Acid digestion

Before instrumental analysis, an acid digestion procedure is usually applied to dissolve the nanoclay particles with a strong acid (*e.g.*, nitric acid, hydrochloride acid, hydrofluoric acid, or their combination). Standard methods for the acid digestion of nanoclay are set by the US Environmental Protection Agency (EPA) including Method 3050B (Acid digestion of sediments, sludges, and soils), Method 3051A (Microwave assisted acid digestion of sediments, sludges, soils, and oils) and Method 3052 (Microwave assisted acid digestion of siliceous and organically based matrices). There are several advantages of acid digestion [Caroli 2007]: (a) more efficient atomization of the homogenous solution for AAS analysis or ionization of the homogenous solution for ICP-MS analysis compared with that of the suspension; (b) avoidance of probable blockage within the instrument caused by the large particles; and (c) more precise measurement of elements in a homogenous solution than in a suspension where particles may not be evenly dispersed.

2.7.1.2 AAS technique

AAS (Figure 2.10) is applied for the quantification of a specific element (either metallic or non-metallic) in a liquid or solid sample [Welz & Sperling 2007]. The elemental analysis is based on the absorption of light by free atoms at atomizing stage. Most of the elements within nanoclay, from the major elements like Si, Al and Mg, to some minor elements like Fe, Ca and Na, can be analyzed by this technique. AAS is classified into two major categories depending on the type of atomizer used to atomize the element: flame AAS and electrothermal AAS. Flame AAS uses flame as the atomizer consisting of an air-acetylene flame or a nitrous oxide-acetylene flame. An air-acetylene flame generates a temperature of 2300 ºC which is sufficient to atomize

many elements simultaneously. To atomize some elements with good affinity to oxygen (*e.g.*, Al or Si), an N_2O-acetylene flame is adopted with a temperature of up to 2700 ºC to sufficiently break down the compound of these elements. Electrothermal AAS or graphite furnace AAS uses a graphite tube as the atomizer heated by a low-voltage high-current power supply to achieve a temperature of up to 3000 ºC. Some elements (*e.g.*, V, Mo, or B) with atomization temperatures out of the range of flame AAS can be analyzed by this technique.

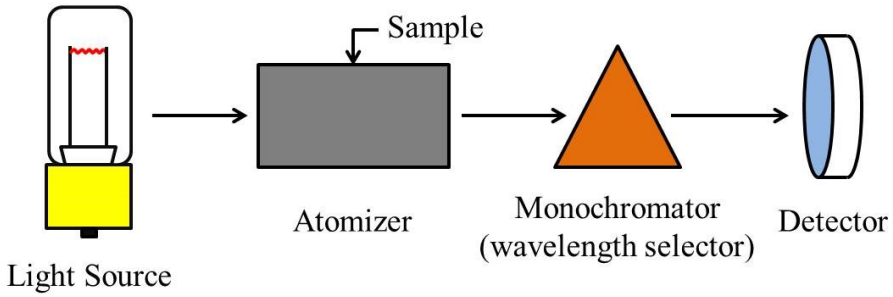

Figure 2.10 Schematic diagram of the working principle of AAS method.

Quantification of an element in the sample requires a calibration curve obtained by preparing a series of standard solutions of that element with known concentrations and recording the absorbance at each concentration. The absorbance-concentration relationship follows the Beer-Lambert Law where the absorbance is proportional to the element concentration. To detect nanoclay, the use of pure nanoclay particles as the standards should be straightforward, but there are some inherent disadvantages such as the variation of elemental composition of nanoclay from batch to batch, or the uneven dispersion of nanoclay particles in the solvent. To overcome these disadvantages, reference standards are used which are soluble in water and stable in composition. The limit of detection (LOD) varies with types of elements and sample preparation procedures. A LOD of ppm level (mg L^{-1}) is usually gained by using flame AAS, while a lower LOD (ppb level

or μg L^{-1}) can be achieved with graphite furnace AAS.

2.7.1.3 ICP-MS technique

ICP-MS is a powerful technique for rapid multi-elemental analysis of a variety of samples [Beauchemin 2006; Thomas 2008]. The instrument consists of an ICP source coupled with a mass spectrometer (Figure 2.11). Argon gas is normally applied in the ICP source to generate plasma with a temperature of up to 10,000 ºC, so that nearly all the elements are efficiently atomized. Before injection into the ICP source, the sample is converted to aerosol by using a nebulizer (for liquid sample) or a laser ablation technique (for solid sample). Once the aerosol sample is introduced into the ICP source, the elements within the sample are dissociated into gaseous atoms and then ionized. The ionized elements are further selected from the plasma and passed through the mass spectrometer where they are separated according to the mass-to-charge (m/z) ratio and detected. The separation of ions is done by either a magnetic sector analyzer or a quadrupole analyzer, while the latter one is commonly used. ICP-MS is more sensitive than AAS due to the highly efficient ionization by ICP source and the low background noise. A LOD of ppt level (ng L^{-1}) or sub-ppb level can be achieved for most elements.

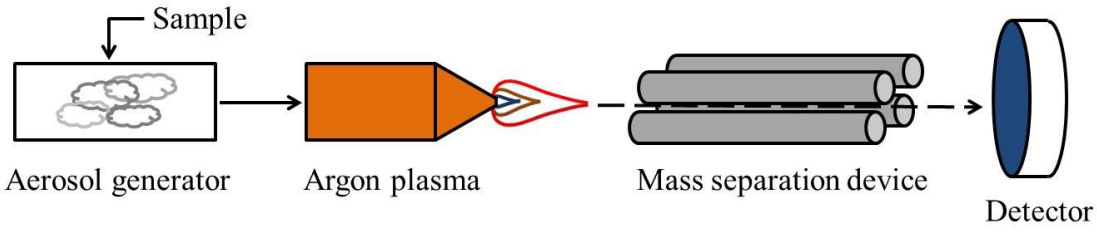

Figure 2.11 Schematic diagram of the working principle of ICP-MS method.

2.7.2 Characterization

2.7.2.1 Size and shape

A variety of size techniques are available for the measurement of particle size and size distribution [Powers *et al.* 2006]. In an aqueous system, dynamic light scattering (DLS) is commonly applied and the particle size is calculated by the Stokes-Einstein equation [Atkins 1998]:

$$r = \frac{K_B T}{6\pi\eta D} \tag{2.12}$$

where D is the translational diffusion coefficient of the particle estimated by the cumulant method [Frisken 2001]. The measurement of size and size distribution is simple if particles are monodispersed. When particles are polydispersed, a progressive measurement is carried out to accurately describe the size distribution [Masuda 1971]. The measurement requires the separation of polydispersed particles which can be achieved by using field-flow fractionation [Gidding *et al.* 1976].

Differential mobility analysis and laser diffraction/static light scattering are usually applied for the measurement of particles at solid state. Electron microscopy such as scanning electron microscopy (SEM) or transmission electron microscopy (TEM) is another type of technique that provides clear images of dry particles, although the image is only two-dimensional which may not reflect the real particle size and shape due to the orientation effects.

2.7.2.2 Structure and morphology

X-ray diffraction (XRD) and electron microscopy are the commonly used methods to characterize nanoclay structure and morphology in the polymer. XRD provides direct measurement of the interlayer spacing (or *d*-spacing) of nanoclay; the working principle is

shown in Figure 2.12. The incident beams (with a wavelength of λ) hit the basal plane of two adjacent clay layers (with a distance of d) at an angle θ and are diffracted at the same angle. A travelling difference of the beams between the two planes is produced and expressed as $2d\sin(\theta)$. If this distance is an integer (generally 1 is used) of the wavelength, construction interference occurs and is expressed by the Bragg's law [Cowley 1995]:

$$d = \frac{\lambda}{2\sin(\theta)} \tag{2.13}$$

XRD cannot provide any information regarding the spatial distribution of nanoclay particles in the polymer. To provide what XRD is missing, TEM is appled allowing a qualitative analysis on the structure and morphology of nanoclay particles in the polymer. SEM is also capable of producing images of the polymer surface containing nanoclay particles with a three-dimensional appearance, while the resolution is not as good as TEM.

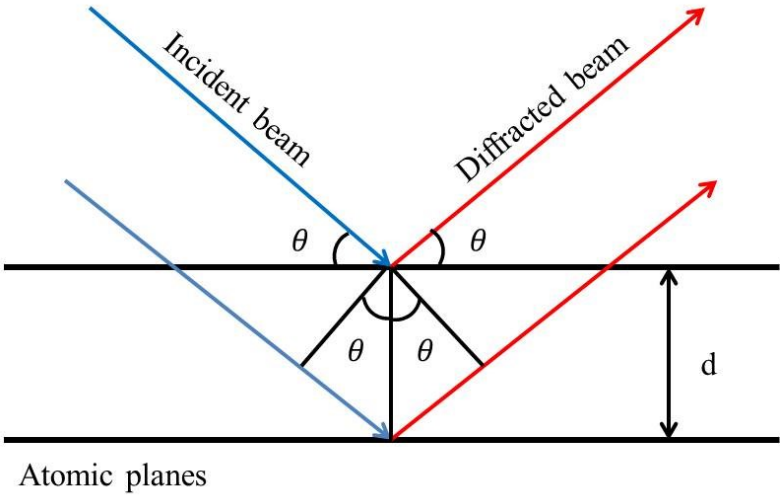

Figure 2.12 Schematic illustration of Bragg's Law.

Investigation of nanoclay structure and morphology in liquid is a challenge for electron

microscopy as it is mainly operated in a vacuum environment. Direct exposure of a liquid sample to the vacuum could cause sample alternation and dehydration artifacts [Mavrocordatos *et al.* 2007]. Cryogenic transmission electron microscopy (cryo-TEM) had been used to solve these problems [Putaux *et al.* 1999; Chalaye *et al.* 2001; Herrera *et al.* 2004]. This technique requires the quenching of a liquid sample in a cold liquid (*e.g.*, liquid ethane) and the observation of the quenched sample at cryogenic temperatures (*e.g.*, liquid nitrogen temperature).

2.7.2.3 Surface area

Surface area is an important character of nanoclay. An increase in surface area enhances the surface reactivity and sorption behavior [Tiede *et al.* 2008]. The specific surface area (SSA) of nanoclay particles can be measured by using a surface area and porosity analyzer. The test is conducted by measuring the adsorption of inert gas molecules (*e.g.*, nitrogen, argon, carbon dioxide, or krypton) by the dry and clean clay powder under vacuum. Since the gas molecules are very small in size, the measurement is only slightly affected by the particle aggregation/agglomeration. The SSA is calculated by applying the Brunauer-Emmett-Teller (BET) sorption isotherm equation [Allen 2004] to the measured adsorption of gas molecules.

The surface area of nanoclay particles in an aqueous system can be determined by conductometric titration with a standard methyl blue solution [Hang & Brindley 1970; Yukselen & Kaya 2008; Abayazeed & EI-Hinnawi 2011]. The methyl blue molecules are adsorbed by nanoclay particles through ion exchange; and the surface area is calculated at the end point of titration with the equation [Abayazeed & EI-Hinnawi 2011]:

$$SSA = \frac{m_{MB}}{319.9} \cdot N_A \cdot A_{MB}/M \tag{2.14}$$

where m_{MB} is the mass of methyl blue (with a molecular weight of 319.9) adsorbed at the end

point of titration, N_A is Avogadro's number 6.02×10^{23} mol^{-1}, A_{MB} *i*s the area of a single methyl blue molecule which is assumed to be 130 $Å^2$ [Hang & Brindley 1970], M is the mass of dry methyl blue to be dissolved in one liter of distilled water. Other cationic surfactants could also be used for titration such as dodecylamine hydrochloride [Kalb & Curry 1969].

2.7.2.4 Surface charge

Surface charge is another important character of nanoclay as it impacts the particle stability especially in suspension [Powers *et al.* 2006; Tiede *et al.* 2008]. A large negative or positive surface charge of particles improves their dispersion in suspension due to the large repelling force among the particles. Otherwise, particles tend to flocculate or aggregate when the surface charge is close to neutral. A particle in suspension has a liquid layer surround it which can be divided into two parts: an inner layer (Stern layer) where ions are strongly bound to the particle and an outer layer (diffuse layer) where the ions are weakly associated. The potential at the boundary of the outer layer (slipping plane) is called zeta potential (Figure 2.13) which is used as an indicator of the surface charge. There are several factors that affect the zeta potential of nanoclay in suspension. One factor is pH as the nanoclay surface is more negatively charged in a base solution, but tends to turn neutral or even positive in an acid solution [Ijagbemi *et al.* 2009; Pawar & Bohidar 2009]. Another factor is salt concentration as the increase of salt concentration (*e.g.*, Na^+, Li^+, or Ca^{2+}) leads to the increase of zeta potential [Yukselen & Erzin 2008]. The zeta potential could also be affected by the surfactant such as type of surfactant and amount of surfactant attached to the nanoclay [Marras *et al.* 2007; Mahesh *et al.* 2011].

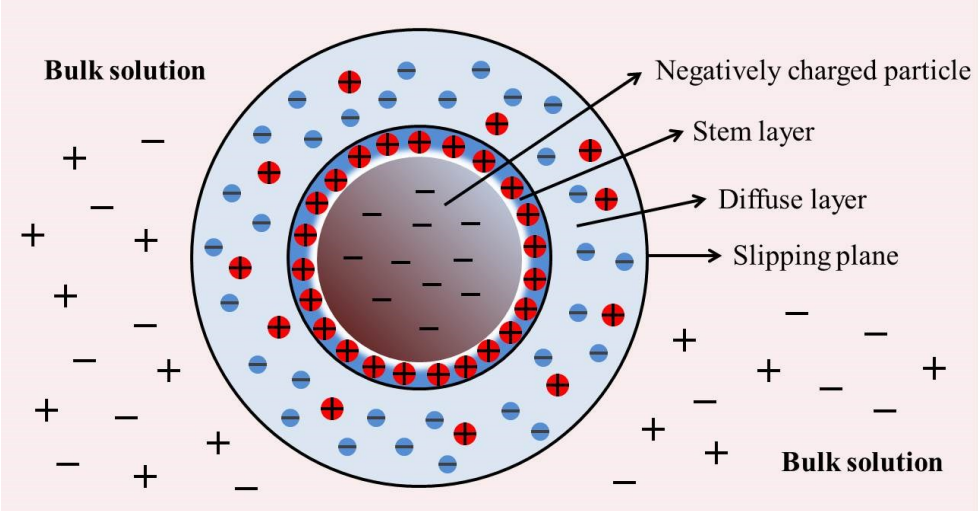

Figure 2.13 Schematic illustration of zeta potential, adapted from the brochure of Malvern Nanosizer Nano ZS.

Typical methods for the measurement of zeta potential of nanoclay in suspension include microelectrophoresis [Marras *et al.* 2007; Pawar & Bohidar 2009], electrophoretic light scattering [Isherwood & Jennings 1983; Mahesh *et al.* 2011] and potentiometric titration [Tombacz & Szekeres 2004; Yukselen & Erzin, 2008; Ijagbemi *et al.* 2009]. Microelectrophoresis is a method to investigate the electrophoresis of dispersed particles. The apparatus contains two chambers with an electrode in each chamber and a capillary cell that connects the two chambers. The movement of particles induced by the direct current voltage on the electrodes is observed by an optical microscope placed above the capillary cell. The electrical conductivity of the suspension, the mobility and observed size of particles are correlated to the zeta potential. Electrophoretic light scattering measures the frequency shift or phase shift of incident laser beams scattered by the dispersed particles. The zeta potential is obtained by correlating the shift to the electrophoretic mobility of particles based on Smoluchowski's theory [Marras *et al.* 2007]. Potentiometric titration measures the electric potential drop over the

suspension between two electrodes: an indicator electrode and a reference electrode. For the measurement of nanoclay with negative charged surface, potentiometric titration of protons is carried out. The proton adsorption by nanoclay surface is recorded at the isoelectric point (also described by the pH of zero net proton charge) of titration and converted to zeta potential.

2.7.2.5 Aggregation

Nanoclay particles may remain dispersed or aggregated in suspension depending on the clay-clay and clay-solvent interactions. Aggregation occurs with an increase in particle size due to the attraction among particles (van der Waals forces or hydrophobic interactions) or the binding to other molecules such as oligomer, polymer and proteins. Aggregation of nanoclay particles is influenced by the surrounding environments (*e.g.*, solvent type, salt concentration, or pH) and the surface treatment of nanoclay (*e.g.*, organo-modification). The aggregation could happen in both acid (low pH) and base (high pH) environments although the mechanisms are different [Tombacz & Szekeres 2004; Borgnino 2013]. Edge-to-face aggregation is usually found in a low pH environment, while face-to-face aggregation happens in a high pH environment. Salt concentration has an effect on the particle stability as an increase in salt concentration could facilitate the aggregation of nanoclay particles in an aqueous suspension. Surface modification such as organo-modification makes nanoclay particles less stable in an aqueous suspension, resulting in aggregation [Marras *et al.* 2007; Mahesh *et al.* 2011].

Many instrumental techniques used for particle size measurement can also be applied to the aggregation study. Among these techniques, light scattering is commonly applied not only to the static measurement but also the kinetic study of nanoclay aggregation.

BIBLIOGRAPHY

BIBLIOGRAPHY

Abayazeed, S.D.; EI-Hinnawi, E. Characterizatin of Ehyptian smectitic clay deposits by methylene blue adsorption. *Am. J. Appl. Sci.* **2011**, 8, 1282-1286.

Acharya, H.; Pramanik, M.; Srivastava, S.K.; Bhowmick, A.K. Synthesis and evaluation of high-performance ethylene-polylene-diene terpolymer/organoclay nanoscale composites. *J. Appl. Polym. Sci.* **2004**, 93, 2429-2436.

Ajayan, P.M.; Schadler, L.S.; Braun, P.V. Nanocomposite Science and Technology. Wiley-VCH: Weinheim, Deutschland, 2003, Chapter 2.

Alexandre, M. and Dubois, P. Polymer-layered silicate nanocomposites: preparation, properties and uses of a new class of materials. *Mater. Sci. Engng. R.* **2000**, 28, 1-63.

Allen, T. Particle Size Measurement, Vol 1: Powder Sampling and Particle Size Measurement, 5th Ed., Chapman & Hall: London, UK, 2004.

Aranda, P.; Ruiz-Hitzky, E. Poly(ethylene oxide)-silicate intercalation materials. *Chem. Mater.* **1992**, 4, 1395-1403.

ASTM D4754-11. Standard Test Method for Two-Sided Liquid Extraction of Plastic Materials Using FDA Migration Cell. ASTM International, West Conshohocken, PA, USA

ASTM D1239-07. Standard Test Method for Resistance of Plastic Films to Extraction by Chemicals. ASTM International, West Conshohocken, PA, USA.

Atkins, P.W. 1998. Physical chemistry, 6th Edition. Oxford University Press: Oxford, UK, 1998, pp. 1014.

Avella, M.; De Vlieger, J.J.; Errico, M.E.; Fischer, S.; Vacca, P. and Volpe, M.G. Biodegradable starch/clay nanocomposite films for food packaging applications. *Food Chem.* **2005**, 93, 467-474.

Awad, W.H.; Beyer, G.; Benderly, D.; Ijdo, W.L.; Songtipya, P.; Jimenez-Casco, M.D.M.; Manias, E.; Wilkie, C.A. Material properties of nanoclay PVC composites. *Polymer* **2009**, 50, 1857-1867.

Baek, M.; Lee, J.A.; Choi, S.J. Toxicological effects of a cationic clay, montmorillonite *in vitro* and *in vivo*. *Mol. Cell Toxicol.* **2012**, 8, 95-101.

Bayens B.; Bradbury M.H. A mechanistic description of Ni and Zn sorption on Na-montmorillonite: titration and sorption measurement. *J. Contam. Hydrol.* **1997**, 27, 199-222.

Beauchemin, D. Inductively coupled plasma mass spectrometry. *Anal. Chem.* **2006**, 78, 4111-4136.

Bergaya, F.; Theng, B.K.G.; Lagaly, G. Handbook of Clay Science. Elsever Science: Welwyn, UK, 2006.

Bergman, J.S.; Chen, H.; Giannelis, E.P.; Thomas, M.G.; Coates, G.W. Synthesis and charaterization of polyolefin-silicate nanocomposites: a catalyst intercalation and in situ polymerization apporach. *J. Chem. Soc. Chem. Commun.* **1999**, 21, 2179-2180.

Blumstein, A. Polymerization of adsorbed monolayers: II. Thermal degradation of the inserted polymers. *J. Polym. Sci. A* **1965**, 3, 2665-2673.

Borgnino, L. Experimental determination of the colloidal stability of Fe(III)-montmorillonite: effects of organic matter ionic strength and pH conditions. *Colloids Surf. A* **2013**, 423, 178-187.

Bradbury M.H.; Bayens B. Modelling the sorption of Zn and Ni on Ca-montmorillonite, Geochim. *Cosmochim. Acta* **1999**, 63, 325–336.

Brandsch, J.; Mercea, P.; Ruter, M.; Tosa, V.; Piringer, O.G. 2002. Migration modelling as a tool for quality assurance of food packaging. *Food Addi. Cont.* **2002**, 19, 29-41.

Burgentzle, D.; Duchet, J.; Gerard, J.F.; Jupin, A.; Fillon, B. Solvent-based nanocomposite coatings I. Dispersion of organophilic montmorillonite in organic solvents. *J. Colloid Interf. Sci.* **2004**, 278, 26-39.

Cadambi, R.M. and Ghassemieh, E. Mechanism of gas permeation in processed HNBR/nanoclay composites. *Adv. Polym. Technol.* **2013**, 32, 103-118.

Caroli, S. The determination of chemical elements in food: applications for atomic and mass spectrometry. John Wiley & Sons: Hoboken, New Jersey, USA, 2007.

Carrera, M.C.; Erdmann, E.; Destefanis, H.A. Barrier properties and structure study of nanocomposite of HDPE/montmorillonite modified with polyvinylalcohol. *J. Chem.* **2013,** 7 pages, ID 679567.

Cases, J.M.; Berend, I.; Besson, G.; Francois, M.; Uriot, J.P.; Thomas, F.; Poirier, J.E. Mechanism of adsorption and desorption of water vapor by homoionic montmorillonite. 1. The sodium-exchanged form. *Langmuir* **1992**, 8, 2730-2739.

Chalaye, S.; Bourgeat-Lami, E.; Putaux, J.L.; Lang, J. Synthesis of composite latex particles filled with silica. Control of the composite particles composition. *Macromol. Symp.* **2001**, 169, 89-96.

Chau, C.F.; Wu, S.H.; Yen G.C. The development of regulation for food nanotechnology. *Trends Food Sci. Technol.* **2007**, 18, 269-280.

Chaudhary, A.K.; Jayaraman, K. Extrusion of linear polypropylene-clay nanocomposite foams. *Polym. Eng. Sci.* **2011**, 51, 1749-1756.

Chen, L.; Wong, S. C.; Liu, T.X.; Lu, X.H.; He, C.B. Deformation mechanisms of nanoclay-reinforced maleic anhydride-modified polypropylene. *J. Polym. Sci. B* **2004**, 42, 2759-2768.

Chow, W.S.; Mohd Ishak, Z.A.; Karger-Kocsis, J. Atomic force microscopy study on blend morphology and clay dispersion in polyamide-6/polypropylene/organoclay systems. *J. Polym. Sci. B* **2005**, 43, 1198-1204.

Chung, D.; Papadakis, S.E.; Yam, K.L. Simple models for assessing migration from food-packaging films. *Food Addit. Contam.* **2002**, 19, 611-617.

Cowley, J.M. Diffraction Physics, Third Revised Edition. Elsevier Science: Amsterdam, Holland, 1995.

Crank, J. The Mathematics of Diffusion. Oxford University Press: Oxford, England, 1975.

Davis, C.H.; Mathias, L.J.; Gilman, J.W.; Schiraldi, D.A.; Shields, J.R.; Trulove, P.; Sutto, T.E.; Delong, H.C. Effects of melt-processing conditions on the quality of poly(ethylene terephthalate) montmorillonite clay nanocomposites. *J. Polym. Sci. B* **2002**, 40, 2661-2666.

De A. Prado, L.A.S.; Karthikeyan, C.S.; Schulte, K.; Nunes, S.P.; de Torriani, I.L. Organic modification of layered silicates: structural and thermal charaterizations. *J. Non-cryst. Solids* **2005**, 351, 970-975.

Di Gianni, A.; Amerio, E.; Monticelli, O.; Bongiovanni, R. Preparation of polymer/clay mineral nanocomposites via dispersion of silylated montmorillonite in a UV curable epoxy matrix. *Appl. Clay Sci.* **2008**, 42, 116-124.

Diaz. C.A.; Xia, Y.; Rubino, M.; Auras, R.; Jayaraman, K.; Hotchkiss, J. Fluorescent labeling and tracking of nanoclay. *Nanoscale* **2013**, 5, 164-168.

[EFSA] European Food Safety Authority. The Potential Risks Arising from Nanoscience and Nanotechnologies on Food and Feed Safety. *EFSA J.* **2009**, 958, 1-39. Available from: http://www.efsa.europa.eu/en/efsajournal/doc/958.pdf

[FDA] Food and Drug Administration. 2013. FDA Nanotechnology Regulatory Science Research Plan. Available from: http://www.fda.gov/ScienceResearch/SpecialTopics/Nanotechnology/ucm273325.htm

[FDA] Food and Drug Administration. 2007. Guidance for Industry: Preparation of Food Contact Notifications and Food Additive Petitions for Food Contact Substances: Chemistry Recommendations. Available from: http://www.fda.gov/Food/GuidanceRegulation/GuidanceDocumentsRegulatoryInformation/ucm081818.htm

Fornes, T.D.; Yoon, P.J.; Keskkula, H.; Paul, D.R. Nylon 6 nanocomposites: the effect of matrix molecular weight. *Polymer* **2001**, 42, 9929-9940.

Frisken, B.J. Revisiting the method of cumulants for the analysis of dynamic light-scattering data. *Appl. Optics* **2001**, 40, 4087-4091.

Frounchi, M.; Dourbash A. Oxygen barrier properties of poly(ethylene terephthalate) nanocomposite films. *Macromol. Mater. Eng.* **2009**, 294, 68-74.

Gidding, J.C.; Yang, F.J.; Myers, M.N. Flow field-flow fractionation: a versatile new separation method. *Science* **1976**, 193, 1244-1245.

Gilbert, S.G.; Miltz, J.; Giacin, J.R. Transport consideration of potential migrants from food packaging material. *J. Food Process. Preserv.* **1980**, 4, 27-49.

Golebiewski, J.; Galeski, A. Thermal stability of nanoclay polypropylene composites by simultaneous DSC and TGA. *Compos. Sci. Technol.* **2007**, 67, 3442-344.

Gysell, M. The interaction of synthetic nanoparticles with biological systems. PhD Thesis, School of Biomedical Sciences, University of Queensland, Australia, 2011.

Hamdani, M.; Feigenbaum, A.; Vergnaud, J.M. Prediction worst case migration from packaging to food using mathematical models. *Food Addit. Contam.* **1997**, 14, 499-506.

Hang, P.T.; Brindley, G.W. Methylene blue absorption by clay minerals. Determination of surface areas and cation exchange capacities (Clay-Organic Studies XVIII). *Clays Clay Miner.* **1970**, 18, 203-212.

Hansen, C.M. Hansen Solubility Parameters, A User's Handbook. CRC Press: Boca Raton, FL, USA, 1999.

Hao, J.; Lewin, M.; Wilkie, C.A.; Wang, J. Additional evidence for the migration of clay upon heating of clay-polypropylene nanocomposites from X-ray photoelectron spectroscopy (XPS). *Polym. Degrad. Stabil.* **2006**, 91, 2482-2485.

Helmroth, I.E.; Bekhuis, H.A.M.; Linssen, J.P.H. and Dekker, M. Direct measurement of additive migration from low-density polyethylene as a function of space and time. *J. Appl. Polym. Sci.* **2002**, 86, 3185-3190.

Hensen, E.J.M.; Smit, B. Why clays swell. *J. Phys. Chem. B* **2002**, 106, 12664-12667.

Herrera, N.N.; Letoffe, J.M.; Putaux, J.L.; David, L.; Bourgreat-Lami, E. Aqueous dispersions of silence-functionalized laponite clay platelets. A first step toward the elaboration of water-based polymer/clay nanocomposite. *Langmuir* **2004**, 20, 1564-1571.

Ho, D. L.; Glinka, C. J. Effects of solvent solubility parameters on organoclay dispersions. *Chem. Mater.* **2003**, 15, 1309-1312.

Hussain, F.; Hojjati, M.; Okamoto, M.; Gorga, R.E. Review article: polymer-matrix nanocomposites, processing, manufacturing, and application: an overview. *J. Compos. Mater.* **2006**, 40, 1511-1575.

Ianchis, R.; Cinteza, L.O.; Donescu, D.; Petcu, C.; Corobea, M.C.; Somoghi, R.; Ghiurea, M.; Spataru, C. Implications of silylated montmorillonite on montmorillonite-polyacrylate nanocomposites. *Appl. Clay Sci.* **2011**, 52, 96-103.

Ianchis, R.; Corobea, M.C.; Conescu, D.; Rosca, I.D.; Cinteza, L.O.; Nistor, L.C.; Vasile, E.; Marin, A.; Preda, S. Advanced functionalization of organocaly nanoparticles by silylation and their polystyrene nanocomposites obtained by miniemulsion polymerization. *J. Nanopart. Res.* **2012**, 14, 1233-1236.

Ijagbemi, C.O.; Baek, M.H.; Kim, D.S. Montmorillonite surface properties and sorption characteristics for heavy metal removal from aqueous solutions. *J. Hazard. Mater.* **2009**, 166, 538-546.

Ikhsan, J.; Wells, J.D.; Johnson, B.B.; Angove, M.J. Surface complexation modeling of the sorption of Zn(II) by montmorillonite. *Colloids Surf. A* **2005**, 252, 33–41.

Inacio, A.S.; Mesquita, K.A.; Baptista, M.; Ramalho-Samtos, J.; Vaz, W.L.C.; Vieira, O.V. In vitro surfactant structure-toxicity relationships: implications for surfactant use in sexually transmitted infection prophlaxis and contraception. Published online at PLOS ONE, May 2011. Available from: http://www.plosone.org/article/info%3Adoi%2F10.1371%2Fjournal.pone.0019850

Isherwood, R.; Jennings, B.R. Surface-charge determination of crocidolite proticles in suspension. *Clay Miner.* **1983**, 18, 313-323.

Jeon, H.G.; Jung, H.T.; Lee, S.W.; Hudson, S.D. Morphology of polymer solicate nanocomposites. High density polyethylene and a nitrile. *Polym. Bull.* **1998**, 41, 107-113.

Jimenez, G.; Ogata, N.; Kawai, H.; Ogihara, T. Structure and thermal/mechanical properties of poly(ε-caprolactone)-clay blend. *J. Appl. Polym. Sci.* **1997**, 64, 2211-2220.

Kaci, M.; Remili, C.; Bruzaud, S.; Grohens, Y. Effect of photooxidation on polystyrene/cloisite 15A nanocomposites under accelerated UV exposure. *Academ. J. Manufac. Eng.* **2010**, 8, 61-66.

Kalb, G.W.; Curry, R.B. Determination of surface area by surfactant adsorption in aqueous suspension-I. Dodecylamine hydrochloride. *Clays Clay Miner.* **1969**, 17, 47-57.

Karayanni, S.T.; Demertzis, P.G.; Kontominas, M.G. Adsorption of vinylchloride onto plasticized polyvinylchloride by classical partition in the presence of various food simulating solvents: migration aspects. *Lebensm. Wiss. Technol.* **1987**, 20, 202-206.

Kaya A.; Oren A.H. Adsorption of zinc from aqueous solutions to bentonite. *J. Hazard. Mater. B* **2005**, 125, 183–189.

Ke, Y.C.; Long, C.; Qi, Z. Crystallization, properties, and crystal and nanoscale morphology of PET-clay nanocomposites. *J. Appl. Polym. Sci.* **1999**, 71, 1139-1146.

Kojima, Y.; Usuki, A.; Kawasumi, M.; Okada, A.; Kurauchi, T.; Kamigaito, O. One-pot synthesis of nylon 6-clay hybrid. *J. Polym. Sci. A* **1993**, 31, 1755-1758.

Koszinowski, J.; Piringer, O. Food/package compatibility and migration. *J. Plast. Film Sheet* **1987**, 3, 96-111.

Krishnamachari, P.; Zhang, J.; Lou, J. Z.; Yan, J. Z.; Uitenham, L. Biodegradable poly(lactic acid)/clay nanocomposites by melt intercalation: a study of morphological, thermal, and mechanical properties. *Int. J. Polym. Analy. Charact.* **2009**, 14, 336-350.

Lauterwasser, C. Opportunities and Risks of Nanotechnologies. London: Allianz AG, Centre for Technology/OECD, 2005.

Lee, J.H.; Jung, D.; Hong, C. E.; Rhee, K. Y.; Advani, S. G. Properties of polyethylene-layered silicate nanocomposites prepared by melt intercalation with a PP-g-MA compatibilizer. *Compos. Sci. Technol.* **2005**, 65, 1996-2002.

Lewin, M. Surface barrier formation in the pyrolysis and combustion of nanocomposites. *Rec. Adv. Flame Retard. Polym. Mater.* **2002**, 13, 84-96.

Lewin, M. Reflections on migration of clay and structural changes in nanocomposites. *Polym. Adv. Technol.* **2006**, 17, 758-763.

Li, P.R.; Wei, J.C.; Chiu, Y.F.; Su, H.L.; Peng, F.C.; Lin, J.J. Evaluation on cytotoxicity and genotoxicity of the exfoliated silicate nanoclay. *ACS Appl. Mater. Interf.* **2010**, 2, 1608-1613.

Limm, W.; Holifield, H.C. Effects of temperature and mixing on polymer adjuvant migration to corn oil and water. *Food Addit. Contam.* **1995**, 12, 609-624.

Lin, D.; Tian, X.; Wu, F.; Xing, B. Fate and transport of engineered nanomaterials in the environment. *J. Environ. Qual.* **2010**, 39, 1896-1908.

Liu, A.D.; Xie, T.X.; Yang, G.S. Comparison of polyamide-6 nanocomposites based on pristine and organic montmorillonite obtained via anionic ring-opening polymerization. *Macromol. Rapic Commun.* **2006**, 27, 1572-1577.

Liu, T.X.; Lim, K.P.; Tjiu, W.C.; Pramoda, K.P.; Chen, Z.K. Preparation and characterization of nylon 11/organoclay nanocomposites. *Polymer* **2003**, 44, 3529-3535.

Lordan, S.; Kennedy, J.E.; Higginbotham, C.L. Cytotoxic effects induced by unmodified and organically modified nanoclays in the human hepatic HepG2 cell line. *J. Appl. Toxicol.* **2011**, 31, 27-35.

Lowry, G.V.; Gregory, K.B.; Apte, S.C.; Lead, J.R. Transformations of nanomaterials in the environment. *Environ, Sci. Technol.* **2012**, 46, 6893-6899.

Mahesh, K.R.V.; Murthy, H.N.N.; Kumaraswamy, B.E.; Raghavendra, N.; Sridhar, R.; Krishna, M.; Pattar, N.; Pal, R.; Sherigara, B.S. Synthesis and characterization of organomodified Na-MMT using cation and anion surfactants. *Front. Chem. China* **2011**, 6, 153-158.

Maiti, P.; Yamada, K.; Okamoto, M.; Ueda, K.; Okamoto, K. New polylactide/layered silicate nanocomposites: role of organoclays. *Chem. Mater.* **2002**, 14, 4654-4661.

Manias, E. Origins of materials properties enhancement in polymer/clay nanocomposites. Nanocomposites 2001, Delivering New Value to Plastics, Jun. 25-27, 2001, Chicago, IL, ECM Publishers, IL, USA, 2001, pp. 1-11.

Marras, S.I.; Tsimpliaraki, A.; Zuburtikudis, I.; Panayiotou, C. Thermal and colloidal behavior of amine-treated clays: the roe of amphiphilic organic cation concentration. *J. Colloid Interf. Sci.* **2007**, 315, 520-527.

Masuda, H.I.K. Theroetical study of the scatter of experimental data due to particle size distribution. *J. Chem. Eng. Jpn.* **1971**, 4, 60-67.

Mauricio-Iglesias, M.; Peyron, S.; Guillard, V.; Gontard, N. Wheat gluten nanocomposite films as food-contact materials: migration tests and impact of a novel food stabilization technology (high pressure). *J. Appl. Polym. Sci.* **2010**, 116, 2526-2535.

Mavrocordatos, D.; Perret, D.; Leppard, G.G. Stratigies and advances in the characterization of environmental colloids by electron microscopy. In: Wilkinson, K.J.; Lead, J.R. Environmental Colloids and Particles: Behaviour, Structure and Charaterization. John Wiley & Sons: published online, 2007.

Messersmith, P.B.; Giannelis, E.P. Polymer-layered silicate nanocomposites: in-situ intercalative polymerization of ε-caprolactone in layered silicates. *Chem. Mater.* **1993**, 5, 1064-1066.

Morawiec, J.; Pawlak, A.; Slouf, M.; Galeski, A.; Piorkowska, E.; Krasnikowa, N. Preparation and properties of compatibilized LDPE/organo-modified montmorillonite nanocomposites. *Eur. Polym. J.* **2005**, 41, 1115-1122.

Nazarenko, S.; Meneghetti, P.; Julmon, P.; Olson, B.G.; Qutubuddin, S. Gas barrier of polystyrene montmorillonite clay nanocomposites: effect of mineral layer aggregation. *J. Polym. Sci. B* **2007**, 45, 1733-1753.

Newman, A.C.D. The Interaction of Water with Clay Mineral Surfaces. In Chemistry of Clays and Clay minerals. Longman Scientific and Technical Publisher: Birmingham, AL, USA, 1987, pp. 237.

Nielsen, L. Platelet particles enhance barrier of polymer by forming tortuous path. *J. Macromol. Sci. Chem.* **1967**, Al (5), 929-942.

Nitva, G.; Nair, G.T.; Mony, U.; Chennazhi, K.P.; Nair S.V. In vitro evaluation of electrospun PCL/nanoclay composite scaffold for bone tissue engineering. *J. Mater. Sci. Mater. Med.* **2012**, 23, 1749-1761.

Noh, M.H.; Jang, L.W.; Lee, D.C. Intercalation of styrene-acryonitrile copolymer in layered silicate by emulsion polymerization. *J. Appl. Polym. Sci.* **1999**, 74, 179-188.

Ogata, N.; Jimenez, G.; Kawai, H.; Ogihara, T. Structure and thermal/mechanical properties of poly(L-lactide)-clay blend. *J. Polym. Sci. B* **1997**, 35, 389-396.

Okada, A.; Kawasumi, M.; Usuki, A.; Kojima, Y.; Kurauchi, T.; Kamigaito, O. Synthesis and properties of nylon-6/clay hybrids. In: Schaefer, D.W.; Mark, J.E. Polymer based molecular composites. MRS Symposium Proceedings, Pittsburgh, 1990, 171, 45-50.

Okamoto, M.; Morita, S.; Taguchi, H.; Kim, Y.H.; Kotaka, T.; Tateyama, H. Synthesis and structure of smectic clay/poly(methyl methacrylate) and clay polystyrene nanocomposites via in situ intercalative polymerization. *Polymer* **2000**, 41, 3887-3890.

Okamoto, M.; Morita, S.; Kotaka, T. Dispersed structure and ionic conductivity of smectic clay/polymer nanocomposites. *Polymer* **2001**, 42, 2685-2688.

Okutomo, S.; Kuroda, K.; Ogawa, M. Preparation and characterization of silylated-nagadiites. *Appl. Clay Sci.* **1999**, 15, 253-264.

Osaka, A.; Usuki, A. The chemistry of polymer-clay hybrids. *Mater. Sci. Eng.* **1995**, C3, 109-115.

Pandey, P.; Bhattacharyya, A.R.; Gutch, P.K.; Chauhan, R.S.; Pant, S.C. Polyvinyl alcohol fuller's earth clay nanocomposite films. *J. Appl. Poly. Sci.* **2010**, 115, 3005-3012.

Pashaei S.; Siddaramaiah; Syed, A.A. Investigation on thermal, mechanical and morphological behaviours of organo nanoclay incorporated expoxy nanocomposites. *ARPN J. Eng. Appl. Sci.* **2010**, 5, 76-86.

Passaglia, E.; Bertoldo, M.; Ceriegi, S.; Sulcis, R.; Narducci, P.; Conzatti, L. Oxygen and water barrier properties of MMT nanocomposites from low density polyethylene or EPM with grafted succinic groups. *J. Nanosci. Nanotechnol.* **2008**, 8, 1690-1699.

Pastore, H.O.; Frache, A.; Boccaleri, E.; Marchese, L.; Camino, G. Heat induced structure modifications in polymer-layered silicate nanocomposites. *Macromol. Mater. Eng.* **2004**, 289, 783-786.

Patel, H.A.; Somani, R.S.; Bajaj, H.C.; Jasra, R.V. Nanoclays for polymer nanocomposites, paints, inks, greases and cosmetics formulations, drug delivery vehicle and waste water treatment. *Bull. Mater. Sci.* **2006**, 29, 133-145.

Pawar, N.; Bohidar, H.B. Hydrophobic hydration mediated universal self-association off colloidal nanoclay particles. *Colloids Surf. A* **2009**, 333, 120-125.

Pereira de Abreu, D.A.; Paseiro Losada, P.; Angulo, I.; Cruz, J.M. Development of new polyolefin films with nanoclays for application in food packaging. *Eur. Polym. J.* **2007**, 43, 2229-2243.

Picard, E.; Vermogen, A.; Gerard, J.F.; Espuche, E. Barrier properties of nylon 6-montmorillonite nanocomposite membranes prepared by melt blending: influence of the clay content and dispersion state: consequences on modeling. *J. Membrane Sci.* **2007**, 292, 133-144.

Piringer, O.G.; Bieber, W.; Figge, K., Baner, A.L.; Franz, R. Alternative fatty food simulants for migration testing of polymeric food contact materials. *Food Addi. Contam.* **1992**, 9, 137-148.

Powers, K.W.; Brown, S.C.; Krishna, V.B.; Wasdo, S.C.; Moudgil, B.M.; Roberts, S.M. Research strategies for safety evaluation of nanomaterials. Part VI. Characterization of nanoscale particles for toxicological evaluaton. *Toxicol. Sci.* **2006**, 90, 296-303.

Praseetha, P.N.; Surej, R.C.; George, K.E. Insitu polymerization of styrene using nanoclay and optimization of strength using central composite design. *Int. J.Eng. Res. Appl.* **2012**, 2, 1045-1049.

Putaux, J.L.; Buléon, R.; Borsali, H.; Chanzy, H. Ultrastructural aspects of phytoglycogen from cryo-TEM and quasi-elastic light scattering data. *Int. J. Biol. Macromol.* **1999**, 26, 145-150.

Rathi, S.; Dahiya, J.B. Polyamide 66/nanoclay composite: synthesis, thermal and flammability properties. *Adv. Mat. Lett.* **2012**, 3, 381-387.

Reichert, P.; Nitz, H.; Klinke, S.; Brandsch, R.; Thomann, R.; Mulhaupt, R. Poly(propylene)/organoclay nanocomposite formation. *Macromol. Mater. Engng.* **2000**, 275, 8-17.

Routledge, E.J.; Sumpter, J.P. Estrogenic activity of surfactants and some of their degradation products assessed using a recombinant yeast screen. *Environ. Toxicol. Chem.* **2009**, 15, 241-248.

Saad, A.L.G.; Dimitry, O.I.H. Studies pf particle dispersion in plasticized poly(vinyl chloride)/montmorillonite nanocomposites. *J. Appl. Polym. Sci.* **2012**, 123, 1407-1420.

Sanchez-Garcia, M.D.; Gimenez, E.; Lagaron, J.M. Novel PET nanocomposites of interest in food packaging applications and comparative barrier performance with biopolyester nanocomposites. *J. Plast. Film Sheet.* **2007**, 23, 133-148.

Sarkar, M.; Dana, K.; Ghatak, S.; Banerjee, A. Polypropylene-clay composite prepared from Indian bentonite. *Bull. Mater. Sci.* **2008**, 31, 23-28.

Schmidt, B.; Petersen, J.H.; Bender Koch, C.; Plackett, D.; Johansen, N.R.; Katiyar, V.; Larsen, E.H. Combining asymmetrical flow field-flow fractionation with light-scattering and inductively coupled plasma mass spectrometric detection for characterization of nanoclay used in biopolymer nanocomposites. *Food Addit. Contam.* **2009**, 26, 1619-1627.

Schmidt, B.; Katiyar, V.; Plackett, D.; Larsen, E.H.; Gerds, N.; Koch, C.B.; Petersen, J.H. Migration of nano-sized layered double hydroxide platelets from polylactide nanocomposite films. *Food Addit. Contam.* **2011**, 28, 956-966.

Scott, R.L.; Hilderbrand, J. Regular Solutions. Prentice-Hall: Englewood Cliffs, NJ, USA, 1962.

Shen, L.; Phang, I. Y.; Chen, L.; Liu, T. X.; Zeng, K. Y. Nanoindentation and morphological studies on nylon 66 nanocomposites. I. Effect of clay loading. *Polymer* **2004**, 45, 3341-3349.

Shiraz, N.Z.; Enferad, E.; Monfared, A.; Mojarrad, M.A. Preparation of nanocomposite based on exfoliation of montmorillonite in acrylamide thermosensitive polymer. *ISRN Polym. Sci.* **2013**, Volume 2013, 5 pages, ID 280897.

Silvestre, C.; Duraccio, D.; Cimmino, S. Food packaging based on polymer nanomaterials. *Prog. Poly. Sci.* **2011**, 36, 1766-1782.

Simon, P.; Joner, E. Conceivable interactions of biopersistent nanoparticles with food matrix and living systems following from their physicochemical properties. *J. Food Nutr. Res.* **2008**, 47, 51-59.

Simon, P.; Chaudhry, Q.; Bakos, D. Migration of engineered nanoparticles from polymer packaging to food–a physicochemical view. *J. Food Nutr. Res.* **2008**, 47, 105-113.

Sinha Ray, S.; Maiti, P.; Okamoto, M.; Yamada, K.; Ueda, K. New polylactide/layered silicate nanocomposites. 1. Preparation, characterization and properties. *Macromolecule* **2002**, 35, 3104-3110.

Sinha Ray, S.; Okamoto, M. Polymer/layered silicate nanocomposites: a review from preparation to processing. *Prog. Polym. Sci.* **2003**, 28, 1539-1641.

Snyder, R.C.; Breder, C.V. New FDA migration cell used to study migration of styrene from polystyrene into various solvents. *Anal. Chem.* **1985**, 68, 770-775.

Sonnenschein, C.; Soto, A.M. An updated review of environmental estrogen and androgen mimics and antagonists. *J. Steroid Biochem. Mol. Biol.* **1998**, 65, 143-150.

Strawhecker, K.E.; Manias, E. Structure and properties of poly(vinyl alcohol)/Na^+ montmorillonite nanocomposites. *Chem. Mater.* **2000**, 12, 2943-2949.

Subramani, S.; Choi, S.W.; Lee, J.Y.; Kin, J.H. Aqueous dispersion of novel silylated (polyurethane-acrylic hybrid/clay) nanocmposite. *Polymer* **2007**, 48, 4691-4703.

Talmage, S.S. Environmental and Human safety of major surfactants: alcohol ethoxylates and alkylphenol ethoxylates. CRE Press: Boca Raton, FL, USA, 1994.

Tang, Y.; Hu, Y.; Li, B.; Liu, L.; Wang, Z.; Chen, Z.; Fan, W. Polypropylene/montmorillonite nanocomposites and intumescent, flame-retardant montmorillonite synergism in polypropylene nanocomposites. *J. Poly. Sci. A* **2004**, 42, 663-6173.

Tang, Y.; Lewin, M.; Pearce, E.M. Effects of annealing on the migration behavior of PA6/clay nanocomposites. *Macromol. Rapid Comm.* **2006**, 27, 1545-1549.

Tang, Y.; Lewin, M. New aspects of migration and flam retardancy in polymer nanocomposites. *Polym. Degrad. Stabil.* **2008**, 93, 1986-1995.

Thomas, R. Practical Guide to ICP-MS: A Tutorial for Beginners, Second Edition. CRC Press: Boca Raton, FL, USA, 2008.

Tiede, K.; Alistair, B.A.; Boxall, A.B.A.; Tear, S.P.; Lewis, J.; David, H.; Hassellov. Detection and characterization of engineered nanoparticles in food and the environment. *Food Addit. Contam.* **2008**, 25, 795-821.

Tombacz, E.; Szekeres, M. Colloidal behavior of aqueous montmorillonite suspensions: the specific role of PH in the presence of indifferent electrolytes. *Appl. Clay Sci.* **2004**, 27, 75-94.

Tudor, J.; Willington, L.; O'Hare, D.; Royan, B. Intercalation of catalytically active metal complexes in phyllosilicates and their application as propene polymerization catalyst. *Chem. Commun.* **1996**, 2031-2032.

Uddin, F. Clays, nanoclays, and montmorillonite minerals. *Metall. Mater. Trans. A* **2008**, 39, 2804-2814.

Vaia, R.A.; Ishii, H.; Giannelis, E.P. Synthesis and properties of two-dimensional nanostructures by direct intercalation of polymer melts in layered silicates. *Chem. Mater.* **1993**, 5, 1694-1696.

Vaia, R.A.; Teukolsky, R.K.; Giannelis, E.P. Interlayer structure and molecular environment of alkylammonium layered silicates. *Chem. Mater.* **1994**, 6, 1017-1022.

Veli S.; Alyuz B. Adsorption of copper and zinc from aqueous solutions by using natural clay. *J. Hazard. Mater.* **2007**, 149, 226-233.

Venhus, S.H.; Mehrvar, M. Health effects, environmental impacts, and photochemical degradation of selected surfactants in water. *Int. J. Photoenergy* **2004**, 6, 115-125.

Verma, N.K.; Moore, E.; Blau, W.; Volkov, Y.; Ramesh Babu, P. Cytotoxicity evaluation of nanoclays in human epithelial cell line A549 using high content screening and real-time impedance analysis. *J. Nanopart. Res.* **2012**, 14, 1137-1147.

Von der Kammer, F.; Ferquson, P.L.; Holden, P.A.; Masion, A.; Rogers, K.R.; Klaine, S.J.; Koelmans, A.A.; Home, N.; Unrine, J.M. Analysis of engineered nanomaterials in complex matrices (environment and biota): general considerations and conceptual case studies. *Environ. Toxicol. Chem.* **2012**, 31, 32-49.

Welz, B.; Sperling, M. Atomic Absorption Spectrometry, Third Edition. Wiley-VCH: published online, 2007.

Westerhoff, P.; Nowack, B. Searching for global descriptors of engineered nanomaterial fate and transport in the environment. *Acc. Chem. Res.* **2013**, 46, 844-853.

Whitley, H.D.; Smith, D.E. Free energy, energy, and entropy of swelling in Cs-, Na-, and Sr-montmorillonite clays. *J. Chem. Phys.* **2004**, 120, 5387–5395.

Widya, T.; Macosko, C.W. Nanoclay-modified rigid polyurethane foam. *J. Macromol. Sci. B* **2005**, 44, 897-908.

Xie, W.; Gao, Z.M.; Liu, K.; Pan, W.P.; Vaia, R.; Hunter, D.; Singh, A. Thermal characterization of organically modified montmorillonite. *Thermochimica Acta* **2001**, 367-368, 339-350.

Yariv, S. 2002. Organo-clay complexes and interactions. New York: Marcel Dekker, Inc., NY, USA, 68, 69 & 84-89, pp. 515-519.

Ying, G.G. Fate, behavior and effects of surfactants and their degradation products in the environment. *Environ. Int.* **2006**, 32, 417-431.

Yukselen, Y.; Erzin, Y. Artificial neural networks approach for zeta potential of montmorillonite in the presence of different cations. *Environ. Geol.* **2008**, 54, 1059-1066.

Yukselen, Y.; Kaya, A. Suitability of the methylene blue test for surface area, cation exchange capacity and swell potential determination of clayey soils. *Eng. Geol.* **2008**, 102, 38-45.

Zammarano, M.; Gilman, J.W.; Nyden, M.; Pearce, E.M.; Lewin, M. The role of oxidation in the migration mechanism of layered silicate in poly(propylene) nanocomposites. *Macromol. Rapid Comm.* **2006**, 27, 693-696.

Zanetti, M.; Camino, G.; Thomann, R.; Mulhaupt, R. Synthesis and thermal behavior of layered silicate-EVA nanocomposites. *Polymer* **2001**, 42, 4501-4507.

Zanetti, M.; Kashiwagi, T.; Falqui, L.; Camino, G. Cone calorimeter combustion and gasification studies of polymer layered silicate nanocomposites. *Chem. Mater.* **2002**, 14, 881-887.

Zhao, X.; Urano, K.; Ogasawara, S. Adsorption of poly(ethylene vinyl alcohol) from aqueous solution on montmorillonite clays. *Colloid Polym. Sci.* **1989**, 267, 899-906.

Zheng, Y.; Zaoui, A.; Shahrour, I. A theroretical study of swelling and shrinking of hydrated Wyoming montmorillonite. *Appl. Clay Sci.* **2011**, 51, 177-181.

Zhu, J.; Morgan, A.B.; Lamelas, F.J.; Wilkie, C.A. Fire properties of polystyrene-clay nanocomposites. *Chem. Mater.* **2001**, 13, 3774-3780.

Zhu, Y.; Xu, Y.; Tong, L.; Xu, Z.; Fang, Z. Influence of polarity on the preferential intercalation behavior of clay in immischible polypropylene/polystyrene blend. *J. Appl. Polym. Sci.* **2008**, 110, 3130-3139.

CHAPTER 3: Detection and Quantification of Montmorillonite Nanoclay in Water-Ethanol Solutions by Graphite Furnace Atomic Absorption Spectrometry

A paper was published based on this chapter:

Xia, Y.; Rubino, M.; Auras, R. 2013. Detection and quantification of montmorillonite nanoclay in water-ethanol solutions by graphite furnace atomic absorption spectrometry. *Food Additives and Contaminants* 30: 2177-2183.

3.1 Introduction

In the past decades, engineered nanomaterials (ENMs) with at least one dimension within the nanoscale (1-100 nm) have been widely used in the manufacture of nanocomposites providing improved performance and properties [Polyakova & Hubert 2001; Han & Yu 2006; Bal & Samal 2007; Pereira de Abreu *et al.* 2007; Duncan 2011]. The market share for nanocomposites was US$920 million in 2011 and is estimated to grow to over US$2.4 billion by 2016 [BCC Research 2012]. As the use of nanocomposites has expanded, there are increasing concerns regarding the transport and fate of ENMs and the associated environmental impacts and health risks due to the exposure to ENMs [Colvin 2003; Farre *et al.* 2011; Yokel & MacPhail 2011; Badireddy *et al.* 2012; Lowry *et al.* 2012]. However, information about the exposure to ENMs is not sufficient and the effects of ENMs on biological systems and environments are not well understood [Thomas *et al.* 2006; Savolainen *et al.* 2010; EFSA 2011]. The U.S. National Research Council has recently addressed the urgency of understanding the risks associated with ENMs, with emphasis on the transport and fate of nanoparticles within different biological systems and environments [NRC 2012].

As one of the ENMs, nanoclays, such as organo-modified montmorillonite (O-MMT), are extensively used due to their efficiency and low cost, and account for about half of the nanocomposite market [BCC Research 2012]. The market for polymer-clay nanocomposites reached over 450 million kg (1 billion lbs) in 2009, with applications in different fields such as packaging, automotive, coatings, and construction [Patel *et al.* 2006]. MMT belongs to the smectite family, also known as 2:1 phillosilicates. The crystal structure of MMTconsists of two silica tetrahedral sheets fused to an edge-shared alumina octahedral sheet [Sinha Ray & Okamoto 2003]. MMT is usually in the form of tactoids, which are the stacks of parallel clay platelets with

about 1 nm interlayer space. The interlayer space contains exchangeable cations (*e.g.*, Na^+ or K^+) that can be replaced by organic cationic surfactants (*e.g.*, alkylammonium or alkylphosphonium cations) to improve the compatibility of the nanoclay with the polymer [De A. Prado *et al.* 2005].

The addition of O-MMT into the polymers has been reported with improved mechanical and barrier properties [Sinha Ray & Okamoto 2003; Choudalakis & Gotsis 2009], which enables the potential use of polymer-clay nanocomposites in food packaging applications, such as bottles for beer and carbonated drinks, and wrap films for a variety of foods [Akbari *et al.* 2006; Chaudhry *et al.* 2008; Silvestre *et al.* 2011]. Recently, more attention has been placed on the transport of nanoclays within different systems especially in food packaging systems, due to the potential release of nanoclays into the packaged foods which may adversely affect human health [Chaudhry *et al.* 2008; Mauricio-Iglesias *et al.* 2010; Diaz *et al.* 2013]. A major research challenge in this area is the lack of methodologies for tracking and detecting nanoparticles in different environments [Tiede *et al.* 2008; EFSA 2009; Stamm *et al.* 2012]. Current approaches for tracking and detecting nanoclay particles in liquid systems are focused on elemental analysis by mainly using atomic absorption spectrometry (AAS) and inductively coupled plasma mass spectroscopy (ICP-MS) [Avella *et al.* 2005; Schmidt *et al.* 2009; Mauricio-Iglesias *et al.* 2010; Schmidt *et al.* 2011]. Acid digestion procedures on nanoclay particles are applied to obtain homogenous solutions, as required by these techniques [EPA 1996; EPA 2007]. However, the digestion procedures are time consuming and inconvenient and introduce issues with the clay concentration, which affects the suitability for real-time transport studies. On the other hand, in some transport studies of nanoclays, only the elemental concentrations have been reported. Little attention has been focused on nanoclay quantification and characteristics in different media, although the understanding of these factors is essential to evaluate the potential risks of

nanoclays [Chau *et al.* 2007; Linsinger *et al.* 2013]. Thus, methodologies for the rapid and reliable detection of nanoclay in different media are highly sought to properly understand the transport of nanoclays within different systems and to understand their behavior in solution.

The overall aim of this work was to develop a methodology for the rapid and reliable measurement of O-MMT concentration in solution by correlation with the Si and Al concentrations. Water and ethanol were selected because both solvents and their combinations are commonly used to simulate a variety of food systems [FDA 2007]. First, a graphite furnace atomic absorption spectrometry (GFAAS) method was adopted for the direct multi-elemental analysis of O-MMT in suspensions without prior acid digestion. Second, the stability of O-MMT dispersed in water and/or ethanol as a function of time was evaluated. Finally, a correlation was established between the amounts of Si and Al and the O-MMT concentration in solution. The correlation was validated with elemental composition results for the O-MMT obtained by X-ray fluorescence (XRF) spectrometry.

3.2 Materials and methods

3.2.1 Characterization of O-MMT

The organo-modified nanoclay (Nanomer® I.44P) was obtained from Nanocor (Hoffman Estates, IL, USA). It contains about 65 % montmorillonite (MMT) and 35 % surfactant (dimethyl dialkyl (C14-C18) amine), and is herein referred to as O-MMT. The particle size of O-MMT, as demonstrated by the supplier, was mainly below 10 μm. The specific surface area (SSA) of the O-MMT was measured (in duplicate) with an ASAP 2020 accelerated surface area and porosity analyzer (Micromeritics Instrument Corporation, Atlanta, GA, USA). Before analysis, the O-MMT powder (~0.3 g) was degassed at 160 °C under a vacuum of 100 mTorr

(13.33 Pa) for 16 h to remove any absorbed water. The SSA was obtained by applying the Brunauer-Emmett-Teller (BET) sorption isotherm equation [Allen 2004] to the measured adsorption of nitrogen gas (N_2) at 77 K (-196 °C).

The zeta potential of O-MMT in various water-ethanol solutions, as an indication of the surface charge, was measured by using a Malvern Zetasizer (model Nano-ZS, Malvern Instruments Inc., Houston, TX, USA) and Smoluchowski's model [Marras *et al.* 2007]. Nanoclay suspensions of 200 mg L^{-1} were prepared in three different solvent systems (water, ethanol, and water:ethanol [1:1]) and stirred for 24 h at 23 °C. All the measurements were conducted at 25 ± 0.1 °C with at least 10 runs on each sample suspension.

The elemental composition of O-MMT was measured by an X-ray fluorescence spectrometry (XRF) method. The test was done according to a previously established procedure [Deering *et al.* 2008]. Briefly, 1 g of O-MMT powder (pre-dried) was combined with 9 g of lithium tetraborate ($Li_2B_4O_7$) and 0.5 g of ammonium nitrate (NH_4NO_3, used as oxidizer) in a platinum crucible and placed on an orbital mixing stage and fused at 1000 °C for 20-30 min. The melt was poured into a platinum mold to form a glass disk and the disk was analyzed by XRF using a Bruker S-4 system (Bruker Co., Billerica, MA, USA). XRF major-element analysis was performed using a fundamental parameter data reduction method and Bruker Spectra Plus software; O-MMT samples were tested in triplicate.

3.2.2 Preparation of O-MMT suspensions

A stock suspension of 200 mg L^{-1} was prepared by dispersing 40 mg of O-MMT in 200 mL of ethanol (100%) and sonicating (VWR ultrasonic cleaner water bath, Model 75HT, 35 kHz, VWR International LLC., Radnor, PA, USA) the mixture in a 250 mL beaker for 30 min before

further dilution with water or ethanol. Sonication helps to break down the O-MMT clusters and achieve a better dispersion [Herrera-Alonso *et al.* 2009; Santos *et al.* 2011].

3.2.3 Graphite furnace atomic absorption spectrometry (GFAAS)

Elemental analysis of O-MMT was conducted with a Hitachi Z-9000 simultaneous multi-element atomic absorption spectrometer (Hitachi High-Technologies Co., Tokyo, Japan) equipped with a HGA-700 atomizer and an autosampler system. A graphite tube–type cuvette was used as the atomization furnace with a temperature program as follows: (a) drying at 120 °C for 30 s; (b) converting to ash from 710 to 990 °C for 30 s; (c) atomizing at 3000 °C for 10 s; and (d) cleaning at 3000 °C for 3 s. Detection of Si and Al was performed by injecting 20 µL sample solution into the graphite furnace and recording the absorbance at 251.6 and 309.3 nm, respectively, with hollow cathode lamps (Hamamatsu Photonics Corp., Japan) set at 15 mA.

Si and Al standard solutions of 1000 mg L^{-1} (PerkinElmer Inc., MA, USA), made with $(NH_4)_2SiF_6$ and $Al(NO_3)_3$ as solutes, were diluted with deionized water in the 50 mL PP centrifuge tube and used to establish the external calibration curves. A good linear range was achieved for the Si standard solution between 0.03 and 0.5 mg L^{-1} ($R^2 = 0.999$) and for the Al standard solution between 0.012 and 0.2 mg L^{-1} ($R^2 = 0.998$). The lower limits of quantification (LOQ) of the method (based on a signal-to-noise ratio of 10) were 0.03 mg L^{-1} for Si and 0.01 mg L^{-1} for Al. The calibration curves generated from the Si and Al standards were used to determine the amount of Si and Al in nanoclay suspensions. The LOQ can be further improved by using the concentration function of the instrument. This was carried out by repeat injections (up to 25 times) of the sample via the auto sampler and execution via the drying stage. For instance, LOQ of 8 µg L^{-1} for Si and 3 µg L^{-1} for Al were achieved by injecting the sample 6

times to give one absorbance data point.

3.2.4 Stability of the dispersion of O-MMT in solution

To study the stability of O-MMT dispersed in different water:ethanol solvent systems, the stock suspension of O-MMT was diluted to 5 mg L^{-1} with water:ethanol at 5 different vol/vol ratios (1:0, 2:1, 1:1, 1:2 and 0:1). The final suspensions were mechanically agitated with a vortex mixer (Scientific Industries, Inc., NY, USA) for 30 s prior to GFAAS measurements to maintain the homogeneous dispersion of the nanoclay. To indicate the dispersion stability of O-MMT, the Si and Al absorbance of the O-MMT suspensions (conducted in triplicate) was recorded every 2 min up to 36 min.

The effect of the surfactant on O-MMT dispersion was also evaluated. The dimethyl dialkyl (C14-C18) amine (Sigma-Aldrich, St. Louis, MO, USA) was added to the stock suspension of O-MMT, which was further diluted to 5 mg L^{-1} with deionized water to achieve final suspensions with surfactant:O-MMT ratios of 1:1 and 5:1. Si and Al absorbance of the suspensions (conducted in triplicate) was recorded every 2 min up to 36 min.

3.3 Results and discussion

3.3.1 Properties of O-MMT

The zeta potential of O-MMT was 38.2 ± 1.8 mV in water (pH = 7), 11.6 ± 0.8 mV in the 1:1 water-ethanol mixture, and -23.6 ± 0.8 mV in ethanol. The measured O-MMT surface area was 12.4 $m^2 g^{-1}$. The theoretical SSA of fully exfoliated O-MMT nanoclay has been estimated as 750 $m^2 g^{-1}$ [Nikolaidis *et al.* 2011]. A measured SSA may be affected by the aggregation state of the clay particles and type of methods used. The BET sorption isotherm equation gives the

external surface area on the basis of N_2 adsorption. Therefore, the measured SSA value may be far less than the theoretical one. Si and Al contents within the nanoclay, based on the XRF analysis, were 20.14 ± 0.06 % and 7.70 ± 0.02 % wt/wt, respectively, with a Si/Al ratio of 2.58 ± 0.01.

3.3.2 Dispersion of O-MMT in different solvent systems

Measurement of O-MMT concentration in a suspended solvent system requires a homogenous and stable dispersion of the O-MMT within the time frame the sample is analyzed to guarantee that the real concentration of O-MMT in solution is measured. Dispersion of O-MMT can be affected by the interaction between the O-MMT and the solvent system. Since organo-modification of MMT changes the surface from hydrophilic to organophilic, a poor dispersion of O-MMT nanoparticles would be expected in water. Aggregation behavior of MMT in water after organo-modification along with an increase in zeta potential from negative toward positive has been reported [Marras *et al.* 2007; Mahesh *et al.* 2011]. On the other hand, a better dispersion of O-MMT particles in ethanol would be expected due to the relatively good affinity between the organic solvent and organic surfactant, as previously reported by the adsorption of ethanol into the interlayer space and the swelling of nanoclay particles [Burgentzle *et al.* 2004].

Si and Al absorbance of 5 mg L^{-1} nanoclay suspensions made with different water/ethanol ratios was recorded from up to 18 injections (over about 36 min) and data are shown in Figure 3.1. Maximum absorbance values were obtained for both Si and Al in suspensions with pure ethanol and with a water/ethanol ratio of 1:2, and no obvious decreasing trend was observed for the absorbance with time (slope β = zero; $P > 0.05$). As water content in the suspension increased (water/ethanol ratios of 1:1 and 2:1), a decreasing trend for absorbance was observed, indicating

an ongoing precipitation of O-MMT particles as a function of time. In pure water, the Si and Al absorbance reached minimum values, which were about 1/5 of those in pure ethanol. Generally, precipitation of nanoclay particles happens both in ethanol and water, which could be explained by the solubility parameter of the solvent [Ho & Glinka 2003]. However, a more stable dispersion of O-MMT particles was achieved in ethanol than in water within the short period of time studied as indicated in Figure 3.1. In addition, sonication and mechanical agitation helped to stabilize the dispersion of O-MMT particles and slow down their precipitation.

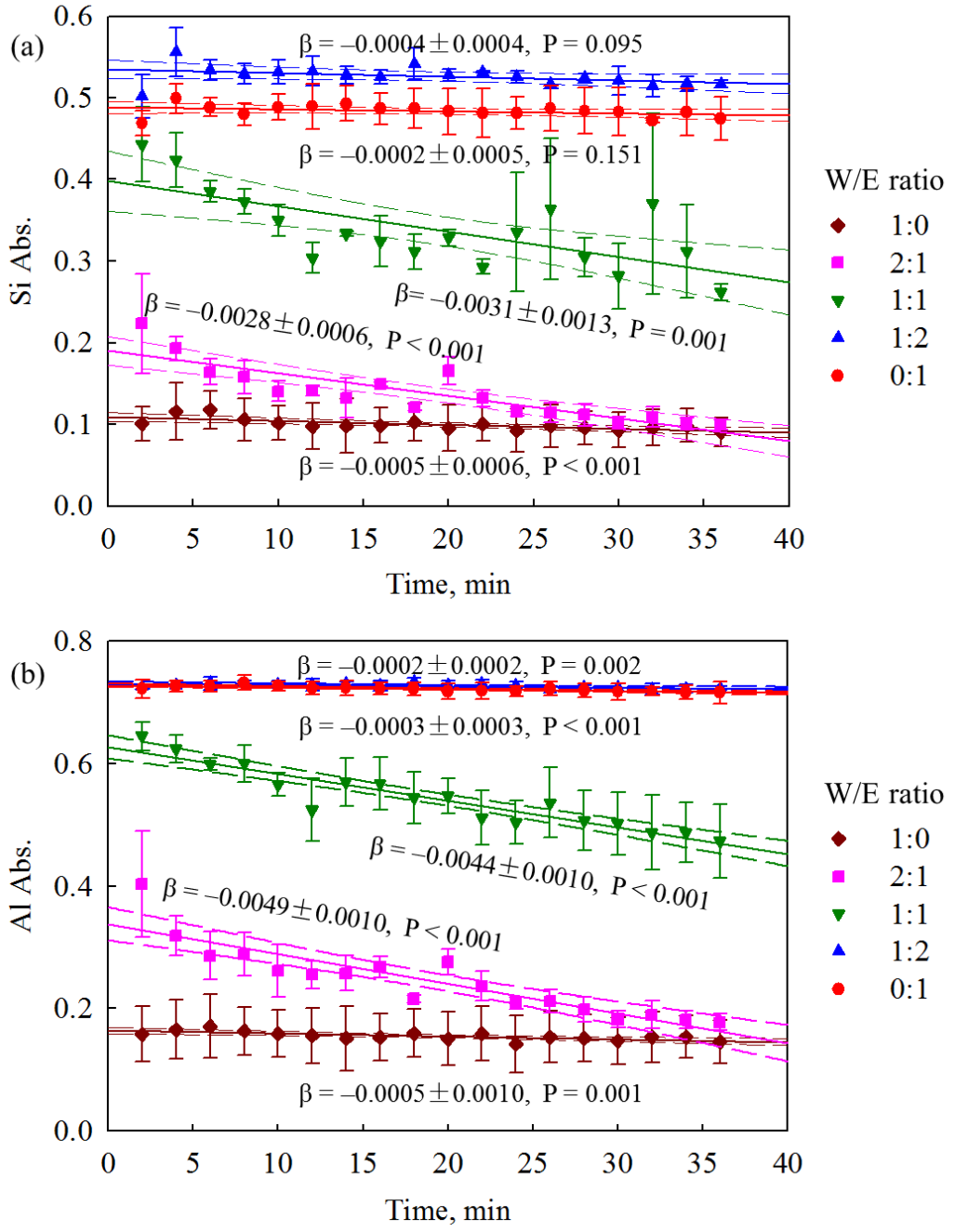

Figure 3.1 Absorbance of (a) Si and (b) Al as a function of time in nanoclay suspension (5 mg L^{-1}) at water/ethanol ratios of 1:0, 2:1, 1:1, 1:2 and 0:1. Linear regression (solid line) was performed with the 95 % confidence interval (CI) band (dashed line). Slopes of each regression line are also reported with the 95 % CI and P value.

The dispersion of O-MMT in water could be improved by adding a surfactant (dimethyl dialkyl amine) that has bi-affinity to water and the nanoclay. Figure 3.2 shows the Si and Al absorbance of nanoclay suspensions (5 mg L^{-1}) with added surfactant (5 and 25 mg L^{-1} surfactant) and without surfactant (0 mg L^{-1}, control) in water. Compared with the control, the absorbance was much higher for the sample with a surfactant/nanoclay ratio of 1:1, indicating that a large number of O-MMT particles were dispersed. The absorbance was even higher at the surfactant/nanoclay ratio of 5:1, and the slope β was reduced. However, the absorbance of the suspension in the 5:1 mixture was lower than that in pure ethanol (about 10 % less) and the decreasing trend of absorbance was more obvious compared with that in pure ethanol (Figure 3.1) as indicated by the slope β for the two solutions. The addition of surfactant significantly improved the dispersion of O-MMT in water although not to the extent achieved for the dispersion of O-MMT in ethanol.

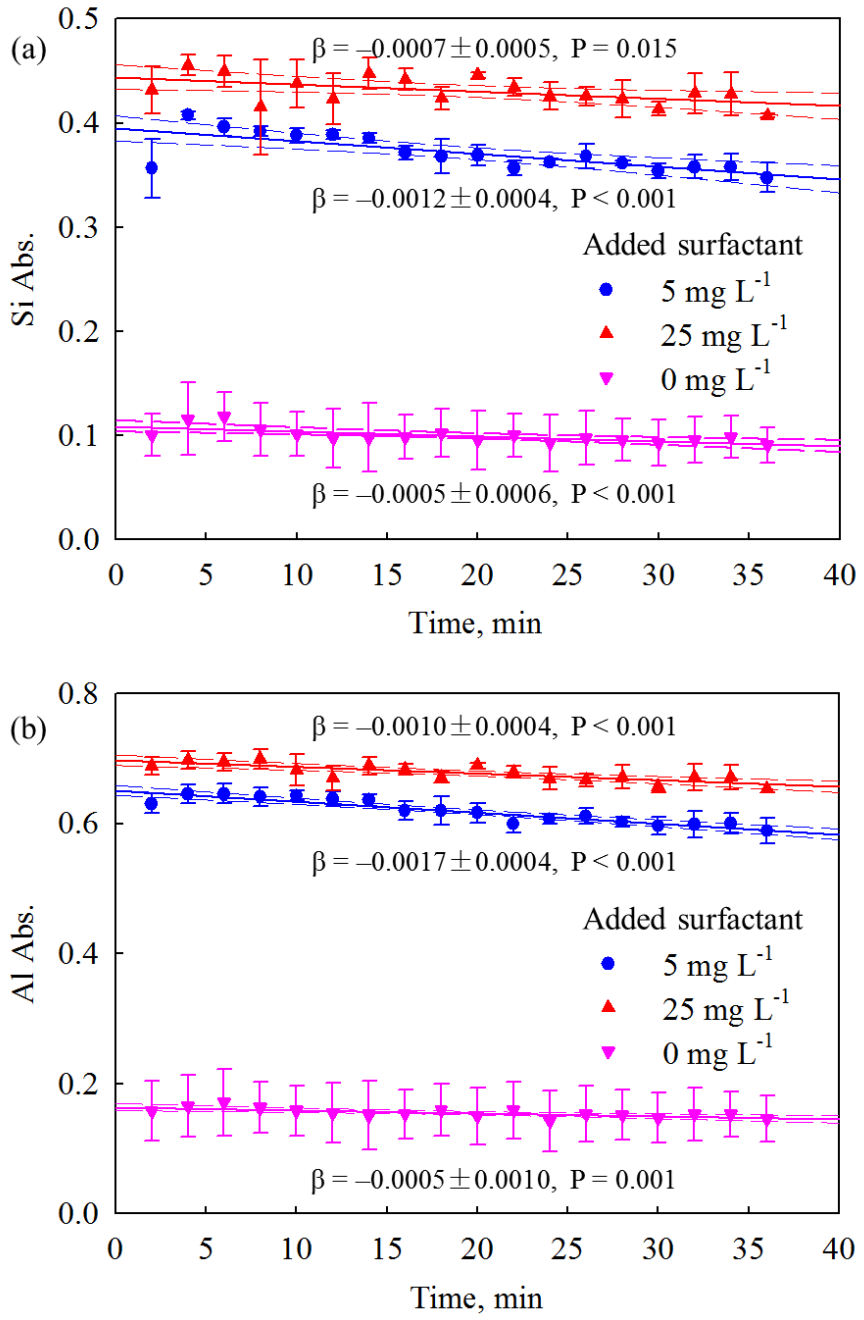

Figure 3.2 Absorbance of (a) Si and (b) Al as a function of time in nanoclay suspension (5 mg L^{-1} in water) with added surfactant of 5, 25 and 0 mg L^{-1}, corresponding to surfactant/nanoclay ratios of 1:1, 5:1 and 0:1 (control). Linear regression (solid line) was performed with the 95 % CI band (dashed line). The slope of each regression line is also given with the 95 % CI and P value.

Dissolution of clay minerals usually happens in aqueous systems. The preferential release of Si compared with Al from montmorillonite occurs due to the abundance of Si at the clay surface and the higher solubility of Si in water [Huang & Keller 1971; Rozalen *et al.* 2008; Sondi *et al.* 2008]. Figure 3.3 shows the change in Si/Al ratios observed over time in various water-ethanol systems. The Si/Al ratio increased with an increase in the water content of the system, which may be attributed to the uneven release of Si and Al from the O-MMT into water along with the precipitation of O-MMT. Therefore, O-MMT quantification in water on the basis of elemental analysis may not give reliable results due to the large dispersion of values and the preferential release of Si. Figure 3.3 confirms that a water/ethanol ratio of 1:2 and pure ethanol can be used to quantify O-MMT in solution, which would be valuable for measuring O-MMT during mass transport experiments such as migration from polymer nanocomposites.

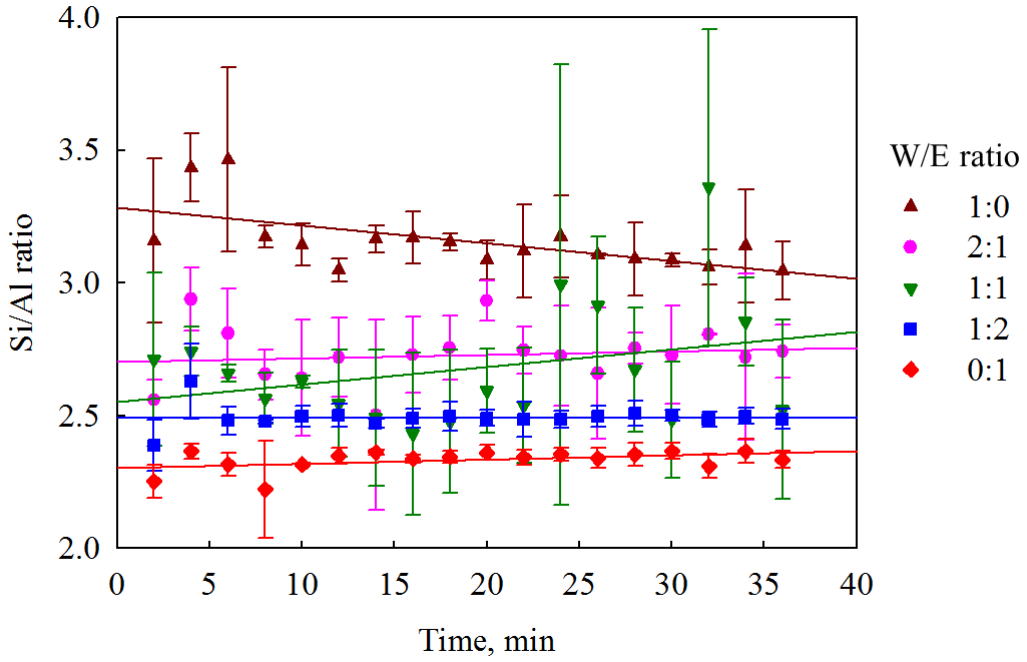

Figure 3.3 Change in Si/Al ratio over time in nanoclay suspension at water/ethanol ratios of 1:0, 2:1, 1:1, 1:2 and 0:1. Solid lines are experimental linear regressions to demonstrate the trends.

3.3.3 Determination of Si and Al content

Although O-MMT concentration cannot be directly measured by the GFAAS equipment or other instruments, the elements of this clay can be identified and quantified in ethanol. Therefore, the elemental (Si and Al) concentrations could be correlated with the O-MMT concentration in solution. A series of O-MMT suspensions with a concentration range of 0.5 to 2 mg L^{-1} were prepared and linear regressions of Si and Al concentrations vs O-MMT concentrations were obtained (Figure 3.4). The slope of each regression line gives the Si and Al contents within the O-MMT, which are 22 ± 1.1 % and 9.3 ± 0.5 % wt/wt, respectively, with a Si/Al ratio of 2.4 ± 0.1. These values are aligned with the values obtained by XRF (Si = 20.14 ± 0.06 %, Al =7.80 ± 0.02 % wt/wt, and a Si/Al ratio of 2.58 ± 0.01). The deviation between the results from two methods might be due to the difference in sample preparation (liquid vs solid samples), the sample analysis method and/or the variation in surfactant content.

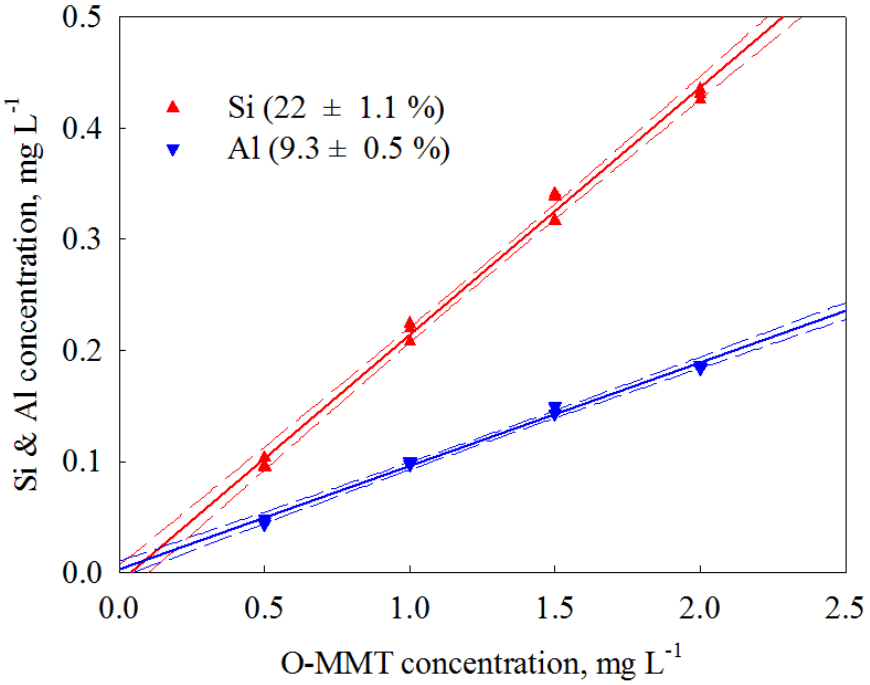

Figure 3.4 Correlations between Si and Al concentrations and O-MMT concentration. Linear regression was applied on Si and Al concentrations vs O-MMR concentration. Si and Al contents in the O-MMT, given by the slope of the regression line, were 22 ± 1.1 % and 9.3 ± 0.5 % wt/wt, respectively, at $P < 0.001$.

3.4 Conclusions

A GFAAS method was developed for a rapid measurement of O-MMT concentration in water-ethanol solutions without the need for acid digestion of the O-MMT sample. Since no digestion was applied, special precautions were taken to ensure the stability of the O-MMT in water-ethanol solutions to perform a reliable measurement on the nanoclay particles. The stabilized dispersion was affected by the interaction between the O-MMT and the water-ethanol solutions. A solution with an ethanol concentration higher than 70 % (vol/vol) was preferred to obtain a good dispersion of O-MMT in the sonicated solutions due to the good affinity between

the solution and the organophilic O-MMT. The dispersion in water was improved by the addition of an organic surfactant. The correlation between Si and Al concentrations and O-MMT concentrations in solution and the Si/Al ratio gave results in good agreement with the expected composition of O-MMT in solution, which was further validated by results obtained with an XRF method. Therefore, GFAAS can be used as a tool for determining the amount (*e.g.*, mass concentration) of O-MMT in suspension by measuring the concentration of Si and Al. This methodology can be applied to measure migration of O-MMT from nanocomposites in contact with food or food simulants. Further work is needed to understand the behavior of O-MMT and other nanoclays in different solvent systems, so that the application of this instrumental methodology can be expanded.

BIBLIOGRAPHY

BIBLIOGRAPHY

Akbari, Z.; Ghomashchi, T.; Aroujalian, A. 2006. Potential of nanotechnology for food packaging industry. Paper presented at ‘‘Nano Micro Technologies in the Food Health Food Industries’’ Conference organized by Institute of Nanotechnology, Oct. 25-26, 2006, Amsterdam.

Allen, T. Particle Size Measurement, Vol 1: Powder Sampling and Particle Size Measurement, 5th Edition, Chapman & Hall: London, UK, 2004.

Avella, M.; De Vlieger, J.J.; Errico, M.E.; Fischer, S.; Vacca, P.; Volpe, M.G. Biodegradable starch/clay nanocomposite films for food packaging applications. *Food Chem.* **2005**, 93, 467-474.

Badireddy, A.R.; Wiesner, M.R.; Liu, J. Detection, characterization, and abundance of engineered nanoparticles in complex waters by hyperspectral imagery with enhance darkfield microscopy. *Environ. Sci. Technol.* **2012**, 46, 10081-10088.

Bal, S.; Samal, S.S. Carbon nanotube reinforced polymer composites-A state of the art. *Bull. Materials Sci.* **2007**, 30, 379-386.

BCC Research. Global Markets for Nanocomposites, Nanoparticles, Nanoclays, and Nanotubes. BCC Research LLC, Wellesley, MA, USA, 2012. Available from: http://www.bccresearch.com/report/nanocomposites-global-markets-nan021e.html

Burgentzle, D.; Duchet, J.; Gerard, J.F.; Jupin, A.; Fillon, B. Solvent-based nanocomposite coatings I. Dispersion of organophilic montmorillonite in organic solvents. *J. Colloid Interf. Sci.* **2004**, 278, 26-39.

Chau, C.F.; Wu, S.H.; Yen, G.C. The development of regulation for food nanotechnology. *Trends Food Sci. Technol.* **2007**, 18, 269-280.

Chaudhry, Q.; Scotter, M.; Blackburn, J.; Ross, B.; Boxall, A.; Castle, L.; Aitken, R.; Watkins, R. Applications and implications of nanotechnologies for the food sector. *Food Addit. Contam.* **2008**, 25, 241-258.

Choudalakis, G.; Gotsis, A.D. Permeability of polymer/clay nanocomposites: A review. *Eur. Polym. J.* **2009**, 45, 967-984.

Colvin, V.L. The potential environmental impact of engineered nanomaterials. *Nature Biotech.* **2003**, 21, 1166-1170.

De A. Prado, L.A.S.; Karthikeyan, C.S.; Schulte, K.; Nunes, S.P.; De Torriani, I.L. Organic modification of layered silicates: structural and thermal charaterizations. *J. Non-cryst. Solids.* **2005**, 351, 970-975.

Deering, C.D.; Cole, J.W.; Vogel, T.A. A rhyolite compositional continuum governed by lower crustal source conditions in the taupo volcanic zone, New Zealand. *J. Petrology.* **2008**, 49, 2245-2276.

Diaz, C.A.; Xia, Y.; Rubino, M.; Auras, R.; Jayaraman, K.; Hotchkiss, J. Fluorescent labeling and tracking of nanoclay. *Nanoscale* **2013**, 5, 164-168.

Duncan, T.V.; Applications of nanotechnology in food packaging and food safety: Barrier materials, antimicrobials and sensors. *J. Colloid Interf. Sci.* **2011**, 363, 1-24.

[EFSA] European Food Safety Authority. The Potential Risks Arising from Nanoscience and Nanotechnologies on Food and Feed Safety. *EFSA J.* **2009**, 958, 1-39. Available from: http://www.efsa.europa.eu/en/efsajournal/doc/958.pdf

[EFSA] European Food Safety Authority. Guidance on the risk assessment of the application of nanoscience and nanotechnologies in the food and feed chain. *EFSA J.* **2011**, 9, 2140. [36 pp]. Available from: http://www.efsa.europa.eu/en/efsajournal/doc/2140.pdf

[EPA] Environmental Protection Agency. Method 3052: Microwave assisted acid digestion of siliceous and organically based matrices, Revision 0. U.S. Environmental Protection Agency, 1996. Available from: http://www.epa.gov/osw/hazard/testmethods/sw846/pdfs/3052.pdf

[EPA] Environmental Protection Agency. Method 3051A: Microwave assisted acid digestion of sediments, sludges, soils, and oils, Revision 1. U.S. Environmental Protection Agency, 2007. Available from: http://www.epa.gov/osw/hazard/testmethods/sw846/pdfs/3051a.pdf

Farre, M.; Sanchis, J.; Barcelo, D. Analysis and assessment of the occurrence, the fate and the behavior of nanomaterials in the environment. *TrAC Trends Anal. Chem.* **2011**, 30, 517-527.

[FDA] Food and Drug Administration. 2007. Guidance for Industry: Preparation of Premarket Submissions for Food Contact Substances: Chemistry Recommendations. Available from: http://www.fda.gov/Food/GuidanceRegulation/GuidanceDocumentsRegulatoryInformation/IngredientsAdditivesGRASPackaging/ucm081818.htm#aii

Han, K.Q.; Yu, M.H. Study of the preparation and properties of UV-blocking fabrics of a PET/TiO2 nanocomposite prepared by in situ polycondensation. *J. Appl. Polym. Sci.* **2006**, 100, 1588-1593.

Herrera-Alonso, J.M.; Marand, E.; Little, J.C.; Cox, S.S. Transport properties in polyurethane/clay nanocomposites as barrier materials: Effect of processing conditions. *J. Membrane. Sci.* **2009**, 337, 208-214.

Ho, D.L.; Glinka, C.J. Effects of solvent solubility parameters on organoclay dispersions. *Chem. Mater.* **2003**, 15, 1309-1312.

Huang, W.H.; Keller, W.D. Dissolution of clay minerals in dilute organic acids at room temperature. *Am. Mineral.* **1971**, 56, 1082-1095.

Linsinger, T.P.; Chaudhry, Q.; Dehalu, V.; Delahaut, P.; Dudkiewicz, A.; Grombe, R.; von der Kammer, F.; Larsen, E.H.; Legros, S.; Loeschner, K.; Peters, R.; Ramsch, R.; Roebben, G.; Tiede, K.; Weigel, S. Validation of methods for the detection and quantification of engineered nanoparticles in food. *Food Chem.* **2013**, 138, 1959-1966.

Lowry, G.V.; Gregory, K.B.; Apte, S.C.; Lead, J.R. Transformations of nanomaterials in the environment. *Environ. Sci. Technol.* **2012**, 46, 6893-6899.

Mahesh, K.R.V.; Murthy, H.N.N.; Kumaraswamy, B.E.; Raghavendra, N.; Sridhar, R.; Krishna, M.; Pattar, N.; Pal, R.; Sherigara, B.S. Synthesis and characterization of organomodified Na-MMT using cation and anion surfactants. *Front. Chem. China.* **2011**, 6, 153-158.

Marras, S.I.; Tsimpliaraki, A.; Zuburtikudis, I.; Panayiotou, C. Thermal and colloidal behavior of amine-treated clays: the role of amphiphilic organic cation concentration. *Colloid Interf. Sci.* **2007**, 315, 520-527.

Mauricio-Iglesias, M.; Peyron, S.; Guillard, V.; Gontard, N. Wheat gluten nanocomposite films as food-contact materials: migration tests and impact of a novel food stabilization technology (high pressure). *J. Appl. Polym. Sci.* **2010**, 116, 2526-2535.

Nikolaidis, A.K.; Achilias, D.S.; Karayannidis, G.P. Synthesis and characterization of PMMA/organomodified montmorillonite nanocomposites prepared by in situ bulk polymerization. *Ind. Eng. Chem. Res.* **2011**, 50, 571-579.

[NRC] National Research Council. A Research Strategy for Environmental, Health, and Safety Aspects of Engineered Nanomaterials. National Academy Press: Washington DC, USA, 2012. Available from: http://www.nap.edu/catalog.php?record_id=13347

Patel, H.A.; Somani, R.S.; Bajaj, H.C.; Jasra, R.V. Nanoclays for polymer nanocomposites, paints, inks, greases and cosmetics formulations, drug delivery vehicle and waste water treatment. *Bull. Mater. Sci.* **2006**, 29, 133-145.

Pereira de Abreu, D.A.; Losada, P.P.; Angulo, I.; Cruz, J.M. Development of new polyolefin films with nanoclays for application in food packaging. *Eur. Polym. J.* **2007**, 43, 2229-2243.

Polyakova, I.G.; Hubert, T. Thermal stability of TiN thin films investigated by DTG/DTA. *Surf. Coatings Technol.* **2001**, 141, 55-61.

Rozalen, M.L.; Huertas, F.J.; Brady, P.V.; Cama, J.; Garcia-Palma, S.; Linares, J. Experimental study of the effect of pH on the kinetics of montmorillonite dissolution at 25 °C. *Geoch. et Cosmoch. Acta* **2008**, 72, 4224-4253.

Santos, K.S.; Bischoff, E.; Liberman, S.A.; Oviedo, M.A.S.; Mauler, R.S. The effects of ultrasound on organoclay dispersion in the PP matrix. *Ultrason. Sonochem.* **2011**, 18, 997-1001.

Savolainen, K.; Alenius, H.; Norppa, H.; Pylkkanen, L.; Tuomi, T.; Kasper, G. Risk assessment of engineered nanomaterials and nanotechnologies-a review. *Toxicology* **2010**, 269, 92-104.

Schmidt, B.; Petersen, J.H.; Bender Koch, C.; Plackett, D.; Johansen, N.R.; Katiyar, V.; Larsen, E.H. Combining asymmetrical flow field-flow fractionation with light-scattering and inductively coupled plasma mass spectrometric detection for characterization of nanoclay used in biopolymer nanocomposites. *Food Addit. Contam.* **2009**, 26, 1619-1627.

Schmidt, B.; Katiyar, V.; Plackett, D.; Larsen, E.H.; Gerds, N.; Koch, C.B.; Petersen, J.H. Migration of nano-sized layered double hydroxide platelets from polylactide nanocomposite films. *Food Addit. Contam.* **2011**, 28, 956-966.

Silvestre, C.; Duraccio, D.; Cimmino, S. Food packaging based on polymer nanomaterials. *Prog. Polym. Sci.* **2011**, 36, 1766-1782.

Sinha Ray, S.; Okamoto, M. Polymer/layered silicate nanocomposites: a review from preparation to processing. *Prog. Polym. Sci.* **2003**, 28, 1539-1641.

Sondi, I.; Tomasie, V.; Filipovie-Vincekovie, N. Release of silicon and aluminum from montmorrilonite surfaces in aqueous systems. *Croat. Chem. Acta* **2008**, 81, 623-629.

Stamm, H.; Gibson, N.; Anklam, E. Detection of nanomaterials in food and consumer products: bridging the gap from legislation to enforcement. *Food Addit. Contam.* **2012**, 29, 1175-1182.

Thomas, T.; Thomas, K.; Sadrieh, N.; Savage, N.; Adair, P.; Bronaugh, R. Research strategies for safety evaluation of nanomaterials, Part VII: Evaluating consumer exposures to nanoscale materials. *Toxicol. Sci.* **2006**, 91, 14-19.

Tiede, K.; Boxall, A.B.; Tear, S.P.; Lewis, J.; David, H.; Hassellov, M. Detection and characterization of engineered nanoparticles in food and the environment. *Food Addit. Contam.* **2008**, 25, 795-821.

Yokel, R.A.; MacPhail, R.C. Engineered nanomaterials: exposures, hazards, and risk prevention. *J. Occup. Med. Toxicol.* **2011**, 6, 7-34.

CHAPTER 4: LC-MS/MS Assay for the Determination of Surfactants Released from Montmorillonite Nanoclay into Food Simulants

A paper was submitted based on this chapter:

Xia, Y.; Rubino, M.; Auras, R. 2014. LC-MS/MS assay for the determination of surfactants released from montmorillonite nanoclay into food simulants. Manuscript submitted.

4.1 Introduction

Nanoclays, including clays and silicates of nano-size dimensions, are extensively used as engineered nanoparticles (ENPs) in polymer nanocomposites. The addition of nanoclays at small loadings can significantly improve the performance of polymer materials, thereby expanding their applications in consumer goods. Montmorillonite (MMT) is a nanoclay obtained from naturally occurring layered silicate minerals with a crystal structure consisting of two silica tetrahedral sheets fused to an edge-shared alumina octahedral sheet [Sinha Ray & Okamoto 2003]. Each MMT layer has a thickness of about 1 nm and a diameter of 20-200 nm [Ajayan *et al.* 2003]. The clay layers are usually parallel stacked to form tactoids with about 1 nm interlayer space (or clay gallery) containing exchangeable cations (*e.g.*, Na^+ or K^+). MMT can be organically modified (O-MMT) by replacing the exchangeable cations with organic cationic surfactants (*e.g.*, alkylammonium cations), which improves the compatibility of the nanoclay with the polymer [De A Prado *et al*. 2005].

Nanocomposites with O-MMT as the nanofiller account for over half of total nanocomposite consumption (estimated at 225,000 metric tons in 2014), and the primary application is in the packaging industry [Patel *et al*. 2006; BCC Research 2014]. There is increasing concern about the potential release of nanoclay particles and surfactants from nanocomposites, either into foods when used as food packaging materials in direct contact with food or into the surrounding environment [Chaudhry *et al*. 2008; Mauricio-Iglesias *et al*. 2010; Gottschalk & Nowack 2011; Diaz *et al*. 2013; Szakal *et al*. 2014]. Although a few studies have addressed the release of nanoclays from nanocomposites, to the best of the authors' knowledge, no attention has been given to the release of surfactants. Some surfactants have been shown to be toxic to ecosystems, animals and humans [Lewis 1991; Talmage 1994; Ying 2006]. Therefore, it

is critical to understand the release of surfactants from nanoclays under different conditions before further investigation of their transport within different environmental or biological systems takes place.

The surfactant used as the organo-modifier of MMT nanoclay is usually not a single compound but a mixture of different components with similar structures. For example, one type of the most commonly used surfactants is quaternary alkylammonium salt with varied alkyl chain lengths. The instrumental method used for the measurement of surfactant should enable the separation of different components in an efficient manner and the subsequent detection of each component. Meanwhile, the measurement should be relatively rapid, which is critical for the real-time transport study. There are some studies on the analysis of surfactants by liquid chromatography [Ferrer & Furlong 2001; Nishikawa *et al.* 2003; Li & Brownawell 2009]. However, separation of various components in the quaternary alkylammonium surfactants was difficult and the analysis time was long in order to achieve a good separation, which will make the method difficult to use for migration studies. In addition, the analysis of surfactant was usually from environmental samples (sewer water, soil, etc.), not from food or food simulants.

The objectives of this study were to (*1*) develop a liquid chromatography-tandem mass spectrometry (LC-MS/MS) method to identify and quantify surfactants in solution; (*2*) apply the method to measure and describe the release of surfactants from O-MMT into solvents used as food simulants; and (*3*) investigate the effect of different factors (temperature, sonication and simulant type) on surfactant release.

4.2 Materials and methods

4.2.1 Nanoclays and surfactants

Two types of O-MMT nanoclay were used in this study. Nanomer® I.44P (herein referred

to as I44P clay) was obtained from Nanocor (Aberdeen, MS, USA) containing 65 wt% MMT and 35 wt% surfactant, and it is normally included in nanocomposites with polyolefins such as polyethylene (PE) and polypropylene (PP). Cloisite® 93A (herein referred to as Cloisite clay) was obtained from Southern Clay Products (Gonzales, TX, USA) containing 60 wt% MMT and 40 wt% surfactant, and it is commonly used in nanocomposites with nylon. The surfactant for I44P clay (dimethyl dihydrogenated tallow amine or Arquad® 2HT-75, around 75 wt% purity) and the surfactant for Cloisite clay (methyl dihydrogenated tallow amine or Armeen® M2HT, around 90 wt% purity) were obtained from AkzoNobel (IL, USA). According to the supplier and the MSDS, both surfactants consist of two alkyl chains (hydrogenated tallow) ranging from 12 to 18 carbons with mainly C_{16} and C_{18} (>96 wt%). Therefore, only the three main components of each surfactant were considered for analysis, designated as $C_{16}C_{16}$-Arquad/Armeen, $C_{16}C_{18}$-Arquad or Armeen and $C_{18}C_{18}$-Arquad or Armeen.

4.2.2 Thermogravimetric analysis

The heat stability of the surfactant within each nanoclay was characterized by thermogravimetric analysis (TGA) with a Q-50 thermogravimetric analyzer (TA Instruments Inc., New Castle, DE, USA). A heating cycle from room temperature to 700 °C at a ramp rate of 10 °C min^{-1} was used. The experiment was conducted in a high-purity flowing nitrogen atmosphere (70 cm^3 min^{-1}) to avoid oxidation, and the weight loss was recorded.

4.2.3 Release experiments

The release of surfactant from O-MMT into food simulants was evaluated as a function of temperature, sonication or simulant type and detected by using an LC-MS/MS method. The food simulants used included ethanol (100 %), 50 % ethanol (ethanol/water, 1:1) and water. Both

solvents and combinations are commonly used to simulate a wide variety of food systems [FDA 2007].

For the first test to assess the effect of temperature, nanoclay suspensions (60 mg L^{-1}, containing about 21 mg L^{-1} surfactant for I44P clay and 24 mg L^{-1} surfactant for Cloisite clay) were prepared by carefully weighing 2.4 mg of I44P or Cloisite clay into amber glass vials (25 × 95 mm) and adding 40 mL ethanol into each vial. For each nanoclay type, a total of 9 vials were prepared, which were then divided into three groups (3 vials per group) and one group of vials was held in an oven set at 22, 40 or 70 °C for up to 24 h. For another temperature test, Cloisite clay was heated in a Q-50 thermogravimetric analyzer at 240 °C for 7 min, and then dispersed in ethanol at a concentration of 60 mg L^{-1}. The suspension was transferred to 3 vials (40 mL per vial), and the vials were stored at 40 °C for up to 24 h.

To assess the effect of sonication on the release of surfactant, nanoclay suspensions were prepared in ethanol (60 mg L^{-1}) as described above. For each nanoclay type, 6 vials were prepared: 3 vials were sonicated (Model FS30 ultrasonic cleaner, 35 kHz, Fisher Scientific Co., Pittsburg, PA, USA) at 40 °C for up to 6 h, and the remaining 3 vials (control) were also exposed to 40 °C but without sonication.

To evaluate the effect of simulant type, nanoclay suspensions in ethanol, 50 % ethanol or water (60 mg L^{-1}) were prepared in amber glass vials, in triplicate, as described above. All vials were held at 40 °C for up to 24 h.

4.2.4 LC-MS/MS analysis

Measurement of the surfactant in solution was carried out by an LC-MS/MS method developed for this purpose. A Waters Quattro micro mass spectrometer (Waters Co., MA, USA)

coupled to a Shimadzu LC-20AD HPLC system (Shimadzu Scientific Instruments, MO, USA) and a SIL 5000 auto-sampler was used. The system was operated by using Waters MassLynx 4.0 software.

Separation of different components of the surfactant with the HPLC was achieved on a Waters Symmetry C18 column (3.5 μm, 2.1 × 100 mm) with a Symmetry guard column operated at 30 °C. A gradient elution was performed at a flow rate of 0.2 mL min^{-1} for 15 min with a binary mobile phase consisting of (A) 0.1 % formic acid in water and (B) methanol. The gradient program was set as follows: 0-2 min, 20 % B; 2-3 min, 20-80 % B; 3-5 min, 80-95 % B; 5-13 min, 95 % B; and 13-15 min, 20 % B.

Composition analysis of each surfactant was conducted by setting the MS detector at electrospray ionization in positive mode (ESI^+) and single ion recording (SIR). Calculation of the contents of three main components ($C_{16}C_{16}$, $C_{16}C_{18}$ and $C_{18}C_{18}$) was based on their peak areas in a standard solution. The capillary voltage, extractor voltage and radio frequency (Rf) lens were set at 3.5 kV, 3 V and 0, respectively. The cone gas (nitrogen) and desolvation gas (argon) were set at 30 L h^{-1} and 600 L h^{-1}, respectively. A cone voltage of 60 V, a source temperature of 100 °C and a desolvation temperature of 350 °C were used.

Detection of the three main components of each surfactant were carried out by setting the MS detector at ESI^+ and performing data acquisition in multiple reaction monitoring (MRM) mode. The conditions of MRM are summarized in Table 4.1. The capillary voltage, extractor volt and Rf lens were set at 3.17 kV, 2 V and 0.1, respectively. The cone gas (nitrogen) and desolvation gas (argon) were set at 30 L h^{-1} and 600 L h^{-1}, respectively. A source temperature of 100 °C and a desolvation temperature of 350 °C were used. The source cone voltage and the collision voltage for the transition of each component were optimized by using the

QuanOptimize function of the software.

Table 4.1 MS parameters for multiple reaction monitoring of surfactant components.

Component	Precursor ion (m/z)	Daughter ion (m/z)	Dwell (s)	Cone volt. (V)	Collision volt. (eV)
$C_{16}C_{16}$-Arquad	494.55	270.34	0.3	60	44
$C_{16}C_{18}$-Arquad	522.60	270.33	0.3	60	44
$C_{18}C_{18}$-Arquad	494.55	298.40	0.3	60	44
$C_{16}C_{16}$-Armeen	480.33	256.33	0.3	60	38
$C_{16}C_{18}$-Armeen	508.38	256.29	0.3	60	44
$C_{18}C_{18}$-Armeen	536.38	284.28	0.3	60	44

4.2.5 Calibration curve and sample preparation

Standard solutions of each surfactant in ethanol, with concentrations ranging from 0.1 to 5 mg L^{-1}, were used to establish the external calibration curves for each component of the surfactant. A sample aliquot (1 mL) from the release experiments at each sampling time was transferred from each amber glass vial to a 20-mL clear glass vial and diluted to 3 mL with the same solvent as in the amber glass vial. Meanwhile, at each sampling time the amber glass vial was compensated with 1 mL solvent to maintain a total volume of 40 mL. Each sample was filtered with a Waters GHP filter (13 mm, 0.2 μm) before injection into the HPLC. Each standard solution was injected 3 times and each sample solution was injected twice. The injection volume was 10 μL.

4.3 Results and discussion

4.3.1 Performance of LC-MS/MS method

The LC-MS/MS chromatographs obtained for the three main components of each surfactant are shown in Figure 4.1. Separation of the different components was achieved, with retention times from 7.1 to 8.3 min. Both surfactants had a similar retention time profile for each of the three components, due to the similarity in their molecular structures (Table 4.2). The limit of quantification (LOQ) was 25 μg L^{-1} for both surfactants using the $C_{18}C_{18}$ component as the marker. The contents of the three components ($C_{16}C_{16}$, $C_{16}C_{18}$ and $C_{18}C_{18}$) of each surfactant determined by the LC-MS/MS method are listed in Table 4.2. With the composition of the surfactant known, a calibration curve for each component of the surfactant can be established and used to estimate the amount of each component released from nanoclay into the solvent. Total surfactant concentration in the solvent was calculated as the summation of the concentration of each component.

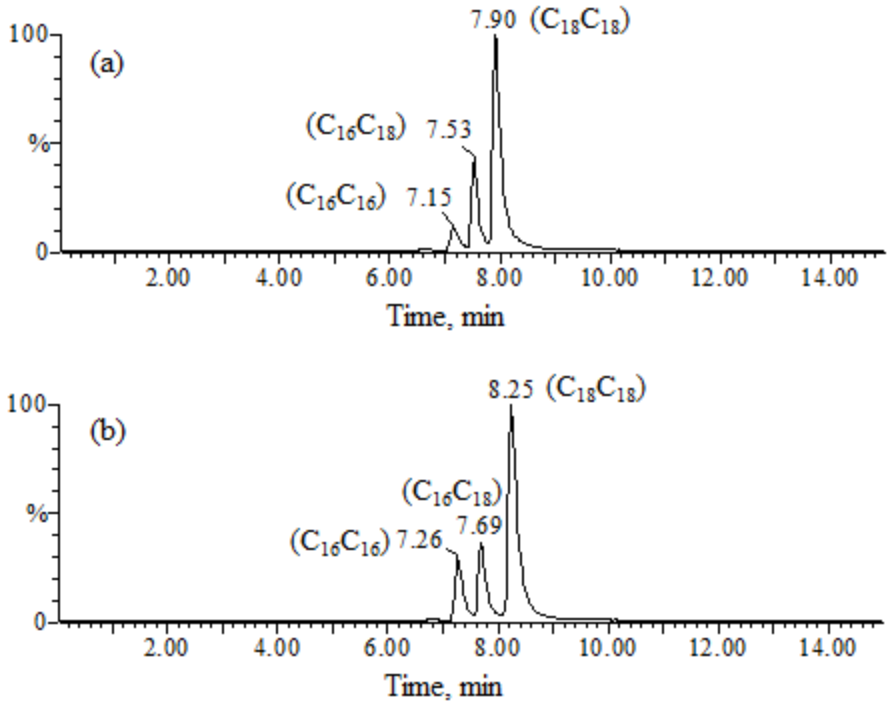

Figure 4.1 LC-MS/MS chromatograms obtained for the three main components of (a) Arquad 2HT-75 and (b) Armeen M2HT surfactants in 5 mg L^{-1} standard solution.

Table 4.2 Molecular structure and composition of the surfactants.

Surfactant	Structure	Component	wt%
Arquad 2HT-75	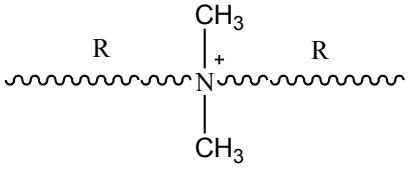	$C_{16}C_{16}$	16
		$C_{16}C_{18}$	41
		$C_{18}C_{18}$	43
Armeen M2HT	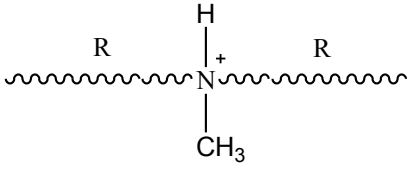	$C_{16}C_{16}$	11
		$C_{16}C_{18}$	40
		$C_{18}C_{18}$	49

Note: R represents 12 to 18 carbon alkyl chains with mainly C_{16} and C_{18} chains.

4.3.2 Effect of temperature on surfactant release

The surfactants were released at a higher rate from the nanoclays as the temperature of the suspension increased (Figure 4.2). Figure 4.2a shows the release of Arquad surfactant from I44P clay into ethanol, revealing that the surfactant concentration increased during the first 6 h, and then remained at a steady state for the rest of the exposure time. Figure 4.2b indicates that the release of Armeen surfactant from Cloisite clay into ethanol took a longer time to achieve steady state at a high temperature (70 °C) than at lower temperatures (22 and 40 °C). For both nanoclays, the amount of surfactant released into ethanol at steady state was highest at 70 °C (about 5.8 out of 21 mg L^{-1} [28 %] for I44P clay and 3.5 out of 24 mg L^{-1} [15 %] for Cloisite clay) and lowest at 22 °C (about 5.3 out of 21 mg L^{-1} [25 %] for I44P clay and 2.6 out of 24 mg L^{-1} [11 %] for Cloisite clay). I44P clay released more surfactant than Cloisite clay did, which suggests a difference in affinity of each surfactant to the solvent. Another possible explanation for this difference could be the way the two types of nanoclay were processed by the different suppliers.

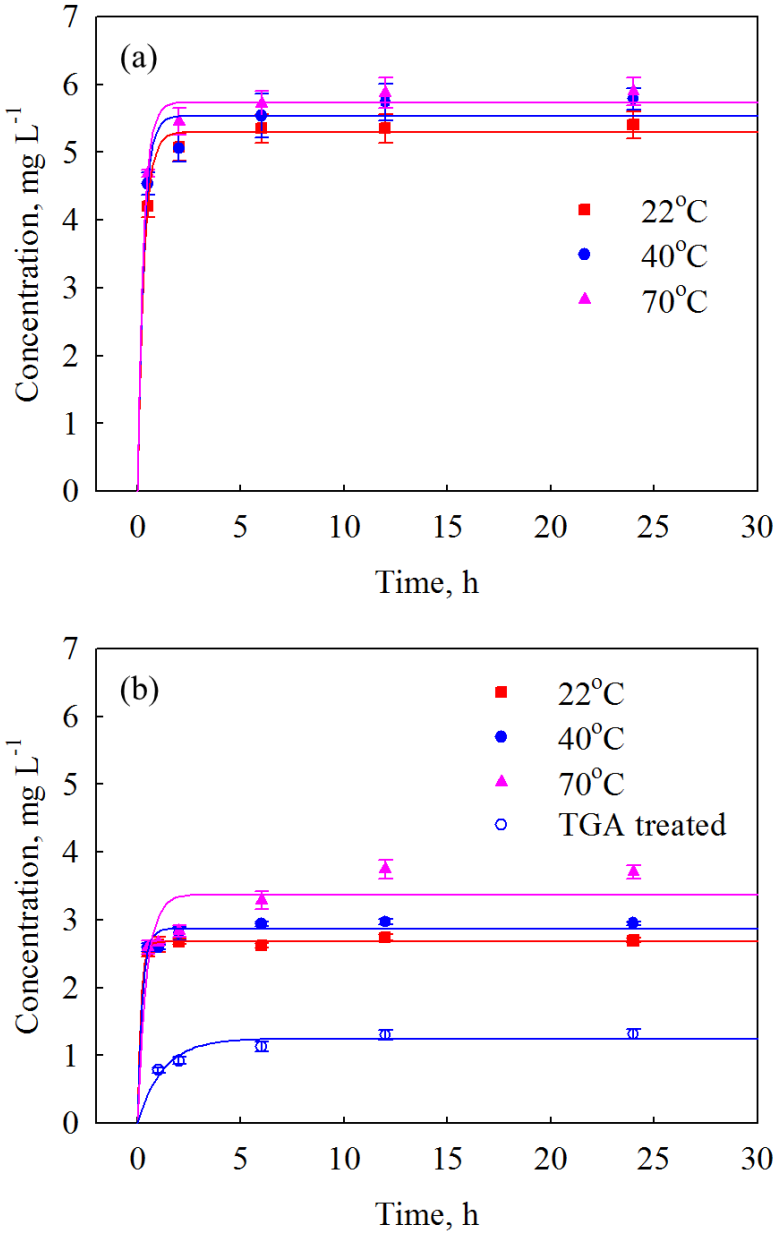

Figure 4.2 Release of surfactant from (a) I44P clay and (b) Cloisite clay into ethanol at various temperatures. Fitted lines are included as a visual guide.

Nanoclays may be affected by exposure to high temperature during film processing. TGA analysis (Figure 4.3) showed an initial thermal decomposition temperature of about 210 °C, which corresponded to the decomposition of the surfactant within the nanoclay and resulting in the weight loss of the nanoclay. Similar result has been reported in other studies on O-MMT [Cervantes-Uc *et al.* 2007]. This temperature is below the processing temperature of some nanocomposites, such as nylon-Cloisite, which are processed at temperatures reaching 240 °C [Nigmatullin *et al.* 2008]. The effect of this high temperature on the release of surfactant is evident when observing the results from TGA-treated Cloisite clay (7 min at 240 °C to simulate the time and temperature of film processing) as shown in Figure 4.2b. Much less surfactant was released from the TGA-treated nanoclay held at 40 °C than from the corresponding untreated sample, probably due to the thermal decomposition of surfactant during the heat treatment indicating that surfactant may be lost during the extrusion process under temperature and pressure although it may release into the polymer matrix.

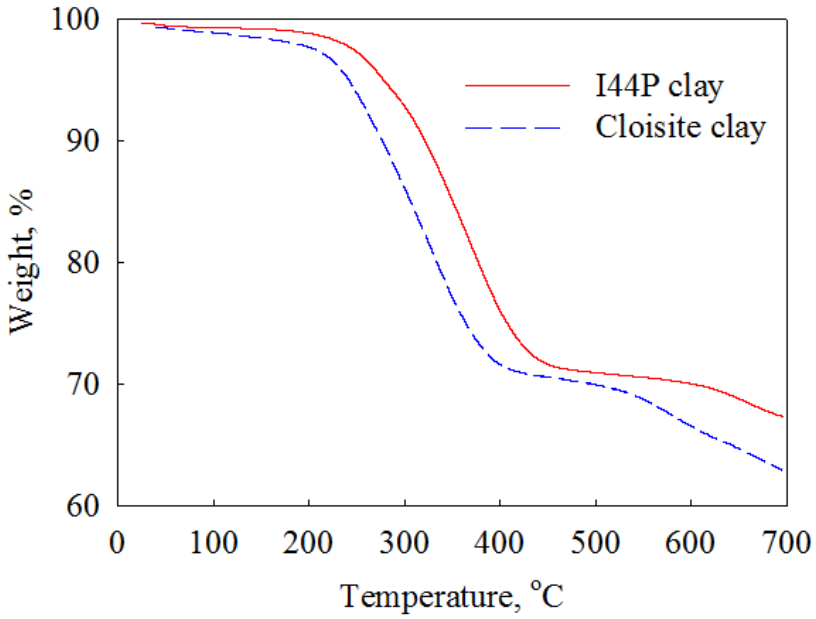

Figure 4.3 TGA curves of I44P clay and Cloisite clay.

4.3.3 Effect of sonication on surfactant release

Sonication is widely applied in food processing and packaging due to its high efficiency in mixing and cleaning. As shown in Figure 4.4, sonication had a significant effect on the release of surfactant from nanoclay. Twice the amount of surfactant was released from both types of nanoclay in the suspensions held at 40 °C after sonication than in suspensions without sonication. Sonication helps to break down the clay clusters into smaller particles [Poli *et al*. 2008]. With smaller particles, more surfactant is exposed to the solvent, leading to an increased amount of surfactant released from the nanoclay.

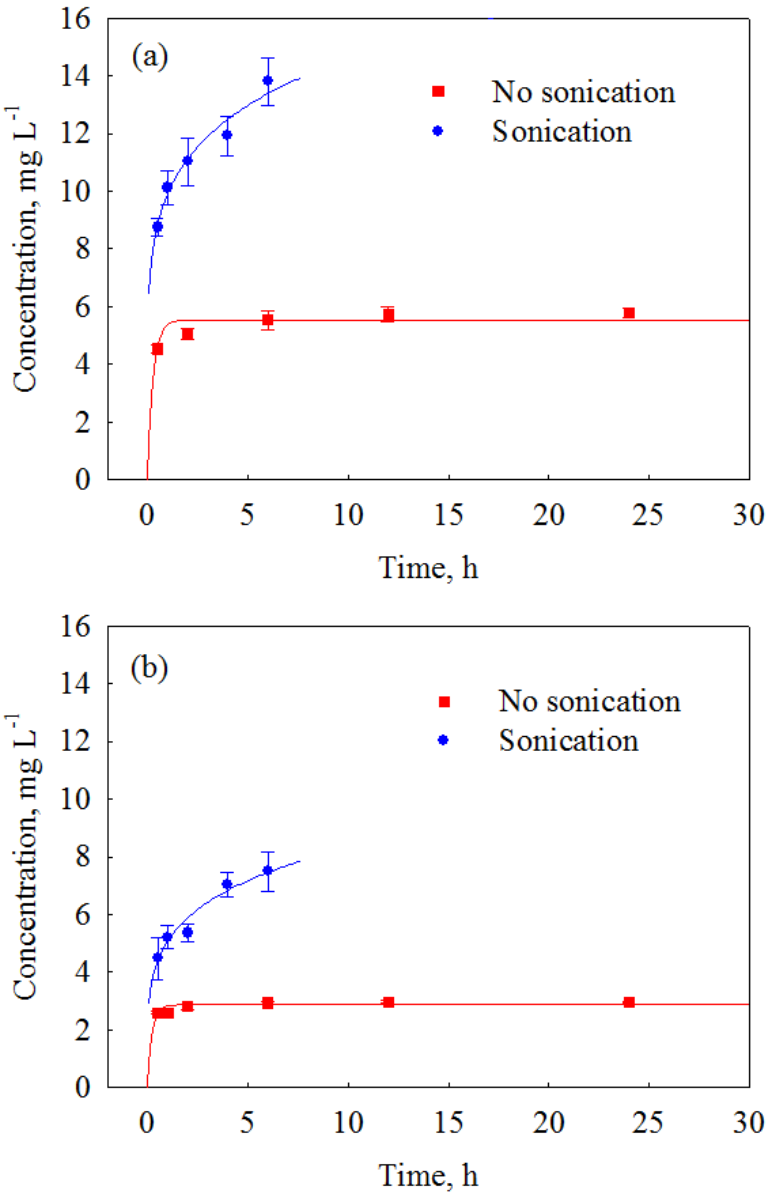

Figure 4.4 Effect of sonication on the release of surfactant from (a) I44P clay and (b) Cloisite clay into ethanol at 40 °C. Fitted lines are included as a visual guide.

4.3.4 Effect of simulant type on surfactant release

Figure 4.5 shows the release of surfactant from nanoclay into three different food simulants (ethanol, 50 % ethanol, or water). Both types of nanoclay released the maximum amount of surfactant into ethanol. Much less surfactant was released from I44P clay (about 1/3 of the maximum amount) into the 1:1 ethanol/water mixture, and even less into water. The level of surfactant released from Cloisite clay into 50 % ethanol or water was below the LOQ. Since organo-modification switches nanoclay from hydrophilic to organophilic, the dispersion of O-MMT in ethanol-water solutions varies with the composition of the solution (ratio of ethanol/water), which in turn plays an impact on the release of surfactant. The previous study (Chapter 3) showed that O-MMT was well dispersed in solutions with high ethanol content (>70 %), while poorly dispersed in solution with high water content (*e.g.*, 50 %) or pure water. Burgentzle et al. have shown that ethanol is efficient in penetrating the clay gallery [Burgentzle *et al.* 2004], which would result in greater exposure of O-MMT to the solvent and promoting the release of surfactant. However, we observed that O-MMT tends to aggregate in solutions with high water content or in pure water due to its hydrophobic nature, which would reduce the amount of nanoclay exposed to the solvent and therefore reduce the release of surfactant from the nanoclay.

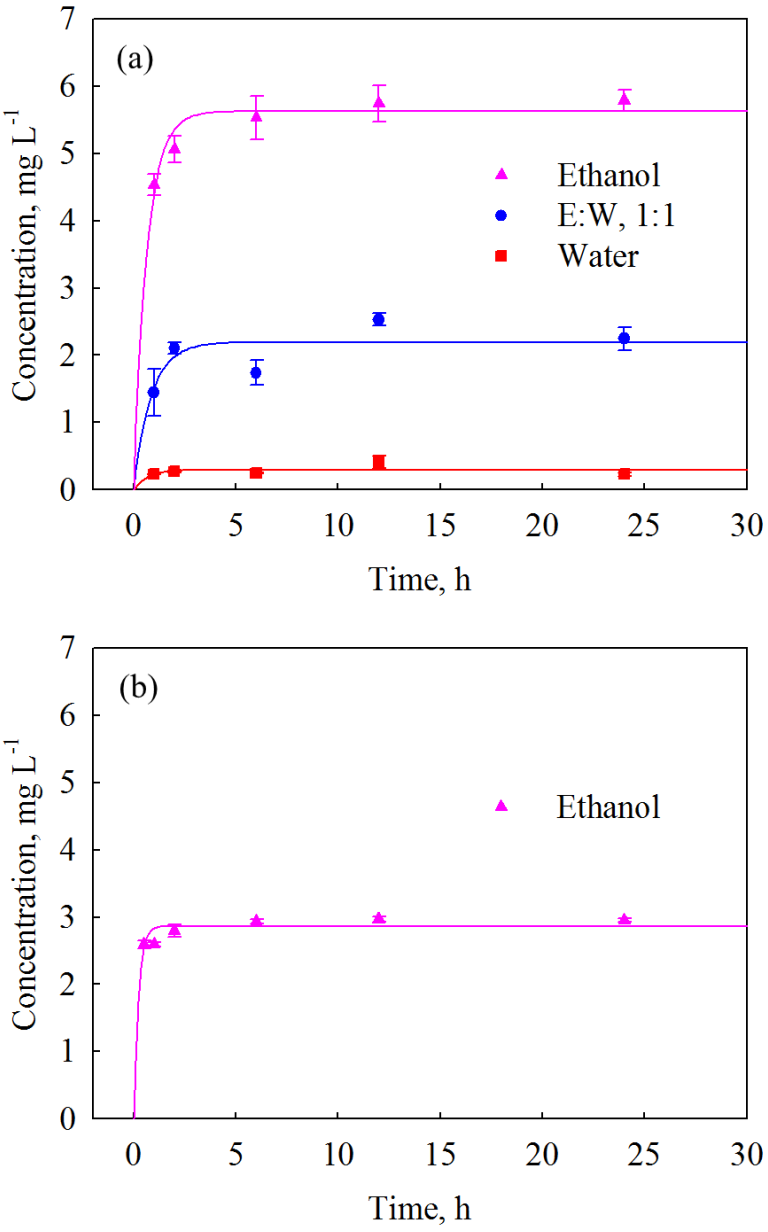

Figure 4.5 Release of surfactant from (a) I44P clay and (b) Cloisite clay into food simulants (ethanol, 50 % ethanol [E:W, 1:1], or water) at 40°C. Release data for surfactant into 50 % ethanol or water in (b) are not shown since surfactant concentrations were below the LOQ. Fitted lines are included as a visual guide.

4.3.5 Solubility parameters

It was assumed that the release of surfactant from nanoclay was influenced by the affinity between the surfactant and the solvent. Such affinity can be estimated based on the solubility parameter δ [Scott & Hilderbrand 1962]. The principle for the use of the solubility parameter is "like dissolves like", which means two substances (liquid or solid) with similar δ values are miscible with each other. The total solubility parameter can be divided into three main components, known as the Hansen solubility parameters [Hansen 1999], which are expressed as δ_D, δ_P and δ_H, and refer to dispersion, polar and hydrogen bonding parameters, respectively. The HSP solubility parameters of the solvent and the surfactant were estimated by the group contribution method [van Krevelen 1997] and converted to the total solubility parameter δ with the equation:

$$\delta = \sqrt{\delta_D^2 + \delta_P^2 + \delta_H^2}$$

The affinity between the surfactant and the solvent was expressed as the difference between solubility parameters of the surfactant and the solvent ($|\delta_S - \delta_L|$) as listed in Table 4.3. The smaller the value of the parameter difference, the better the affinity between the surfactant and the solvent. On the basis of this relationship, the Arquad surfactant for I44P clay had better affinity to ethanol and water than the Armeen surfactant for Cloisite clay. Therefore, the surfactant was more likely to release from I44P clay, resulting in a higher concentration in solution, as shown in Figure 4.5. Moreover, both surfactants showed better affinity to ethanol than to water, so more surfactant was expected to be released into ethanol, which was also confirmed in Figure 4.5.

Table 4.3 Solubility parameter values of solvents and surfactants and the difference between the parameters.

Sample	δ	δ_D	δ_P	δ_H	Parameter difference ($\lvert\delta_S - \delta_L\rvert$)	
	$MPa^{1/2}$	$MPa^{1/2}$	$MPa^{1/2}$	$MPa^{1/2}$	Arquad	Armeen
Ethanol	26.5	15.8	8.8	19.4	8.9	10.4
Water	47.8	15.6	16.0	42.3	30.2	31.7
Arquad	17.6	17.4	0.3	2.8	-	-
Armeen	16.1	15.8	0.6	2.7	-	-

Note: Hansen solubility parameters of ethanol and water were obtained from Hansen (1999); δ_S represents the solubility parameter of the surfactant (the solubility parameter of the $C_{18}C_{18}$ component was used as the solubility parameter of the surfactant), and δ_L represents the solubility parameter of the solvent; molecular weights of $C_{18}C_{18}$-Arquad and $C_{18}C_{18}$-Armeen are 551 g mol^{-1} and 536 g mol^{-1}, respectively; densities of Arquad and Armeen surfactants are 0.88 g cm^{-3} and 0.81 g cm^{-3}, respectively, according to the supplier MSDS datasheet.

4.4 Conclusions

An LC-MS/MS method was developed to identify and quantify the surfactant released from O-MMT into solution. The amount of surfactant released varied under different conditions. Temperature had an effect on the release of surfactant as the amount of surfactant released from the nanoclay into solution increased as the holding temperature increased. However, less surfactant was released when the nanoclay was treated at an ultra-high temperature before suspension, likely due to thermal decomposition of the surfactant. Sonication also had an effect as more surfactant was released into solution under sonication. The effect of simulant type on the

surfactant release can be correlated with the dispersion of nanoclay particles in the solvent as well as the affinity between the surfactant and the solvent. Better dispersion of nanoclay particles was observed in ethanol than in other solvents (*e.g.*, 50 % ethanol or pure water), resulting in a larger nanoclay surface area exposed to the solvent and therefore more surfactant released. Also, the greater release of surfactant into ethanol was facilitated by a better affinity between the surfactant and the solvent due to the similarity in their solubility parameters. The release of surfactant from nanoclay may present a safety concern as the use of nanoclays in polymer nanocomposites for packaging applications becomes more widespread. The instrumental method developed and presented can be applied to measure surfactant release from nanocomposites into food or food simulants.

BIBLIOGRAPHY

BIBLIOGRAPHY

Ajayan, P.M.; Schadler, L.S.; Braun, P.V. Nanocomposite Science and Technology. Wiley-VCH: Weinheim, Deutschland, 2003, Chapter 2.

BCC Research. Global Markets for Nanocomposites, Nanoparticles, Nanoclays, and Nanotubes. BCC Research LLC, Wellesley, MA, USA, 2014. Available from: http://www.bccresearch.com/market-research/nanotechnology/nanocomposites-market-nan021f.html

Burgentzle, D.; Duchet, J.; Gerard, J.F.; Jupin, A.; Fillon, B. Solvent-based nanocomposite coatings I. Dispersion of organophilic montmorillonite in organic solvents. *J. Colloid Interf. Sci.* **2004**, 278, 26–39.

Cervantes-Uc, J.M.; Cauich-Rodriguez, J.V.; Vazquez-Torres, H.; Garfias-Mesias, L.F.; Paul, D.R. Thermal degradation of commercially available organoclays studied by TGA-FTIR. *Thermoch. Acta* **2007**, 457, 92-102.

Chaudhry, Q.; Scotter, M.; Blackburn, J.; Ross, B.; Boxall, A.; Castle, L.; Aitken, R.; Watkins, R. Applications and implications of nanotechnologies for the food sector. *Food Addit. Contam.* **2008**, 25:241–258.

De A Prado, L.A.S.; Karthikeyan, C.S.; Schulte, K.; Nunes, S.P.; De Torriani, I.L. Organic modification of layered silicates: structural and thermal characterizations. *J Non-cryst Solids* **2005**, 351, 970–975.

Diaz, C.A.; Xia, Y.; Rubino, M.; Auras, R.; Jayaraman, K.; Hotchkiss, J. Fluorescent labeling and tracking of nanoclay. *Nanoscale* **2013**, 5, 164–168.

[FDA] Food and Drug Administration. 2007. Guidance for Industry: Preparation of Premarket Submissions for Food Contact Substances: Chemistry Recommendations. Available from: http://www.fda.gov/Food/GuidanceRegulation/GuidanceDocumentsRegulatoryInformation/IngredientsAdditivesGRASPackaging/ucm081818.htm

Ferrer, I.; Furlong, E.T. Identification of alkyl dimethylbenzylammonium surfactants in water samples by solid-phase extraction followed by ion trap LC/MS and LC/MS/MS. *Environ. Sci. Technol.* **2001**, 35, 2583-2588.

Gottschalk, F.; Nowack, B. The release of engineered nanomaterials to the environment. *J. Environ. Monit.* **2011**, 13, 1145–1155.

Hansen, C.M. Hansen Solubility Parameters, A User's Handbook. CRC Press: Boca Raton, FL, USA, 1999.

Lewis, M.A. Chronic and sublethal toxicities of surfactants to aquatic animals: a review and risk assessment. *Water Res.* **1991**, 25, 101–113.

Li, X.; Brownawell, B.J. Analysis of quaternary ammonium compounds in estuarine sediments by LC-ToF-MS: very high positive mass defects of alkylamine lons as powerful diagnostic tools for identification and structural elucidation. *Anal. Chem.* **2009**, 81, 7926-7935.

Mauricio-Iglesias, M.; Peyron, S.; Guillard, V.; Gontard, N. Wheat gluten nanocomposite films as food-contact materials: migration tests and impact of a novel food stabilization technology (high pressure). *J. Appl. Polym. Sci.* **2010**, 116, 2526–2535.

Nigmatullin, R.; Gao, F.; Konovalova, V. Polymer-layered silicate nanocomposites in the design of antimicrobial materials. *J. Mater. Sci.* **2008**, 43, 5728–5733.

Nishikawa, M.; Katagi, M.; Miki, A.; Tsuchihashi, H. Forensic toxicological determination of surfactant by liquid chromatography/electrospray ionization mass spectrometry and liquid chromatrography/electrospray ionization tandem mass spectrometry. *J. Health Sci.* **2003**, 49, 138-148.

Patel, H.A.; Somani, R.S.; Bajaj, H.C.; Jasra, R.V. Nanoclays for polymer nanocomposites, paints, inks, greases and cosmetics formulations, drug delivery vehicle and waste water treatment. *Bull. Mater. Sci.* **2006**, 29, 133–145.

Poli, A.L.; Batista, T.; Schmitt, C.C.; Gessner, F.; Beumann, M.G. Effect of sonication on the particle size of montmorillonite clays. *J. Colloid Interf. Sci.* **2008**, 325, 386–390.

Scott, R.L.; Hilderbrand, J. Regular Solutions. Prentice-Hall: Englewood Cliffs, NJ, USA, 1962.

Sinha Ray, S.; Okamoto, M. Polymer/layered silicate nanocomposites: a review from preparation to processing. *Prog. Polym. Sci.* **2003**, 28, 1539–1641.

Szakal, C.; Roberts, S.M.; Westerhoff, P.; Bartholomaeus, A.; Buck, N.; Illuminato, I.; Canady, R.; Rogers, M. Measurement of nanomaterials in foods: Integrative consideration of challenges and future prospects. *ACS Nano* **2014**, 8, 3128-3135.

Talmage, S.S. Environmental and human safety of major surfactants: alcohol ethoxylates and alkylphenol ethoxylates. A report to the Soap and Detergent Association. CRC Press: Boca Raton, FL, USA, 1994.

Van Krevelen, D.W. Properties of Polymers: Their correlation with Chemical Structure; Their Numerical Estimation and Prediction from Additive Group Contributions. Elsevier: Amsterdam, Netherlands, 1997.

Ying, G.G. Fate, behavior and effects of surfactants and their degradation products in the environment. *Environ. Int.* **2006**, 32, 417–431.

CHAPTER 5: Release of Nanoclay and Surfactant from Polymer-Clay Nanocomposites into a Food Simulant

A paper was submitted based on the main part of this chapter:

Xia, Y.; Rubino, M.; Auras, R. 2014. Release of nanoclay and surfactant from polymer-clay nanocomposites into a food simulant. Manuscript submitted.

5.1 Introduction

The use of nanocomposites consisting of polymers and engineered nanoparticles (ENPs) is expanding rapidly, with global sales of over US$1.2 billion in 2013 rising to an estimated US$4.2 billion by 2019 [BCC Research 2014]. The addition of ENPs at small loadings significantly improves the performance of polymer materials and therefore expands their applications. For example, the use of nanoscale metals enhances the antimicrobial activity and UV resistance of polymers [Han & Yu 2006; Radheshkumar & Munstedt 2006]; the incorporation of carbon nanotubes improves thermal, mechanical and electrical properties of polymers [Kashiwagi *et al.* 2004; Bal & Samal 2007]; and the addition of nanoclays increases the barrier properties and heat stability of polymers [Pereira de Abreu *et al.* 2007; Rathi & Dahiya 2012].

Nanoclays, such as organo-modified montmorillonite (O-MMT), are ENPs increasingly being used in consumer goods due to their low cost, commercial availability, high stability, and relatively simple processing. Nanocomposites with O-MMT as the nanofiller account for over half of total nanocomposite consumption, with the main applications in the automotive parts and packaging industries [Patel *et al.* 2006; BCC Research 2014]. MMT is obtained from naturally occurring layered silicate minerals with a crystal structure consisting of two silica tetrahedral sheets fused to an edge-shared alumina octahedral sheet [Sinha Ray & Okamoto 2003]. The clay layers are usually parallel stacked to form tactoids with about 1 nm interlayer space (or clay gallery) containing exchangeable cations (*e.g.*, Na^+ or K^+). Organo-modification of MMT is carried out by replacing the exchangeable cations with organic cationic surfactants (*e.g.*, alkylammonium cations), to improve compatibility of the nanoclay with the polymer [De A. Prado *et al.* 2005]. Nanoclays are added to several polymer matrices including polypropylene and low density polyethylene to improve their barrier (*e.g.*, to water vapor and gases such as

oxygen and carbon dioxide) and mechanical properties [Pereira de Abreu *et al.* 2007; Choudalakis & Gotsis 2009]. By adding nanoclay, thinner films can be produced having similar strength and barrier properties as thicker films without nanoclay, and solid waste can be reduced. For novel bio-based plastics, such as poly(lactic acid) and thermoplastic starch, the incorporation of nanoclay has expanded the range of applications of these materials by overcoming their performance limitations (*e.g.*, low barrier to moisture, low heat-deflection temperature) [Sinha Ray & Okamoto 2003; Lagaron & Lopez-Rubio 2011].

The cytotoxicity of nanoclays has been evaluated *in vitro* and *in vivo* using different cell models such as human epithelial cells [Verma *et al* 2012], human normal intestinal cells [Baek *et al.* 2012], and human hepatic cells [Lordan *et al* 2011]. Studies have shown that nanoclays tend to penetrate into cells and may affect cell function. Yamashita *et al.* demonstrated that nanosilica particles with diameters of less than 100 nm penetrated and induced structural and functional abnormalities in mouse placenta and caused fetal growth restriction [Yamashita *et al.* 2011]. Verma *et al.* found that the shape and surface area of nanoclays impact cell viability; platelet nanoclays were more cytotoxic than tubular ones [Verma *et al.* 2012]. Also, the potential risks of surfactants used as organo-modifiers of nanoclays have been investigated, revealing that some surfactants are toxic to ecosystems, animals and humans [Talmage 1994; Venhus & Mehrvar 2004; Ying 2006]. Furthermore, the degradation products of phynol-containing surfactants may cause endocrine disruption in wildlife or humans [Sonnenschein & Soto 1998; Routledge & Sumpter 2009].

Nanoparticles including nanoclay may reach biological systems through different routes (Figure 5.1). One route of exposure could occur when nanocomposites are used as packaging materials in contact with food [Chaudhry *et al.* 2008; Silvestre *et al.* 2011]; nanoparticles may be

released from the packaging material into the food. Other routes of exposure could occur when nanocomposites are used in manufacturing or buried in landfills; nanoparticles may be released into the surrounding environment and reach plants, wildlife or humans [Gottschalk & Nowack 2011; Raynor *et al.* 2012].

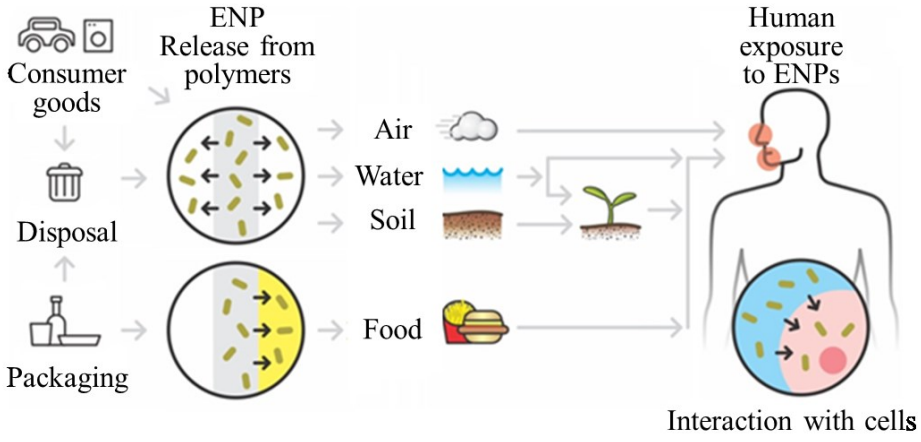

Figure 5.1 Routes of potential nanoparticle exposure to the environment and humans. Copyright © 2014 Maria Rubino & Rafael Auras, School of Packaging, Michigan State University.

The health and safety risks of nanoparticles on humans and the environment are not well understood due to the difficulty in detecting, measuring and characterizing nanoparticles in different media as well as in evaluating exposure levels to nanoparticles [Thomas *et al.* 2006; EFSA 2011; Szakal *et al.* 2014]. To date, release assessments of nanoclay and associated surfactants from nanocomposites are scarce. Gaining knowledge on the transport of these components from nanocomposites when exposed to different conditions is critical to the evaluation of exposure dose and related risk assessment [NRC 2013].

The aim of this study was to investigate the release of nanoclay and surfactant from polymer-clay nanocomposite systems into a food simulant by tracking the nanoclay and

surfactant simultaneously and then correlating the release to interactions among the nanoclay, polymer and solvent. Such interactions could be the exfoliation or aggregation or intercalation of the nanoclay within the polymer, the effect of the solvent either on the swelling of the polymer or on the change of the clay galleries. Two polymers that are well documented in the literature were selected as model systems: polypropylene (PP) and polyamide 6 (PA6). These polymers differ in polarity and chemical composition and, therefore, represent two different groups of polymers.

5.2 Materials and methods

5.2.1 Materials

PP resin (Pro-fax 6523, Appendix 1) was supplied by LyondellBasell Industries (Houston, TX, USA). Maleic anhydride-graft-polypropylene resin (MAPP or Bondyram® 1001, 1 wt% bound maleic anhydride, Appendix 2) was obtained from Polyram Co. (Shelby Township, MI, USA) and used to improve the compatibility between the nanoclay and the polymer [Reichert *et al.* 2000]. PA6 resin (Ultramid® B40 01, Appendix 3) was obtained from BASF (Florham Park, NJ, USA).

Two types of nanoclay were used: Nanomer® I.44P (herein referred to as I44P clay) was obtained from Nanocor (Aberdeen, MS, USA) containing 65 wt% MMT and 35 wt% surfactant (Arquad® 2HT-7), and Cloisite® 93A (herein referred to as Cloisite clay) was obtained from Southern Clay Products (Gonzales, TX, USA) containing 60 wt% MMT and 40 wt% surfactant (Armeen® M2HT). The surfactants used in the nanoclays also were obtained separately (from AkzoNobel, IL, USA): dimethyl dihydrogenated tallow amine or Arquad® 2HT-75 (used in I44P clay), around 75 wt% purity; and methyl dihydrogenated tallow amine or Armeen® M2HT (used in Cloisite clay), around 90 wt% purity. Both surfactants consist of two alkyl chains

(hydrogenated tallow) ranging from 12 to 18 carbons with mainly C16 and C18 (>96 wt%) according to the data sheet from the supplier. Therefore, only three main components of each surfactant were considered for analysis and designated as $C_{16}C_{16}$-Arquad/Armeen, $C_{16}C_{18}$-Arquad or Armeen and $C_{18}C_{18}$-Arquad or Armeen.

5.2.2 Preparation of polymer-clay films

The PP-clay nanocomposite was prepared by initially mixing the PP and MAPP resins for 2 min and then melting in a Haake Rheomix lab mixer (Thermo Electron Co., Newington, NH, USA) at 180 °C and 40 rpm for 5 min. I44P clay was added and further mixing was carried out at 180 °C and 150 rpm for 5 min. The final composition of the PP-clay nanocomposite was 85 wt% PP, 12 wt% MAPP and 3 wt% nanoclay. The PA6-clay nanocomposite was prepared by pre-drying the polymer resin in a vacuum oven at 100 °C for 8 h and then melting in a Haake Rheomix lab mixer at 240 °C and 40 rpm for 5 min. Cloisite clay was added and further mixing was carried out at 240 °C and 150 rpm for 5 min. The final composition of the PA6-clay nanocomposite was 95 wt% PA6 and 5 wt% nanoclay. The type of clay used for each polymer as well as the composition of the nanocomposite was selected to simulate the commercialized product.

The polymer-clay nanocomposites prepared by melt mixing were ground into small pellets and further converted into films. PP-clay films of 22.5 ± 1.1 μm thickness were produced by a Killion blow film extruder (Model KL-100, screw size of 1”, L/D ratio of 30:1, Davis-Standard Corp., Cedar Grove, NJ, USA) with a temperature profile of 193-204 °C (380-400 °F) for the extruder and a screw speed of 14 rpm. PA6-clay films of 21.1 ± 1.2 μm thickness were produced by a Randcastle cast film extruder (Model RCP-0625, screw size of

0.625", L/D ratio of 24:1, Extrusion Systems Inc., Cedar Grove, NJ, USA) with a temperature profile of 238-246 °C (460-475 °F) for the extruder and a screw speed of 45 rpm. Control films without nanoclay (22.8 ± 1.8 μm for PP + MAPP, and 22.1 ± 1.6 μm for PA6) were also prepared in the same manner.

5.2.3 Characterization of polymer-clay films

Thermal properties of both nanocomposite and control films were characterized by differential scanning calorimetry (DSC) and dynamic mechanical analysis (DMA). The melting temperature (T_m) was determined with a Q-100 DSC (TA Instruments, Inc., New Castle, DE, USA) in the first heating cycle from 40 to 260 °C at a ramp rate of 10 °C min^{-1}. The percent crystallinity (X_c) was calculated with the equation below:

$$X_c = \frac{\Delta H_m}{\Delta H_m^0}$$

where ΔH_m is the enthalpy of fusion of the sample, and ΔH_m^0 is the heat of fusion of 100% crystalline polymer. The glass transition temperature (T_g) was recorded by a Q-800 DMA (TA Instruments, Inc.) scanning 5 °C min^{-1} from -50 to 100 °C for PP-based samples and 0 to 120 °C for PA6-based samples. The measurement was carried out in a tension mode with a constant strain of 0.1 %, a constant frequency of 1 Hz and a preload of 0.1 N. All samples were tested in triplicate.

The structure and morphology of the nanocomposite films were characterized by X-ray diffraction (XRD) and transmission electronic microscopy (TEM). XRD analysis was carried out with a Bruker AXS D8 Advance X-ray diffractometer (Bruker Co., Billerica, MA, USA) equipped with a Global Mirror filtered Cu Kα radiation source (wavelength, λ = 0.154 nm) setting at 40 kV and 40 mA. The film sample as well as clay powder (control) was scanned over

a 2 theta range of 0.5 ° to 10 ° at a rate of 0.5 ° min^{-1} and an increment of 0.01 °. TEM analysis was performed with a JEOL 100CX II TEM (JEOL USA Inc., MA, USA). The film sample was embedded in a paraffin block and cut with a microtome into 100-nm thin sections. The microtomed sections were observed in a bright field imaging mode with an acceleration voltage of 120 kV.

5.2.4 Release experiment for polymer-clay films

Two-sided liquid extraction experiments were carried out in accordance with ASTM D4754-11. The apparatus used for the experiment are shown in Figure 5.2. Before the experiments, film samples were washed carefully with water and ethanol to remove any contaminants on the polymer surface. Round disks (2-cm diameter) were cut from nanocomposite films (triplicate) as well as control films (triplicate). To test the release of nanoclay, a 50-mL PP tube was used as the migration cell; 16 film disks (total area = 100 cm^2) of a single material were placed in the tube and the disks were placed on the stainless steel wire and separated by Teflon beads. The tube was filled with 40 mL ethanol (100%) and kept at 22, 40 or 70 °C until the steady state of nanoclay release. Ethanol was used to simulate fatty food according to U.S. Food and Drug Administration (FDA) recommendations on the migration testing of food contact substances [FDA 2007]. A high temperature was used to accelerate the release process also according to the FDA recommendations. In another test, PP-clay films (triplicates) with two different thicknesses (22.5 ± 1.1 μm and 45.6 ± 1.3 μm) were examined at 70 °C for up to 16 d to compare any difference in the nanoclay release. To test the release of surfactant, glass vials (2.5 × 9.5 cm) were used instead of PP tubes as the migration cell to avoid any absorption of surfactant by the tube; 16 disks were placed in each vial as described above

and the extraction with ethanol was conducted at 22, 40 or 70 °C until the steady state of surfactant release. Nanoclay suspensions in ethanol made up of an equivalent amount of nanoclay as in the nanocomposite films were used as a control. For all experiments, multiple samplings were taken from the food simulant at varied time intervals until the end of the experiment.

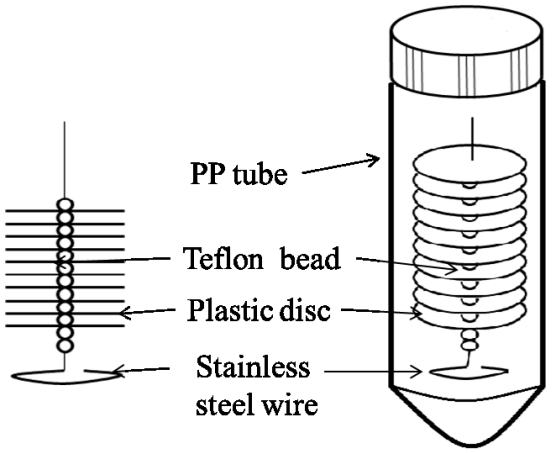

Figure 5.2 Apparatus for two-sided contact migration test.

5.2.5 Evaluation of nanoclay release

Nanoclay concentrations in the solvent were determined by a graphite furnace atomic absorption spectrometry (GFAAS) method as described in Chapter 3. A Hitachi Z-9000 simultaneous multi-element atomic absorption spectrometer (Hitachi High-Technologies Co., Tokyo, Japan) equipped with a HGA-700 atomizer and an autosampler system was used. Si and Al were selected as markers for the nanoclays, and their contents in the nanoclays were evaluated via an X-ray fluorescence (XRF) method as also described in Chapter 3. XRF results for the clays showed that I44P clay contained (20.14 ± 0.06) wt% Si and (7.80 ± 0.02) wt% Al, with a Si/Al ratio of 2.58 ± 0.04; whereas Cloisite clay contained (20.03 ± 0.16) wt% Si and (7.15 ±

0.05) wt% Al, with a Si/Al ratio of 2.80 ± 0.12. Calibration curves generated from Si and Al standards were used to determine the amount of Si and Al released into the solvent. Nanoclay concentrations were calculated by correlating to Si and Al concentrations based on the element contents in the nanoclay.

Before injection into the GFAA spectrometer, the extraction solvent was transferred to a clean PP tube and mixed using a vortex mixer (Scientific Industries Inc., NY, USA) for 30 s to disperse the nanoclay particles. Approximately 2 mL of the solvent was transferred to a sample vial and an injection volume of 20 μL was used for instrumental analysis. After the analysis, the sample solution was returned to the migration cell. All samples were tested in triplicate. Due to the small amount of nanoclay particles in the solvent, a "concentration function" associated to the instrument software was applied to ensure a better detection of the sample by increasing its signal. This function consists of repeating injections of the sample via the auto sampler at the drying stage of the graphite furnace program. Each solvent sample was injected 6 times (20 μL per injection) before the data was recorded. The limit of quantification (LOQ) was 8 μg L^{-1} for Si and 3 μg L^{-1} for Al.

5.2.6 Electron microscopy

The released nanoclay particles were observed by bright field imaging using a JEOL JEM-2200FS field emission TEM (JEOL USA Inc., MA, USA) operating at an acceleration voltage of 200 kV. Composition analysis of the observed particles was carried out with an X-ray energy dispersive spectroscopy (EDS) detector attached to the microscope. To prepare the sample for TEM, 6 droplets of the solvent obtained from the release experiment were dripped on a copper grid coated with a carbon membrane. The carbon memebrane was used to adsorb and

stabilize the particles, and prevent the aggregation of the particles during drying. Three layers of filter paper were placed below the copper grid to absorb the extra solvent. The copper grid was dried under a 100 W lamp for 10 min to evaporate the residual solvent and observed under the microscope.

5.2.7 Liquid chromatography tandem mass spectrometry

Quantification of surfactant in the solvent was performed by a liquid chromatography tandem mass spectrometry (LC-MS/MS) method as described in Chapter 4. A Waters Quattro micro mass spectrometer (Waters Co., MA, USA) coupled to a Shimadzu LC-20AD HPLC system (Shimadzu Scientific Instruments, MO, USA) and a SIL 5000 auto-sampler were used; the system was operated by using Waters MassLynx 4.0 software.

Standard solutions of each surfactant in ethanol, with concentrations ranging from 0.1 to 5 mg L^{-1}, were used to establish the external calibration curve for each component of the surfactant. The LOQ was 25 μg L^{-1} for both surfactants when using $C_{18}C_{18}$ component as the marker. A sample aliquot (1 mL) at each sampling time was transferred from the migration cell to a 20-mL glass vial and diluted with 1 mL ethanol for the Arquad surfactant or 2 mL ethanol for the Armeen surfactant. Meanwhile, at each sampling time the migration cell was compensated with 1 mL ethanol. Each sample was filtered with a Waters GHP filter (13 mm, 0.2 μm, Waters Co., MA, USA) before injection into the HPLC. Each standard solution was injected 3 times and each sample solution was injected twice with an injection volume of 10 μL.

5.2.8 Modeling of surfactant release

Surfactant release from the nanocomposite filmes was described by Equation 2.2.

Diffusion coefficient (*D)*, partition coefficient ($K_{P,F}$) and migrant (surfactant) concentration at equilibrium ($M_{F,\infty}$) were set as the parameters and derived from the equation. Non-linear regression (Appendices 4 to 7) was performed by using MATLAB software (version 7.11.0, The MathWorks, Inc., MA, USA). The migration curve was automatically fitted to the experimental data until the best fit was achieved. The fit of the applied equation to the experimental data was expressed by the root mean square error (RMSE). The smller the RMSE values, the better the methametical model was fitted to the experimental data.

5.3 Results and discussion

5.3.1 Properties of the nanocomposite films

For the thermal properties, as shown in Table 5.1, no significant difference was found for T_g between the nanocomposite and control films, whereas T_m was significantly different. One extra T_m was obtained for PA6 at 212 °C after the addition of nanoclay (DSC curves are in Appendix 8); this peak referred to the γ-crystalline region, which is different from the α-crystalline region formed at 220 °C for pure PA6 [Katoh & Okamoto 2009]. The appearance of the extra T_m was due to good compatibility between the clay layers and PA6 matrix which altered the crystalline phase of PA6, resulting in the formation of new crystalline phase [Wan *et al.* 2012]. Both polymer-clay films had lower X_c than the corresponding control films. The presence of nanoclay particles likely interrupted the arrangement of polymer chains during film processing and, therefore, the formation of crystalline regions.

Table 5.1 Thermal properties of the nanocomposite and control films.

Films	T_m (°C)	ΔH (J g^{-1})	X_c (%) [a]	T_g (°C)
PP (control)	164.2 ± 0.2^{Ab}	109.0 ± 2.4^{A}	45.4 ± 1.0^{A}	1.0 ± 1.2^{A}
PP-clay	162.7 ± 0.2^{B}	101.5 ± 2.1 ^{B}	42.3 ± 0.9^{B}	1.4 ± 2.1^{A}
PA6 (control)	220.2 ± 0.0^{A}	59.5 ± 6.7^{A}	24.8 ± 2.8^{A}	61.5 ± 0.4^{A}
PA6-clay	212.1 ± 0.2^{B} 219.3 ± 0.3^{C}	44.6 ± 4.8^{B}	18.6 ± 2.0^{B}	60.9 ± 0.2^{A}

[a] Heat of fusion of 100% crystalline PP [van der Wal *et al.* 1998] is 207 J g^{-1} and heat of fusion of 100% crystalline PA6 [Illers 1978] is 240 J g^{-1}. [b] Values are the mean ± stdev; for each property within each polymer type, means with different uppercase letters are significantly different ($P < 0.05$, $n = 3$).

Nanoclays, when embedded into the polymer matrix, can be intercalated or even exfoliated by the polymer chains depending on the interaction between the nanoclay and the polymer. The interaction can be determined by assessing the structure and morphology of the nanocomposite. XRD patterns and TEM images for both polymer-clay nanocomposites are shown in Figure 5.3. The gallery distance (*d*-spacing) of I44P clay powder (Figure 5.3a) was 2.66 nm (2θ = 3.32 °) and increased to 3.19 nm (2θ = 2.77 °) after the nanoclay was embedded into PP. That increase was caused by the intercalation of polymer chains into the clay gallery. Partial aggregation of nanoclay particles was found in the PP matrix as shown by the small clusters in the corresponding TEM image (Figure 5.3b). The XRD patterns in Figure 5.3c for the PA6-clay nanocomposite and clay powder shows that nanoclay particles were well exfoliated

since the peak observed for clay powder (2θ = 3.26 °) disappeared in the nanocomposite pattern. The exfoliated structure was also confirmed by the TEM image of the PA6-clay film (Figure 5.3d) in which the nanoclay particles are well separated and homogenously dispersed in the PA6 matrix. A well exfoliated structure can be achieved when there is good thermodynamic affinity between the nanoclay and the polymer matrix; otherwise aggregation of nanoclay particles occurs if the polymer-clay interaction is thermodynamically unfavorable [Paul & Robeson 2008]. Therefore, better interaction was expected between Cloisite clay and PA6 than between I44P clay and PP.

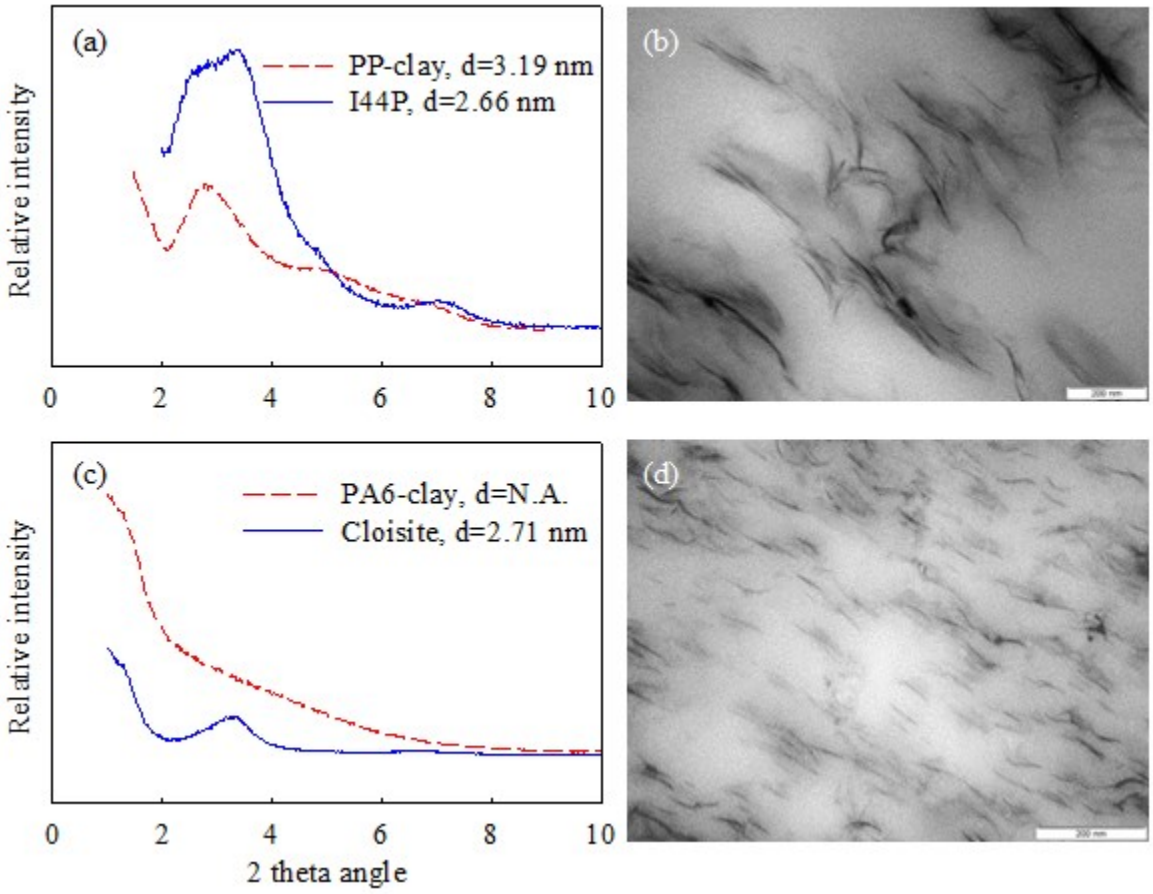

Figure 5.3 XRD patterns for (a) PP-clay and (c) PA6-clay; and TEM images for (b) PP-clay and (d) PA6-clay. Scale bar: 200 nm.

5.3.2 Release of nanoclay from nanocomposite films

Nanoclay released from nanocomposite films was determined by tracking the concentration of Si and Al in the solvent by GFAAS as a function of time. Figure 5.4 shows the Si and Al concentrations in ethanol as a function of time. In order to be certain that the Si and Al measured originated from the nanoclay within the nanocomposite, two independent evaluations were carried out. For the first evaluation, control films were run in parallel with the nanocomposite films. Si and Al concentrations in the solvent in contact with the control films were below the LOQ throughout the release experiment. For the second evaluation, the Si/Al ratio was tracked as a function of time throughout the release experiment, as shown in Figure 5.4. The Si/Al ratio was 2.62 ± 0.25 in the solvent in contact with the PP-clay film and 2.84 ± 0.38 in the solvent in contact with the PA6-clay film. These values were in good agreement with the ones obtained by XRF analysis (Si/Al ratio of 2.58 ± 0.04 for I44P clay, and 2.80 ± 0.12 for Cloisite clay). Therefore, with these two assessments the contamination of Si and Al from other sources such as dust within the film did not represent a concern and the main source of Si and Al was attributed to the nanoclay within the film. On the basis of the Si and Al concentrations in the solvent, the release of nanoclay particles from the polymer-clay films was confirmed. In addition, the increasing trend of Si and Al concentrations at the beginning of the release experiment indicated an initial release of nanoclay particles from the nanocomposite films. Shortly thereafter a steady state was reached, as there was no obvious increase in element concentrations through the end of the experiment.

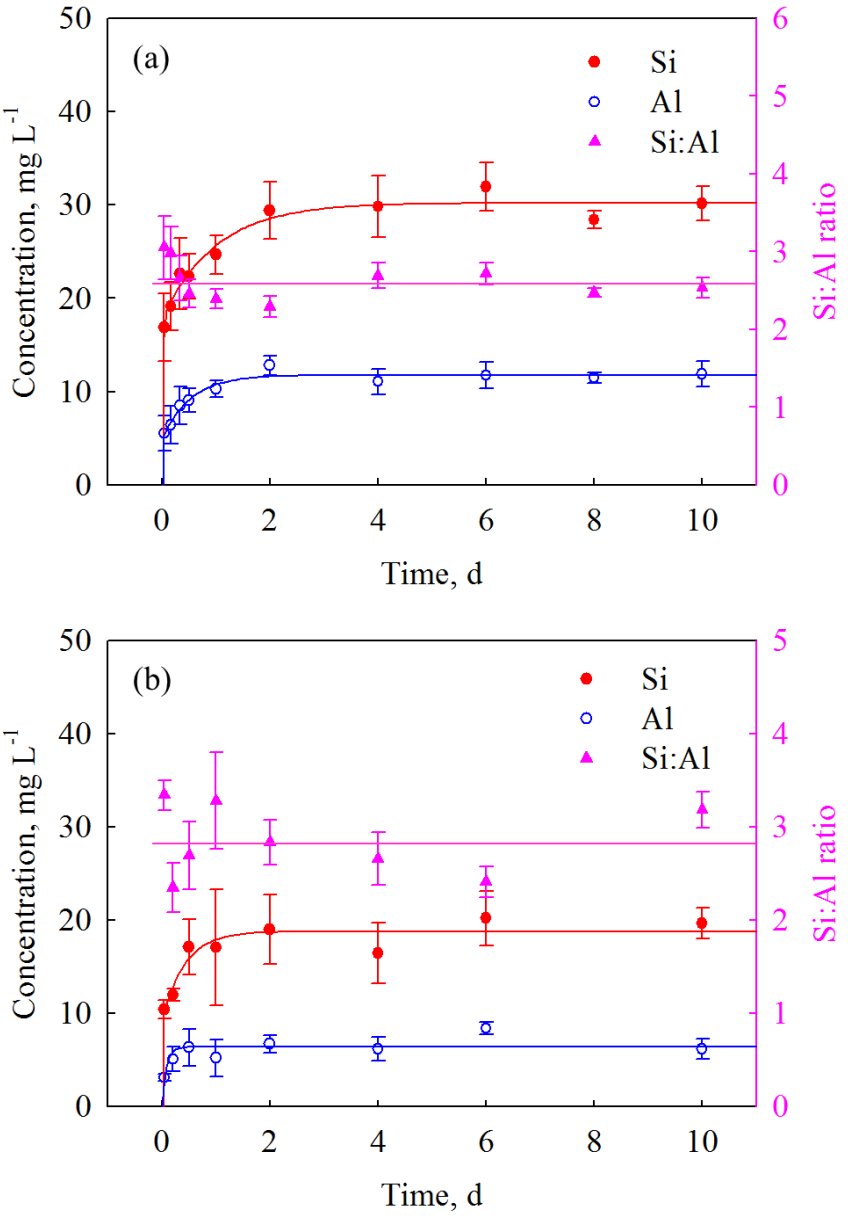

Figure 5.4 Amounts of Si and Al released from (a) PP-clay film and (b) PA6-clay film into ethanol at 70 °C as a function of time. The Si/Al ratio in the solvent as a function of time is also shown. Fitted lines are included as a visual guide.

Al was considered a better marker of nanoclay than Si since there were potentially more contamination sources for Si, such as dusts or impurities in the nanoclay (*e.g.*, quartz). Therefore, Al concentrations were further converted to nanoclay concentrations (Figure 5.5) on the basis of the original Al content in each nanoclay (7.8 % for I44P clay, and 7.2 % for Cloisite clay). Figure 5.5 shows that both PP-clay and PA6-clay films released small amounts of nanoclay particles at the three temperatures (less than 0.15 mg L^{-1} for PP-clay films and less than 0.1 mg L^{-1} for PA6-clay films). Temperature had an effect on the nanoclay release as the nanoclay concentration was higher when the nanocomposite films were exposed to a higher temperature (*e.g.*, 70 °C). The result of nanoclay release partially aligns with Simon's theory that large nanoparticles are difficult to release from the polymer [Simon *et al.* 2008]. However, in the current study, small but significant amounts of nanoclay were released, especially at 70 °C. Although the the total weight of nanoparticle released is small, the number of particles and total surface area of such particles could be large due to the nature of nanoparticles. Additional assessment is needed to evaluate the size of the released particles which may be less than 100 nm being in the range of penetrating cells [Yamashita *et al.* 2011; Verma *et al.* 2012]. More nanoclay particles were released from PP-clay films than from PA6-clay films despite the fact that the initial nanoclay content in PP-clay films (3 wt%) was less than that in PA6-clay films (5 wt%). Such a difference could be explained by the interaction between the nanoclay and the polymer. The exfoliation structure of Cloisite clay in PA6 had a larger surface area interacting with the polymer matrix. The interaction was further mediated through the hydroxyl and amine groups where hydrogen bonding can form at the interface between the nanoclay and the polymer [Sinha Ray & Okamoto 2003]. Hence, there would be a stronger interface between Cloisite clay and PA6, which significantly reduced the mobility of nanoclay particles. In contrast, poor interaction

was found between I44P clay and PP (although some PP was treated with MA to improve the affinity to nanoclay) as indicated by the structure and morphology in Figure 5.3b. A higher mobility was expected for I44P clay particles, which increased their chance of release from the polymer.

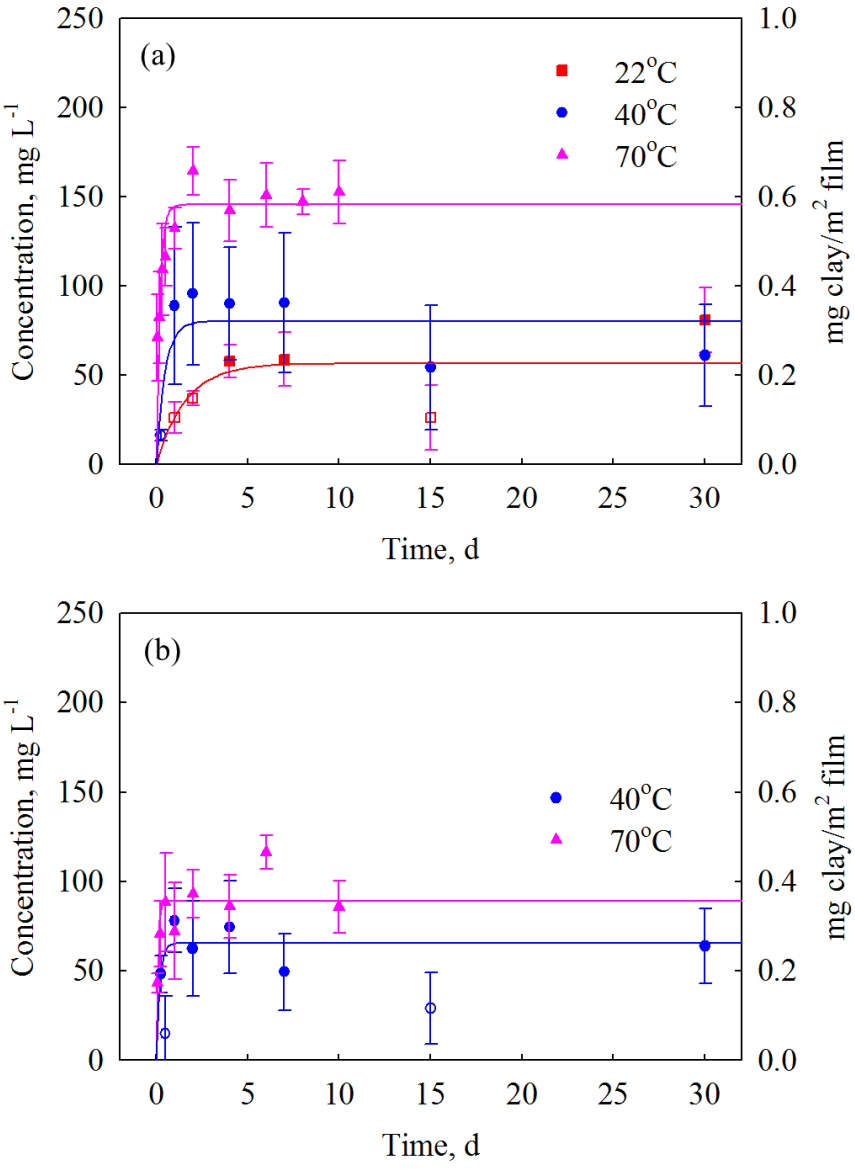

Figure 5.5 Amounts of nanoclay particles released from (a) PP-clay films and (b) PA6-clay films into ethanol at various temperatures as a function of time. Nanoclay concentrations were further converted to mg clay/m^2 film. The hollow data points represent concentrations below the LOQ. Data for nanoclay release from PA6-clay films in (b) at 22 °C are not shown since the concentrations were below the LOQ. Fitted lines are included as a visual guide.

5.3.3 Effect of film thickness on nanoclay release

ASTM D4754-11 recommends a large film surface area exposed to the solvent. This large surface area is critical in order to detect the release of nanoclay particles since the nanocomposite film contains a small amount of nanoclay. To enable the large surface area, the method suggests the film to be cut into many circles and immersed into the solvent, as shown in Figure 5.2. There is a concern if the edge of the film affects the overall nanoclay release, since the release from the edge may be different from the intact surface. In order to address this concern, the release assessment of nanoclay from PP-clay films with two different thicknesses (22.5 ± 1.1 μm and 45.6 ± 1.3 μm) was carried out. As shown in Figure 5.6, regardless of the film thickness, the amount of nanoclay relesased from both films are equivalent, revealing that the edge of the film did not have an obvious effect on the nanoclay release compared to the film surface. It was also revealed that the nanoclay release only occurred at the film surface but not the bulk of the film, as no increase of the nanoclay release was found while the volume of the film was doubled (as the thickness was doubled).

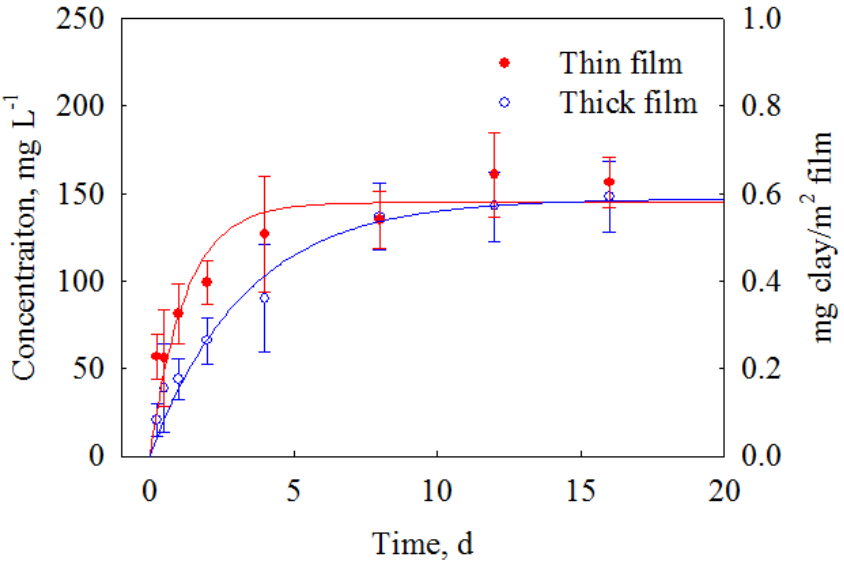

Figure 5.6 Amounts of nanoclay particles released from PP-clay films with different thicknesses into ethanol as a function of time. Nanoclay concentrations were further converted to mg clay/m^2 film. Fitted lines are included as a visual guide.

5.3.4 Characterization of released nanoclay particles

Figure 5.7 shows the nanoclay particles released into the solvent as visualized by TEM. The dark areas within the circles in each image consist of multiple parallel lines representing the stack of clay layers (images with higher magnification of the circled areas are shown in Appendix 9). EDS analysis showed that the particle contains O (48.44 wt%), Si (33.07 wt%) and Al (13.31 wt%), which are the major elements of MMT nanoclay. The Si and Al contents, as determined by EDS analysis, were converted to the corresponding contents in the I44P clay by multiplying by 65 % (*i.e.*, the MMT content in I44P clay; the remaining 35 % is surfactant and does not contain the three elements mentioned above). The resulting values were 21.5 % Si and 8.6 % Al, with a Si/Al ratio of 2.5, similar to the values by XRF analysis of pure I44P clay (20 %

Si and 7.8 % Al, with a Si/Al ratio of 2.6). The nanoclay particles observed under TEM are much larger (500-1000 nm) in one dimension than those in the polymer matrix, probably due to the aggregation of small particles in the solvent after release from the film.

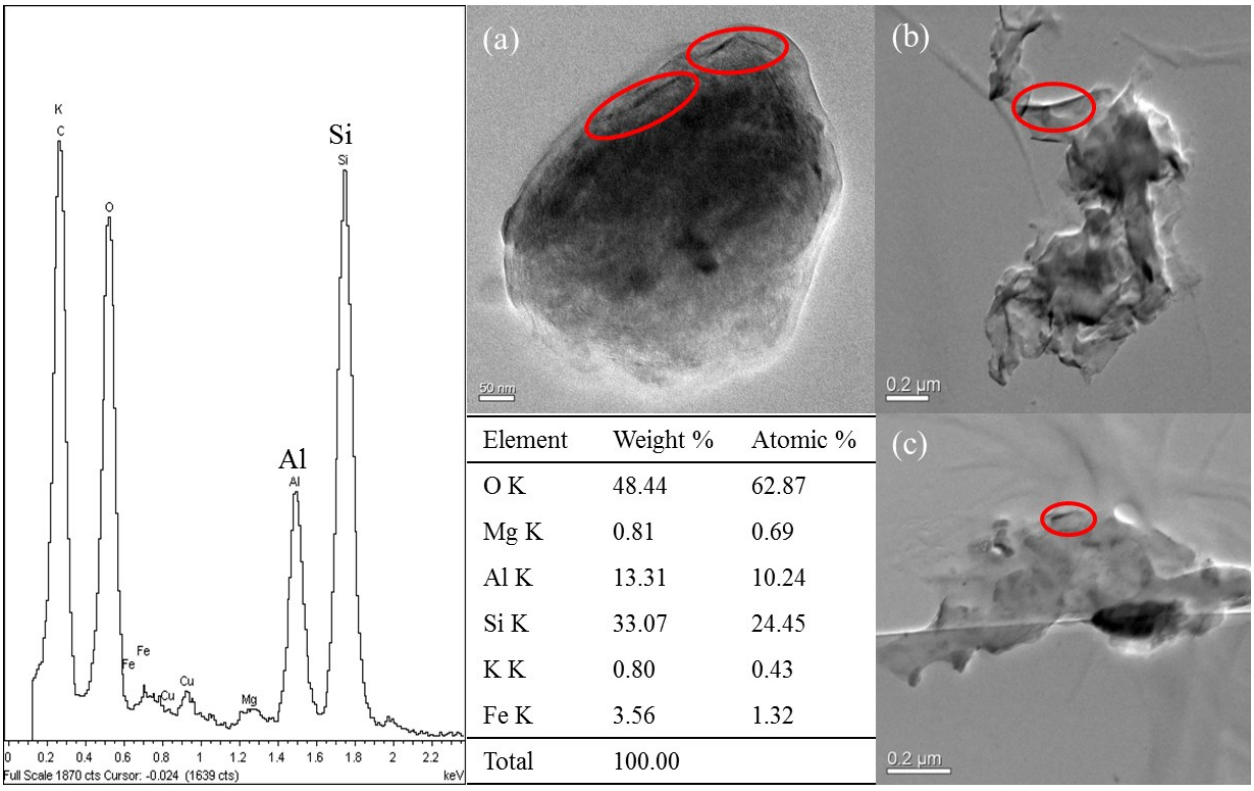

Element	Weight %	Atomic %
O K	48.44	62.87
Mg K	0.81	0.69
Al K	13.31	10.24
Si K	33.07	24.45
K K	0.80	0.43
Fe K	3.56	1.32
Total	100.00	

Figure 5.7 TEM images of released nanoclay particles from the PP-clay film and the corresponding EDS analysis for the particle in image (a). The structures (multiple parallel lines) within the circles exhibit the stacking of clay layers. Scale bar: 50 nm for image (a), 200 nm for images (b) and (c).

5.3.5 Change of d-spacing after solvent exposure

Figure 5.8 shows the results of an initial experiment where solvent exposure caused structural changes to the nanoclay within the nanocomposite film. The *d*-spacing of the nanoclay in the PP-clay film increased from 3.19 to 3.42 nm after exposure to ethanol at 70 °C for 2 h, due

to the absorption of solvent by nanoclay that expanded the clay gallery. After the film was removed from the solvent, the *d*-spacing decreased from 3.42 nm to 2.75 nm over time (XRD patterns are in Appendix 10), to a level that was even below the initial *d*-spacing value (3.19 nm) before exposure to the solvent and similar to the level of the clay powder. Excluding the effect of solvent evaporation, the additional decrease of *d*-spacing was assumed to be due to the release of surfactant, which caused the collapse of the clay gallery.

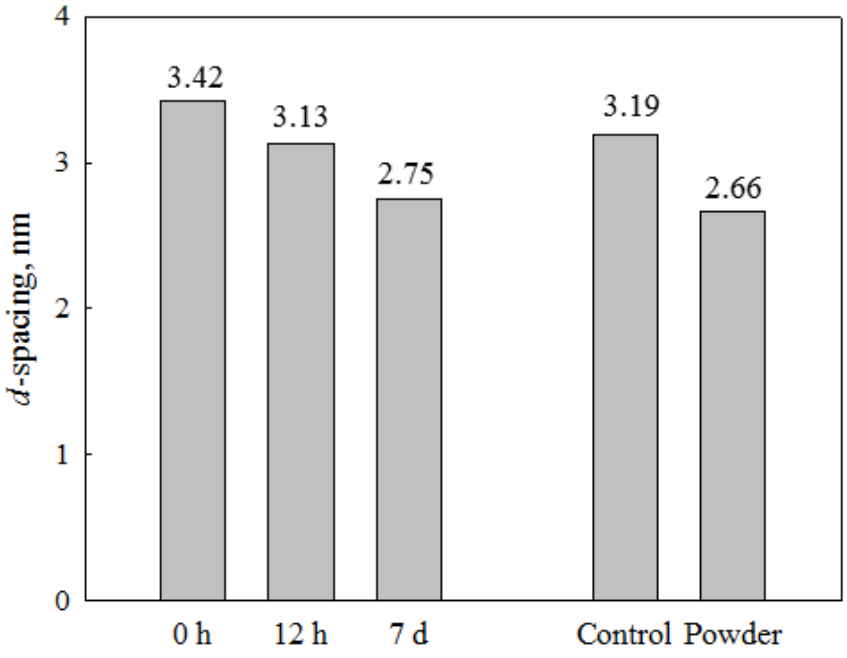

Figure 5.8 Change of *d*-spacing of nanoclay in PP-clay film after immersion in ethanol at 70 °C for 2 h and then exposing to air at room temperature for 0 h, 12 h and 7 d. Control represents PP-clay film before immersion in ethanol, and Powder represents dry clay powder. The experiment was conducted in one replicate.

5.3.6 Release of surfactant from nanocomposite films

The amount of each surfactant component released from nanocomposite films as well as from the nanoclay in suspension as a function of time was calculated using the calibration curve. The total amount of surfactant was interpreted as a summation of the three components ($C_{16}C_{16}$, $C_{16}C_{18}$ and $C_{18}C_{18}$) and the results are shown in Figure 5.9. The surfactant release was affected by temperature as there was more surfactant released from both nanocomposite films at a high temperature (70 °C) than at a low temperature (22 °C) at equilibrium. It took less time to achieve equilibrium of the surfactant release from PP-clay films than from PA6-clay films at all temperatures. The more rapid rate of release of surfactant from the PA6-clay film could be due to the slightly swelling of PA6 in ethanol as reported for other nylon films [McNally *et al.* 1997], while PP has better resistance to the solvent. As a consequence, the solvent easily penetrated the PA6 matrix, swelled the nanoclay particles and interacted with the surfactant.

When comparing the amount of surfactant released from the film and from the nanoclay suspension (control), PA6-clay films released more surfactant than the control did, while less surfactant was released from PP-clay films than that from the control. It was assumed that the amount of surfactant released from the nanocomposite film would not be greater than that released from the corresponding control, because of the probable absorption of surfactant by the polymer. The unusual phenomenon for the PA6-clay film can be explained by the large interfacial forces between the nanoclay and the polymer as demonstrated previously (exfoliated structure of the nanocomposite and the formation of hydrogen bonding between the nanoclay and the polymer). Such interfacial forces facilitate the exfoliation of nanoclay which promote strong friction among the clay layers and the polymer matrix during film processing with a combination of high processing temperature (above the degradation temperature of the O-MMT) [Cervantes-Uc *et al.* 2007], helping the release of extra surfactant from nanoclay surfaces into

the polymer matrix.

Both nanocomposite films released much greater amounts of surfactant (up to 3.5 mg L^{-1} from PP-clay film, and up to 16.2 mg L^{-1} from PA6-clay film) than nanoclay particles (0.15 mg L^{-1} max. from PP-clay film, and 0.1 mg L^{-1} max. from PA6-clay film) into the solvent. Nanoclay particles and surfactants differ in physical properties such as size and shape. Compared with nanoclay particles, the surfactant molecules are smaller in size so they can more easily move within the polymer.

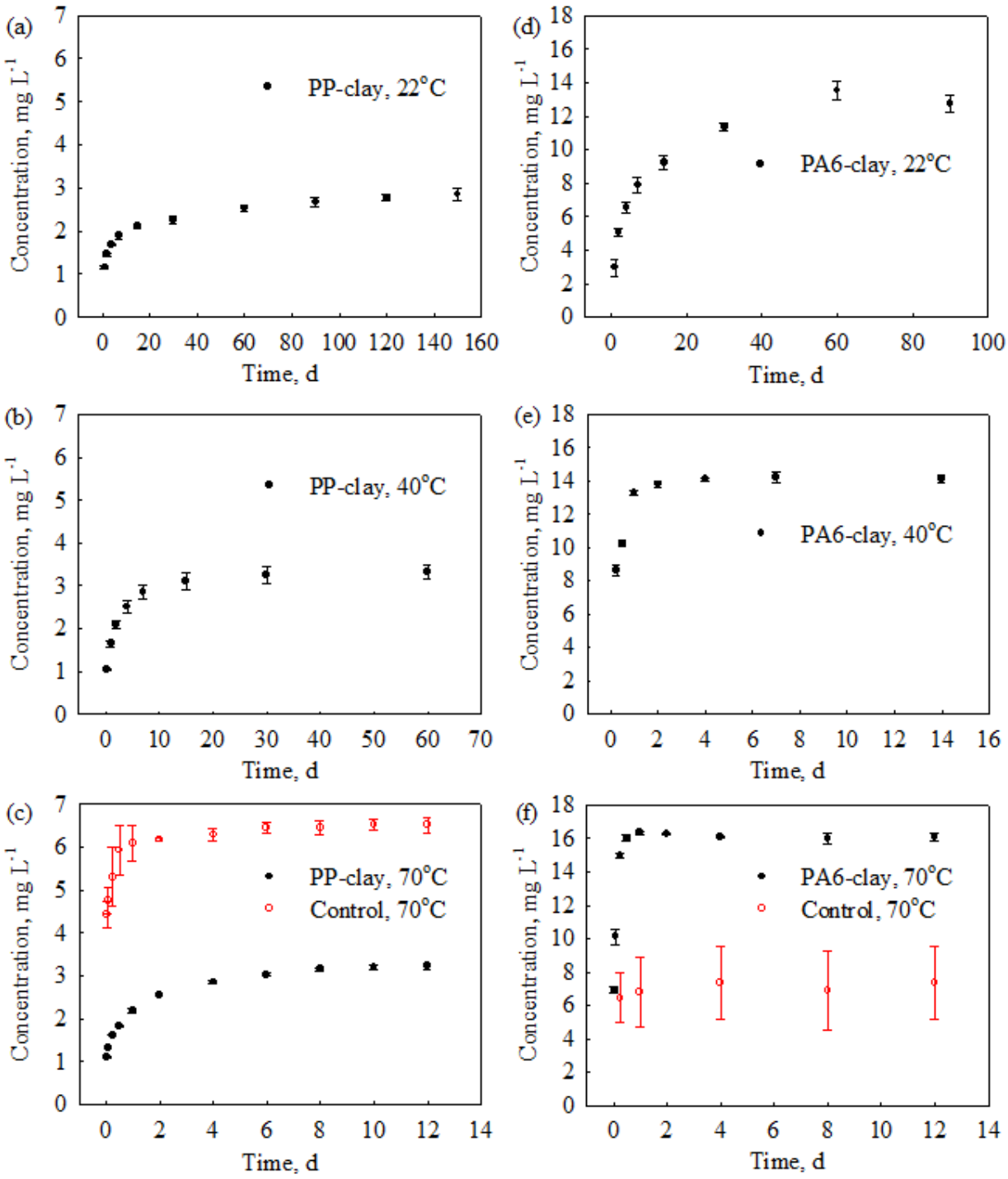

Figure 5.9 Total amount of surfactant released from PP-clay films into ethanol at (a) 22 °C, (b) 40 °C and (c) 70 °C; and from PA6-clay films into ethanol at (d) 22 °C, (e) 40 °C and (f) 70 °C as a function of time. Control represents nanoclay suspensions in ethanol with equivalent amount of nanoclay in nanocomposite films.

5.3.7 Determination of D and $K_{P,F}$

Once the nanoclay were embedded into the polymer, the surfactant may be released from the nanoclay surface into the polymer matrix during the polymer processing or when the nanoclay was in contact with the solvent due to the solvent penetration into the polymer matrix. This part of surfactant was considered as "free" and their release may follow the diffusion behavior of small molecules within the polymer matrix due to the presence of free volume and polymer chain relaxation. To describe the release of "free" surfactant from both nanocomposite films, the Fick's diffusion equation (Equation 2.2) was applied and the related migration curves are shown in Figure 5.10. It seems that the surfactant release exhibits Fickian behavior as the experimental data are closely around the best-fitting curve (entral line). The inner lines beside the best-fitting curve are 95% confidence interval of the curve, and the outer lines indicate 95% prediction interval of the experimental values. The errors of the experimental data are mainly scattered ramdomly around the zero residual line and within two standard residual values, showing good fit between the experimental and the predicted values. The residual plots in (a) and (c) of Figure 5.10 exhibit a trend (decrease first and then increase), revealing that the fiting of the model to cases (a) and (c) is not as good as the other cases.

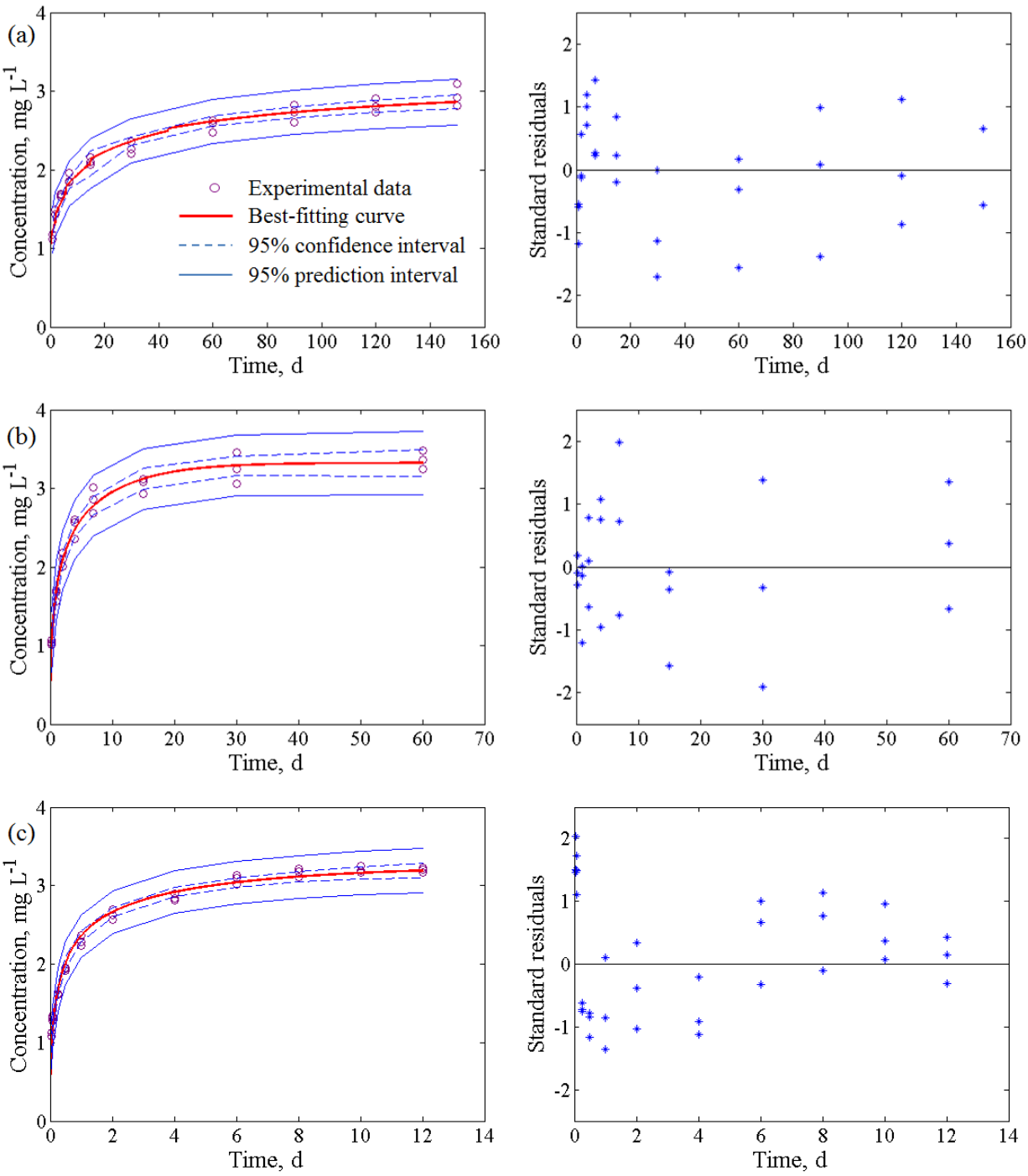

Figure 5.10a Experimental and predicted release of surfactant from PP-clay films into ethanol at (a) 22 °C, (b) 40 °C and (c) 70 °C as a function of time. The associated standard residual plot for each graph is shown in the right with dark line indicating zero residual.

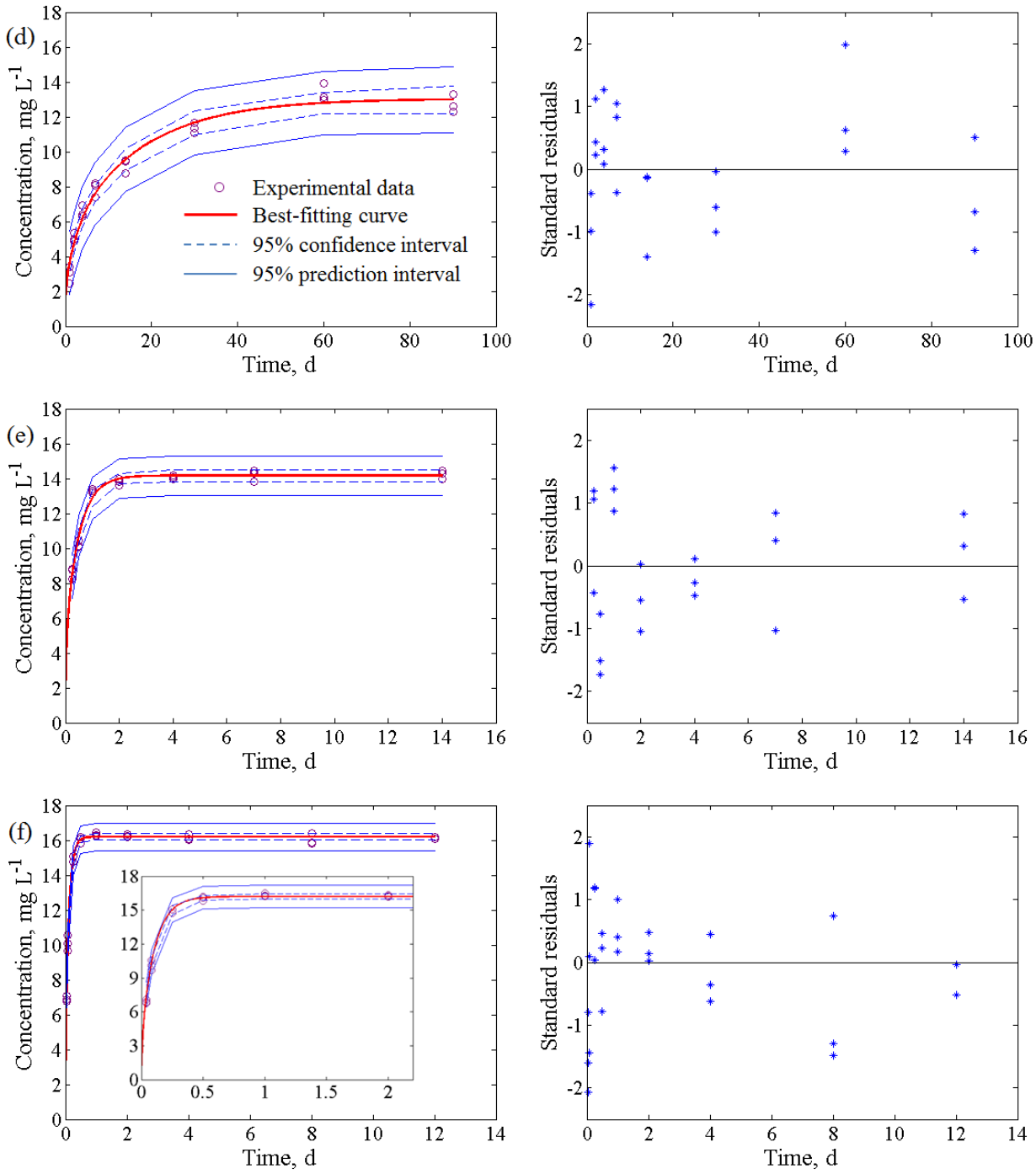

Figure 5.10b Experimental and predicted release of surfactant from PA6-clay films into ethanol at (d) 22 °C, (e) 40 °C and (f) 70 °C as a function of time. The associated standard residual plot for each graph is shown in the right with dark line indicating zero residual.

Table 5.2 lists the parameters including diffusion coefficient (*D)* and partition coefficient ($K_{P,F}$) derived from Equation 2.2. D values were in a scale of 10^{-13} to 10^{-12} cm^2 s^{-1} for the "free" surfactant release from PP-clay films, and 10^{-13} to 10^{-10} cm^2 s^{-1} for the surfactant release from PA6-clay films. Higher *D* values were obtained for PA6-clay films than for PP-clay films at all temperatures, indicating a faster release of free surfactant from PA6-clay films and less time spent to reach the equilibrium of surfactant release, which were in agreement with the experimental result shown in Figure 5.9. $K_{P,F}$ values were smaller at a high temperature (70 °C) than at a low temperature (22 °C) for the surfactant release from both nanocomposite films. A smaller $K_{P,F}$ value could result in a higher surfactant concentration in the solvent at equilibrium of surfactant release as indicated by Equation 2.4. This phenomenon was in a match with the experimental result also shown in Figure 5.9.

It should be noticed that the work presented here is an intial trial to predict the surfactant release from polymer-clay nanocomposites by mathematical models. The surfactant was restricted to those unattached to the nanoclay during the release process. All the parameters derived from the Fick's diffusion equation are theoretical values. For the better utilization of the Fick's diffusion models, future work needs to be carried out to estimate the actual amount of "free" surfactant in the nanocomposite films, to determine the experimental $K_{P,F}$ value. Thus, the theoretical values could be obtained based on the measured experimental values.

Table 5.2 Parameters determined from Equation 2.2 for the surfactant release from nanocomposite films into ethanol under different temperatures.

Material	Temp. °C	$D\times10^{-13}$ $cm^2\ s^{-1}$	α	$K_{P,F}$[a]	$M_{F,\infty}$ mg L^{-1}	RMSE mg L^{-1}
PP-clay	22	0.97±0.26^{Ab}	0.14±0.01^{A}	2725±153^{A}	2.97±0.08^{A}	0.0934
	40	9.38±3.75^{B}	0.22±0.06^{B}	1709±484^{B}	3.33±0.06^{B}	0.1188
	70	30.17±2.51^{C}	0.22±0.01^{B}	1687±63^{B}	3.02±0.08^{C}	0.0568
PA6-clay	22	5.11±1.86^{A}	0.54±0.19^{A}	697±249^{A}	13.15±0.33^{A}	0.5423
	40	248.15±63.18^{B}	1.01±0.39^{A}	374±144^{A}	14.17±0.11^{B}	0.3538
	70	1663.87±88.62^{C}	7.66±3.95^{B}	49±25^{B}	16.20±0.06^{C}	0.2592

Note: [a] $K_{P,F}$ values are estimated from the experimental values and calculated from Equation 2.3.

[b] The values are expressed as mean ± standard error; for each property within each polymer type, means with different uppercase letters are significantly different ($P < 0.05$, $n = 3$).

5.4 Conclusions

The release of both nanoclay particles and surfactant from two nanocomposites was observed in this study. The release of nanoclay particles was dictated by interactions among the nanoclay, the polymer and the solvent. The release process may be described as (a) the penetration of solvent into the polymer matrix causing the interaction between the solvent and the nanoclay within the polymer; and (b) the release of nanoclay particles from the polymer surface due to the slightly swelling of the polymer by the solvent especially at a high temperature. There was a correlation between nanoclay mobility and polymer-clay interaction which was

indicated by the nanocomposite morphology. A well exfoliated morphology represented a better polymer-clay interaction, thereby reducing the release of nanoclay particles. A small amount of nanoclay particles (in μg L^{-1} level) were released from nanocomposites, while the amount of surfactant released from nanocomposites was much larger (in mg L^{-1} level). It should be noticed that sometimes, the film processing may cause extra surfactant release from the nanoclay triggered by the combination of high processing temperature and the strong frictional interaction between the polymer and the nanoclay. This part of surfactant is capable to migrate from the polymer which increases the potential risks of surfactant due to the increase of the exposure dose. The surfactant release followed the diffusion behavior of small molecules within the polymer matrix and can be described by the Fick's diffusion equation. As part of the nanoclay, the release of surfactant caused changes in nanoclay structure which in turn may impact the release of nanoclay particles and the performance of nanocomposite such as strength or barrier properties.

APPENDICES

APPENDIX 1: Technical information of Pro-fax 6523

Table A-1 Technical information of Pro-fax 6523.

Property	
Density - Specific Gravity	0.90 g/cm^3
Melt Flow Rate	4 g/10 min (230 °C/2.16 kg)
Flexural Modulus	1380 MPa (1.3 mm/min)
Flexural Modulus	200000 psi (0.05 in/min)
Tensile Strength @ Yield	33 MPa (50 mm/min)
Tensile Strength @ Yield	4800 psi (2 in/min)
Tensile Elongation @ Yield	12 %
Density	0.90 (23 °C)
Tensile Stress at Yield	30 MPa
Tensile Strain at Yield	12 % (23 °C)
Flexural modulus	1270 MPa (23 °C)
Charpy notched impact strength	6.7 kJ/m² (23 °C)
Notched izod impact strength	6.2 kJ/m² (23 °C)
Notched Izod Impact	53 J/m (23 °C)
Notched Izod Impact	1.0 ft-lb/in (73 °F)
Deformation Temperature Under Load	88 °C (0.45 MPa)
Deformation Temperature Under Load	190 °F (66 psi)

Note: All the data are available at: https://polymers.lyondellbasell.com/portal/site/basell

APPENDIX 2: Technical information of Bondyram® 1001

Table A-2 Technical information of Bondyram® 1001.

Property	ISO Test Method	
Density	1183	0.9 g/cm^3
MFI	1133, 190 °C /2.16 kg	100 °C
Melting point	DSC	160 °C
Maleic anhydride level	FTIR	1 %

Note: All the data are available at: http://www.polyram-usa.com/products-coupling-agents.html

APPENDIX 3: Technical information of Ultramid® B40 01

Table A-3 Technical information of Ultramid® B40 01.

Property	ISO Test Method	
Density	1183	1.13 g/cm^3
Melting Point	3146	220 °C
Water absorption	62	
(23 °C/50% RH)		2.6
(23 °C/Saturation)		9.5
Viscosity Number (0.5% in 96% Sulfuric Acid)	307	250 cm/g
Relative Viscosity (1% in 96% Sulfuric Acid)	307	4
Bulk Density		700 Kg/m
Pellet Shape		cylindrical
Pellet Size		2 to 2.5 mm
Moisture Content	15512	<0.1 %

Note: All the data are available at:

http://iwww.plasticsportal.com/products/dspdf.php?type=iso&param=Ultramid+B40+01

APPENDIX 4: LC-MS/MS data for the modeling of surfactant release from PP-clay films

Table A-4 LC-MS/MS data for the modeling of surfactant release from PP-clay films.

PP-clay, 22°C Mg L^{-1}	Time s	PP-clay, 40°C Mg L^{-1}	Time s	PP-clay, 70°C Mg L^{-1}	Time s
1.175	86400	1.036	21600	1.084	3600
1.178	86400	1.013	21600	1.130	3600
1.121	86400	1.068	21600	1.080	3600
1.493	172800	1.556	86400	1.286	7200
1.433	172800	1.701	86400	1.341	7200
1.431	172800	1.683	86400	1.319	7200
1.694	345600	2.011	172800	1.610	21600
1.650	345600	2.179	172800	1.621	21600
1.677	345600	2.098	172800	1.613	21600
1.851	604800	2.363	345600	1.915	43200
1.958	604800	2.604	345600	1.950	43200
1.846	604800	2.567	345600	1.944	43200
2.060	1296000	2.685	604800	2.236	86400
2.156	1296000	3.013	604800	2.366	86400
2.098	1296000	2.863	604800	2.281	86400
2.205	2592000	2.933	1296000	2.570	172800
2.362	2592000	3.112	1296000	2.692	172800
2.258	2592000	3.078	1296000	2.627	172800
2.471	5184000	3.063	2592000	2.836	345600
2.586	5184000	3.455	2592000	2.899	345600
2.630	5184000	3.250	2592000	2.817	345600
2.602	7776000	3.242	5184000	3.010	518400
2.737	7776000	3.484	5184000	3.129	518400
2.821	7776000	3.367	5184000	3.099	518400
2.726	10368000			3.104	691200
2.797	10368000			3.181	691200
2.909	10368000			3.215	691200
2.809	12960000			3.167	864000
2.920	12960000			3.246	864000
3.093	12960000			3.194	864000
				3.164	1036800
				3.205	1036800
				3.230	1036800

APPENDIX 5: LC-MS/MS data for the modeling of surfactant release from PA6-clay films

Table A-5 LC-MS/MS data for the modeling of surfactant release from PA6-clay films.

PA6-clay, 22°C Mg L^{-1}	Time s	PA6-clay, 40°C Mg L^{-1}	Time s	PA6-clay, 70°C Mg L^{-1}	Time s
3.418	86400	8.798	21600	6.750	3600
2.423	86400	8.222	21600	7.091	3600
3.081	86400	8.748	21600	6.878	3600
5.351	172800	10.155	43200	9.676	7200
4.845	172800	10.079	43200	10.088	7200
4.962	172800	10.421	43200	10.571	7200
6.273	345600	13.304	86400	14.763	21600
6.943	345600	13.181	86400	15.069	21600
6.401	345600	13.420	86400	15.075	21600
8.189	604800	13.792	172800	16.096	43200
8.069	604800	13.996	172800	16.160	43200
7.388	604800	13.614	172800	15.824	43200
9.478	1209600	14.068	345600	16.245	86400
8.761	1209600	13.997	345600	16.307	86400
9.473	1209600	14.204	345600	16.468	86400
11.647	2592000	14.309	604800	16.238	172800
11.099	2592000	13.802	604800	16.205	172800
11.322	2592000	14.462	604800	16.326	172800
13.146	5184000	14.276	1209600	16.034	345600
13.917	5184000	13.979	1209600	16.103	345600
12.958	5184000	14.459	1209600	16.319	345600
12.613	7776000			15.851	691200
13.278	7776000			15.800	691200
12.266	7776000			16.399	691200
				16.192	1036800
				16.059	1036800
				16.061	1036800
				6.750	3600
				7.091	3600

APPENDIX 6: Matlab function program for the fit of Equation 2.2 to the LC-MS/MS data

```
function Mpred = surfactantrelease(beta,t) % the calculations from this program are returned to the script program
% stop the program if a negative beta velue was obtained (parameters in the diffusion equation should always be positive)
if any(beta <= 0)
    Mpred = zeros(size(t));
    return
end

D = beta(1); % predicted best fit difusion coefficient, cm^2/s
mInf = beta(2); % predicted concentration at equilibrium, mg/L
a = beta(3); % predicted best fit alpha values, K_P,F can be obtained based on this value
global L % use thickness L of the nanocomposite films for all programs

% solution toward the infinite series or summation in the Fick's diffusion model (Eq. 2.2)
function x = qyu(n)
    % solve the non-linear equation tan(qn) = -aqn using binary split
    func = @(x) tan(x)+a*x;
    intv = [n*pi - pi/2 + 1e-5, n*pi];
    valv = [func(intv(1)), func(intv(2))];
    while abs(intv(2) - intv(1)) > 1e-6
        val = func((intv(2) + intv(1))/2);
        if sign(val) == sign(valv(1))
            intv(1) = (intv(2) + intv(1))/2;
            valv(1) = val;
        else
            intv(2) = (intv(2) + intv(1))/2;
            valv(2) = val;
        end
    end
    x = mean(intv);
end

Mpred = ones(size(t)); % set 'Mpred' as 1 for all the observation/sampling times

nt=length(t);
for i=1:nt % time loop
    resid = 1;
    counter = 1;
    while abs(resid) > 1e-2 % loop this until the resid is very small (1e-2), the value may be adjusted in order to improve the fitting to the experimental data
        qn = qyu(counter);
```

```
            counter = counter + 1;
            resid = 2*a*(1+a)/(1+a+(a*qn)^2)*exp(-D*10^(-13)*(qn^2)/(L^2)*t(i));
            Mpred(i) = Mpred(i) - resid;
        end
        Mpred(i) = Mpred(i)*mInf;
end
end
```

Note: all words after % are explanation of different commands.

APPENDIX 7: Matlab script program for the fit of Equation 2.2 to the LC-MS/MS data

```
% use Equation 2.2 to describpe the surfactant release
clear
close all
format short

% input orginal data
data = xlsread('matlabdata.xlsx'); % load the data file
Mtobs = data(:,1); % set the values at column 1 as experimental Mt
Mtobs(isnan(Mtobs))=[];
tobs = data(:,2); % set the values at column 2 as time t
tobs(isnan(tobs)) = [];
size_t = size(tobs,1);

global L
L = 0.00211; % thickness of PA6-clay films (0.00225 for PP-clay films), cm
D = 50; % diffusion coefficient, initial guess, 10e-13 cm^2/s
a = 1; % alpha value, initial guess, a = (1/K_P,F) * (V_F/V_P), K_P,F is the patition coefficient
Minf = 15 % concentration at the equilibrium of surfactant release, initial guess, mg/L
beta0(1) = D; % set D value to beta1
beta0(2) = Minf; % set Minf value to beta 2
beta0(3) = a; % set alpha value to beta 3
beta=beta0; % set beta to intial guesses

[beta,resids,J,sigma,mse] = nlinfit(tobs',Mtobs',@surfactantrelease,beta0); % perform non-linear
regression on the experimental data through function program
ci = nlparci(beta,resids,J,0.05) % obtain asymptotic confidence interval and residuals

[Mpred, delta] = nlpredci(@surfactantrelease,tobs,beta,resids,J,0.05,'on','curve'); % obtain
confidence intervals for predicted concentration values ‘Mpred’
[M, deltaobs] = nlpredci(@surfactantrelease,tobs,beta,resids,J,0.05,'on','observation'); % obtain
prediction intervals for the observed concentration values ‘M’

% plot migration curve as M_ana vs t_ana, ‘M_ana’ represents predicted concentrations at a
series of time t_ana
b1=beta(1); % predicted best fit difusion coefficient
b2=beta(2); % predicted best fit concentration at equilibrium of surfactant release
b3=beta(3); % predicted best fit alpha value
Nt = data(size_t,2);
t_ana=0:Nt/1000:Nt; % time ‘t_ana’ starting from 0 to total experimental time length 'Nt’ with
an interval of Nt/1000
Nt_ana=length(t_ana);
```

```
M_ana = surfactantrelease(beta,t_ana);

SS=0;
for i = 1:length(Mpred)
SS = SS + resids(i)^2; % sum of squared error
end
n = length(Mpred);
p = length(beta);
nu = n-p; % degree of freedom
MSE = SS/nu; % mean squared error
rmse = sqrt(MSE); % root mean squared error
covmat = inv(J'*J)*MSE;
stderr_beta1 = sqrt(covmat(1,1)); % obtain standard error in beta1 (diffusion coefficient)
stderr_beta2 = sqrt(covmat(2,2)); % obtain standard error in beta2 (Minf, predicted equilibrium
surfactant concentration)
stderr_beta3 = sqrt(covmat(3,3)); % obtain standard error in beta3 (alpha values, which can be
further converted to partition coefficient K_P,F)
standardresiduals = resids/rmse; % obtain standard residual
asyCIup = Mpred+delta;
asyCIlow = Mpred-delta;
predCIup = M+deltaobs;
predCIlow = M-deltaobs;

figure
hold on
h1(1) = plot(tobs/86400,Mtobs,'o','MarkerEdgeColor',[0.5 0 0.5]); % plot experimental
concentration values with time
h1(2) = plot(t_ana/86400,M_ana,'r', 'LineWidth',2); % plot predicted concentration values with
time
h1(3) = plot(tobs/86400,asyCIup,'--'); % plot upper CI as dashed line
h1(4) = plot(tobs/86400,predCIup,'-'); % plot upper PI as solid line
h1(5) = plot(tobs/86400, asyCIlow,'--'); % plot lower CI as dashed line
h1(6) = plot(tobs/86400, predCIlow,'-'); % plot lower PI as solid line
V=axis;
V(4)=18; % set the max. value of 18 for y-axis of sufactant release from PA6-clay films (set 4
for PP-clay films)
axis(V);
xlabel('Time, d');
ylabel('Concentration, mg L^{-1}');

figure
hold on
h1(1) = plot(tobs/86400,resids,'*'); % plot residuals with time
xlabel('Time, d');
ylabel('Residuals');
```

```
figure
hold on
h1(1) = plot(tobs/86400,standardresiduals,'*'); % plot standard residuals with time
xlabel('Time, d');
ylabel('Standard residuals');

% get the output of the program
beta % multiply by 10^-13 to get the actual diffusion coefficient
ci
MSE
rmse
stderr_beta1
stderr_beta2
stderr_beta3
cond(J) % closer to 0, smaller error of the solution
```

Note: all words after % are explanation of different commands.

APPENDIX 8: DSC curves of PA6 and PA6-clay films

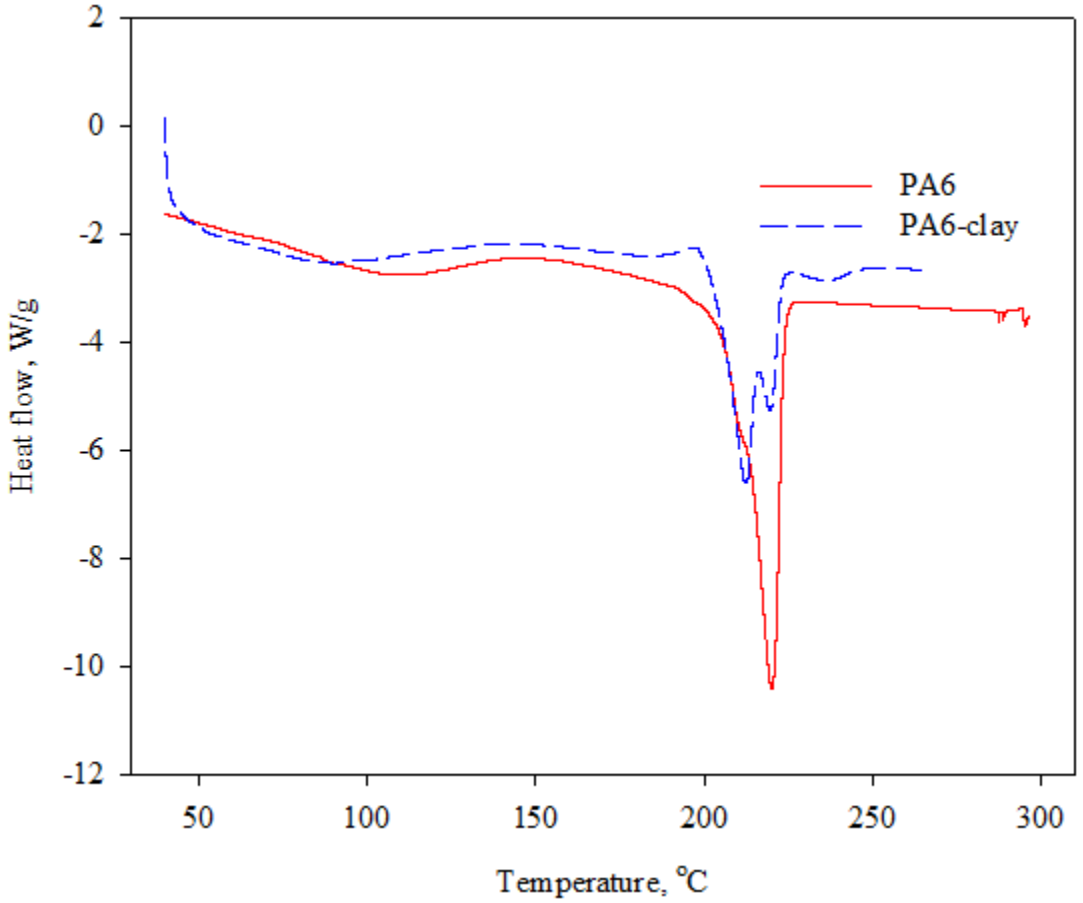

Figure A-1 DSC curves of PA6 and PA6-clay films.

APPENDIX 9: Images of the circled areas in Figure 5.7 (b) and (c)

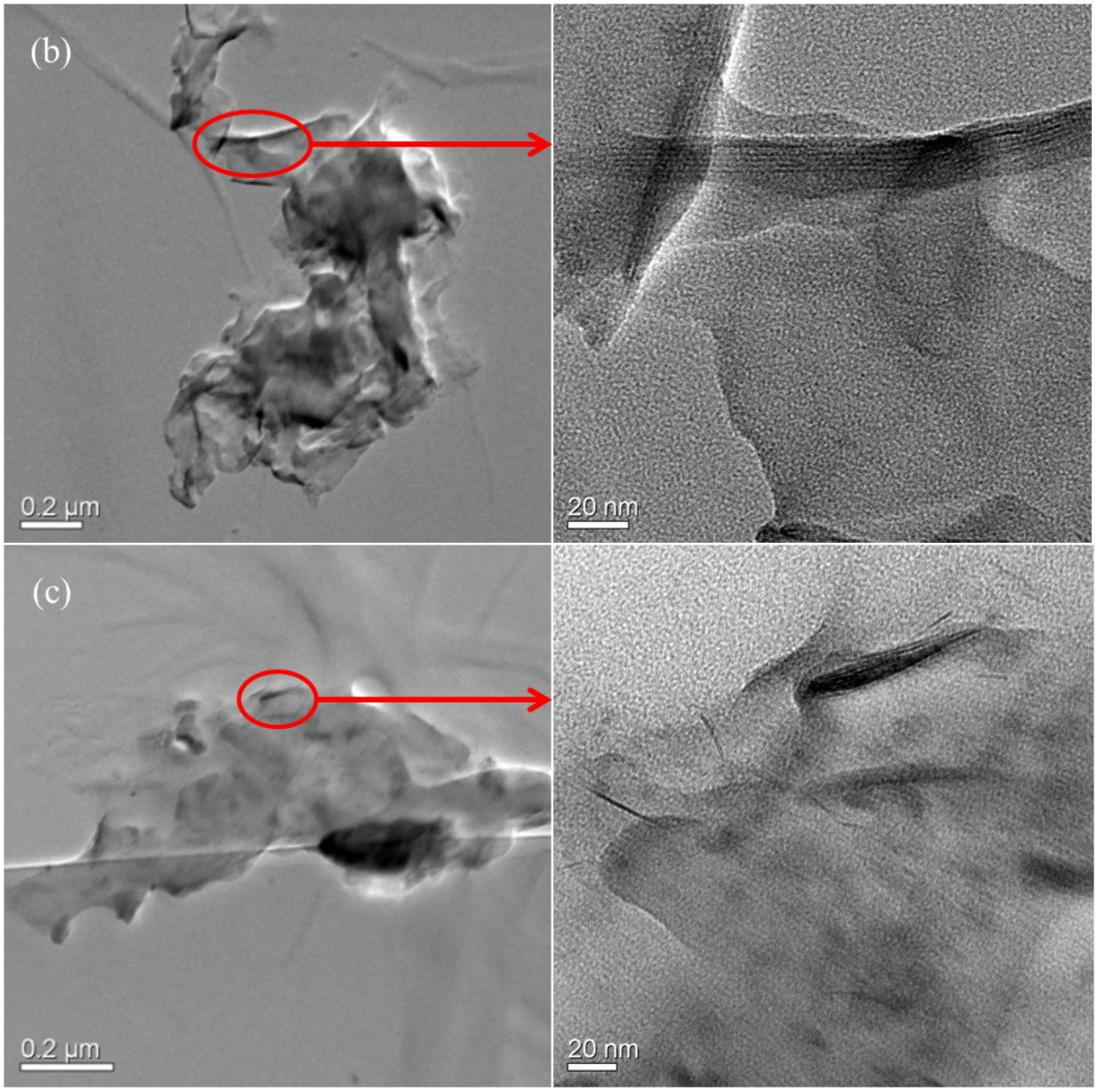

Figure A-2 Images of the circled areas in Figure 5.7 (b) and (c).

Note: Images of the circled area in Figure 5.7 (a) are not available.

APPENDIX 10: XRD patterns of PP-clay film after solvent exposure

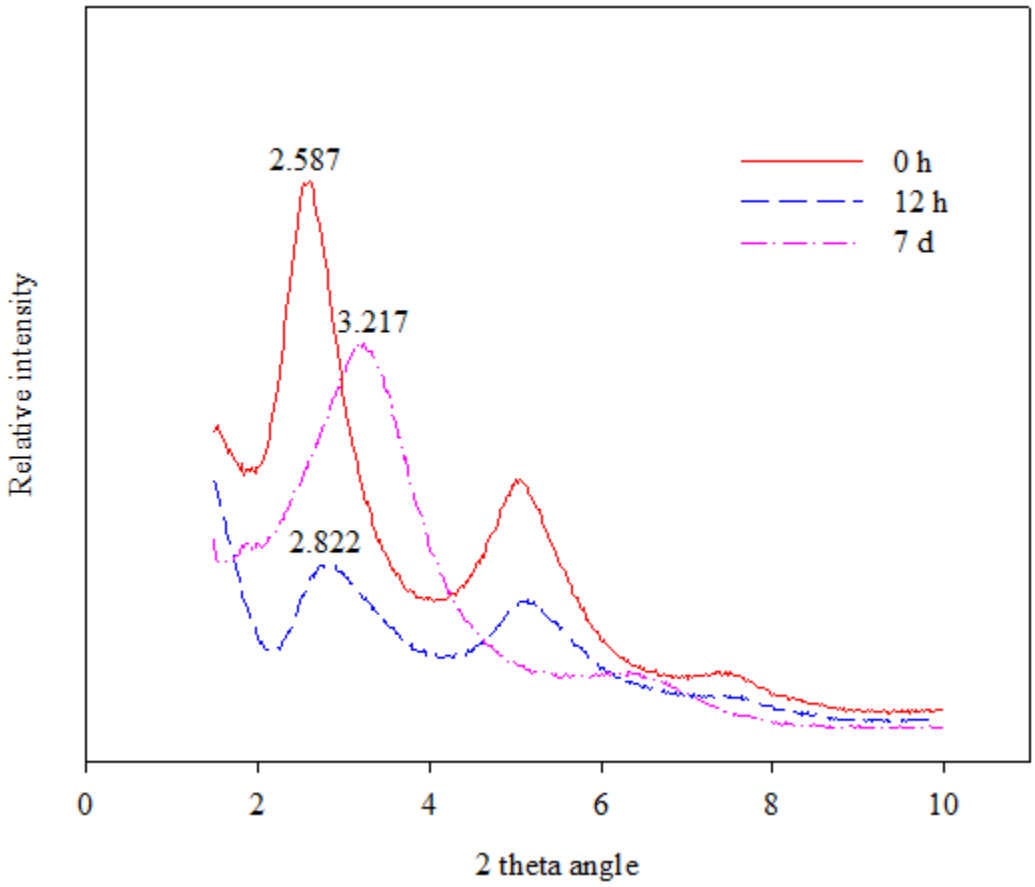

Figure A-3 XRD patterns of PP-clay film after solvent exposure.

Note: The experiment was conducted in one replicate. A PP-clay film was firstly inmmersed in ethanol at 70 °C for 2 h, and then exposed to air at room temperature for 0 h, 12 h and 7 d. XRD pattern of PP-clay film before immersion in ethanol and XRD pattern of dry clay powder can be found in Figure 5.3a

BIBLIOGRAPHY

BIBLIOGRAPHY

Baek, M.; Lee, J.A.; Choi, S.J. Toxicological effects of a cationic clay, montmorillonite *in vitro* and *in vivo*. *Mol. Cell Toxicol.* **2012**, 8, 95-101.

Bal, S.; Samal, S.S. Carbon nanotube reinforced polymer composites-A state of the art. *Bull. Mater. Sci.* **2007**, 30, 379-386.

BCC Research. Global Markets for Nanocomposites, Nanoparticles, Nanoclays, and Nanotubes. BCC Research LLC, Wellesley, MA, USA, 2014. Available from: http://www.bccresearch.com/market-research/nanotechnology/nanocomposites-market-nan021f.html

Cervantes-Uc, J.M.; Cauich-Rodriguez, J.V.; Vazquez-Torres, H.; Garfias-Mesias, L.F.; Paul, D.R. Thermal degradation of commercially available organoclays studied by TGA-FTIR. *Thermoch. Acta* **2007**, 457, 92-102.

Chaudhry, Q.; Scotter, M.; Blackburn, J.; Ross, B.; Boxall, A.; Castle, L.; Aitken, R.; Watkins, R. Applications and implications of nanotechnologies for the food sector. *Food Addit. Contam.* **2008**, 25, 241-258.

Choudalakis, G.; Gotsis, A.D. Permeability of polymer/clay nanocomposites: a review. *Eur. Polym. J.* **2009**, 48, 967-984.

De A. Prado, L.A.S.; Karthikeyan, C.S.; Schulte, K.; Nunes, S.P.; De Torriani, I.L. Organic modification of layered silicates: structural and thermal charaterizations. *J. Non-cryst. Solids* **2005**, 351, 970-975.

[EFSA] European Food Safety Authority. Guidance on the risk assessment of the application of nanoscience and nanotechnologies in the food and feed chain. *EFSA J.* **2011**, 9, 2140 [36 pp]. Available from: http://www.efsa.europa.eu/en/efsajournal/doc/2140.pdf

[FDA] Food and Drug Administration. 2007. Guidance for Industry: Preparation of Food Contact Notifications and Food Additive Petitions for Food Contact Substances: Chemistry Recommendations. Available from: http://www.fda.gov/Food/GuidanceRegulation/GuidanceDocumentsRegulatoryInformation/ucm081818.htm

Gottschalk, F.; Nowack, B. The release of engineered nanomaterials to the environment. *J. Environ. Monit.* **2011**, 13, 1145-1155.

Han, K Q.; Yu, M.H. Study of the preparation and properties of fabrics of a PET/TiO2 nanocomposite prepared by in situ polycondensation. *J. Appl. Polym. Sci.* **2006**, 100, 1588-1593.

Illers, K.H. Polymorphie, Kristallinität und Schmelzwärme von Poly(ε-caprolactam), 2. Kalorimetrische Untersuchungen. *Macromol. Chem.* **1978**, 179, 497-507.

Kashiwagi, T.; Grulke, E.; Hilding, J.; Groth, K.; Harris, R.; Butler, K.; Shields, J.; Kharchenko, S.; Douglas, J. Thermal and flammability properties of polypropylene/carbon nanotube nanocomposites. *Polymer* **2004**, 45, 4227-4239.

Katoh, Y.; Okamoto, M. Crystallization controlled by layered silicates in nylon 6-clay nano-composite. *Polymer* **2009**, 50, 4718-4726.

Lagaron, J.M.; Lopez-Rubio, A. Nanotechnology for bioplastics: opportunities, challenges and strategies. *Trends Food Sci. Tech.* **2011**, 22, 611-617.

Lordan, S.; Kennedy, J.E.; Higginbotham, C.L. Cytotoxic effects induced by unmodified and organically modified nanoclays in the human hepatic HepG2 cell line. *J. Appl. Toxicol.* **2011**, 31, 27-35.

McNally, T.; McNally, G. M.; Ahmad, M. N.; Murphy, W. R.; Kennedy, R. Sorption and diffusion of fuel components in various nylons. In SPE/ANTEC'97 Conference Proceeding Volume III, 1997, pp. 2794-2799.

[NRC] National Research Council. Research Progress on Environmental, Health, and Safety Aspects of Engineered Nanomaterials. National Academy Press, Washington DC, USA, 2013. Available from: http://www.nap.edu/catalog.php?record_id=18475

Patel, H.A.; Somani, R.S.; Bajaj, H.C.; Jasra, R.V. Nanoclays for polymer nanocomposites, paints, inks, greases and cosmetics formulations, drug delivery vehicle and waste water treatment. *Bull. Mater. Sci.* **2006**, 29, 133-145.

Paul, D.R.; Robeson, L.M. Polymer nanotechnology: Nanocomposites. *Polymer* **2008**, 49, 3187-3204.

Pereira de Abreu, D.A.; Paseiro Losada, P.; Angulo, I.; Cruz, J.M. Development of new polyolefin films with nanoclays for application in food packaging. *Eur. Polym. J.* **2007**, 43, 2229-2243.

Radheshkumar, C.; Munstedt, H. Antimicrobial polymers from polypropylene/silver composites-Ag^{+} release measured by anode stripping voltammetry. *React. Funct. Polym.* **2006**, 66, 780-788.

Rathi, S.; Dahiya, J.B. Polyamide 66/nanoclay composite: synthesis, thermal and flammability properties. *Adv. Mater. Lett.* **2012**, 3, 381-387.

Raynor, P.C.; Cebula, J.I.; Spanqenberger, J.S.; Olson, B.A.; Dasch, J.M.; D'Arcy, J.B. Assessing potential nanoparticles release during nanocomposite shredding using direct-reading instruments. *J. Occup. Environ. Hyg.* **2012**, 9, 1-13.

Reichert, P.; Nitz, H.; Klinke, S.; Brandsch, R.; Thomann, R.; Mulhaupt, R. Poly(propylene)/organoclay nanocomposite formation. Macromol. *Mater. Eng.* **2000**, 275, 8-17.

Routledge, E.J.; Sumpter, J.P. Estrogenic activity of surfactants and some of their degradation products assessed using a recombinant yeast screen. *Environ. Toxicol. Chem.* **2009**, 15, 241-248.

Silvestre, C.; Duraccio, D.; Cimmino, S. Food packaging based on polymer nanomaterials. *Prog. Polym. Sci.* **2011**, 36, 1766-1782.

Simon, P.; Chaudhry, Q.; Bakos, D. Migration of engineered nanoparticles from polymer packaging to food – a physicochemical view. *J. Food Nutr. Res.* **2008**, 47, 105-113.

Sinha Ray, S.; Okamoto, M. Polymer/layered silicate nanocomposites: a review from preparation to processing. *Prog. Polym. Sci.* **2003**, 28, 1539-1641.

Sonnenschein, C.; Soto, A.M. An updated review of environmental estrogen and androgen mimics and antagonists. *J. Steroid Biochem. Mol. Biol.* **1998**, 65, 143-150.

Szakal, C.; Roberts, S.M.; Westerhoff, P.; Bartholomaeus, A.; Buck, N.; Illuminato, I.; Canady, R.; Rogers, M. Measurement of nanomaterials in foods: Integrative consideration of challenges and future prospects. *ACS Nano* **2014**, 8, 3128-3135.

Talmage, S.S. Environmental and human safety of major surfactants: alcohol ethoxylates and alkylphenol ethoxylates. A report to the Soap and Detergent Association. CRE Press: Boca Raton, FL, USA, 1994.

Thomas, T.; Thomas, K.; Sadrieh, N.; Savage, N.; Adair, P.; Bronaugh, R. Research strategies for safety evaluation of nanomaterials, Part VII: Evaluating consumer exposures to nanoscale materials. *Toxicol. Sci.* **2006**, 91, 14-19.

Van der Wal, A.; Mulder, J.J.; Gaymans, R.J. Facture of polypropylene: 2. The effect of crystallinity. *Polymer* **1998**, 39, 5477-5481.

Venhus, S.H.; Mehrvar, M. Health effects, environmental impacts, and photochemical degradation of selected surfactants in water. *Int. J. Photoenergy* **2004**, 6, 115-125.

Verma, N.K.; Moore, E.; Blau, W.; Volkov, Y.; Babu, P.R. Cytotoxicity evaluation of nanoclays in human epithelial cell line A549 using high content screening and real-time impedance analysis. *J. Nanopart. Res.* **2012**, 14, 1137-1147.

Wan, T.; Wang, B.; Liao, S.; Clifford, M. Rheological investigation on the interaction of polyamide 6 with clay. *J. Appl. Polym. Sci.* **2012**, 125, E27-E33.

Yamashita, K.; Yoshioka, Y.; Higashisaka, K.; et al. Silica and titanium dioxide nanoparticles cause pregnancy complications in mice. *Nat. Nanotechnol.* **2011**, 6, 321-328.

Ying, G.G. Fate, behavior and effects of surfactants and their degradation products in the environment. *Environ. Int.* **2006**, 32, 417-431.

CHAPTER 6: General Conclusions and Future Work

6.1 General conclusions

For a long time, scientists from the engineering field believe that nanoparticles are not likely to migrate from the polymer because of their huge size. In this research, the release of nanoclay particles from nanocomposites was confirmed as well as the surfactant used as the organo-modifer of nanoclay. The major findings of each study were summarized below.

In Chapter 3, a graphite furnace atomic absorption spectrometry (GFAAS) method was developed to measure O-MMT nanoclay concentration in water-ethanol solutions with Si and Al as markers of the nanoclay. The stability of O-MMT in water-ethanol solutions was investigated in order to achieve a reliable measurement. A good dispersion of O-MMT was obtained in a sonicated solution with an ethanol concentration higher than 70 % (v/v), while the nanoclay dispersion in water can be improved by adding an organic surfactant. Si and Al concentrations were correlated to O-MMT concentrations to give the composition of O-MMT which was in agreement with the results obtained by an X-ray fluorescence (XRF) method. The GFAAS method developed in this study was rapid, reliable and could measure nanoclay at low concentrations (μg L^{-1} level). All these features were critical to the real-time study on the nanoclay release from nanocomopsites.

In Chapter 4, a liquid chromatography tandem mass spectrometry (LC-MS/MS) method was developed to measure the surfactant released from O-MMT nanoclay into food simulants. Two types of O-MMT containing different quaternary alkylammonium surfactants were used. The release of surfactant from O-MMT was evaluated as a function of temperature, sonication and simulant type. More surfactant was released at a higher temperature (*e.g.*, 70 °C) than at a

lower one (*e.g.*, 22 °C), while less surfactant was released if the nanoclay was treated at a temperature above the thermal decomposition temperature of the surfactant. Sonication caused more surfactant release into the food simulant than without sonication. The amount of surfactant released also varied from one food simulant to another. A maxium amount of surfactant release was achieved when the nanoclay particles were dispersed in ethanol, while much less surfactant was released into a water/ethanol mixture (1:1, v/v) or pure water. Such differences could be associated with the affinity between the surfactant and different solvents which were estimated based on the solubility parameters.

In Chapter 5, release assessment of O-MMT nanoclay and surfactant was carried out in accordance with ASTM D4754-11. Two types of polymer-clay nanocomposite films (PP and PA6 with O-MMT nanoclay) were produced and exposed to ethanol as a fatty-food simulant at 22, 40 and 70 °C. The concentration of nanoclay released into ethanol was measured by a GFAAS method; the results showed that both nanocomposites released small amounts of nanoclay particles (μg L^{-1} level). PP-clay films released more nanoclay particles than PA6-clay films did, which could be attributed to the affinity difference between the nanoclay and the polymer. No obvious difference was found in the amount of nanoclay released from PP-clay films with different film thicknesses, revealing that the nanoclay release mainly occurred at the film surface. The amount of surfactant released into ethanol was measured by an LC-MS/MS method. Both nanocomposite films released a substantial amount of surfactant into ethanol (mg L^{-1} level), indicating changes in the nanoclay structure within the nanocomposite while exposed to the solvent. Finally, an initial trial was made to predict the surfactant release from nanocomposite films by the Fick's diffusion model. The parameters that described the release process (*e.g.*, diffusion coefficients and partitiaion coefficients) were derived from the model.

The release of nanoclay and surfactant may occur during the manufacture, use and disposal of nanocomposites, thereby potentially exposing different environments and biological systems to those components. The instrumental methodologies developed for the measurement of nanoclay and surfactant in food simulants can be expanded to evaluate release in other samples like biological or environmental systems. In general, the release of both nanoclay and surfactant may present a safety concern. The outcome of this research provides useful information for determining the exposure doses of the nanocomposite components (while some assumptions may be necessary to translate the experimental results to the actual exposure dose) and eventually enabling risk assessment.

6.2 Future work

This research has addressed some work on the release from polymer-clay nanocomposite systems, especially on the instrumental method development to measure the release of nanoclay and surfactant. However, there are still questions and doubts left behind, and more efforts need to be made at least in two aspects.

Characterization of nanoclay particles in the solvent

Clay particles are usually exfoliated into the polymer matrix during film processing, reducing their size to nanoscale. It is assumed that the smallest particles are more likely to release from the nanocomposite in contact with the solvent. There is a need to understand the physicochemical properties of the released nanoclay particles such as size, shape, surface area and aggregation, which are directly associated with nanoclay toxicity. Some factors need to be taken into account to investigate the behavior of nanoclay particles in the solvent, including

temperature, solvent type and pH.

Characterization of nanoclay particles in the polymer

The release of nanoclay particles from nanocomposites was observed, although the root of cause is not clear. A thorough understanding of the interaction between the nanoclay and the polymer in contact with the solvent is necessary to explore the mechanism of nanoclay release; and then methametical models may be developed to describe the release process. Subsequent study should address the change of material properties (thermal, mechanical, etc.) as well as the morphology and structure when exposing the nanocomposite films to the solvent. In addition, in our previous study, nanoclay particles were successfully labeled with fluorencent tags (Diaz, C.; Xia, Y.; Rubino, M.; Auras, R.; Jayaraman, K.; Hotchkiss, J. Fluorescent labeling and tracking of nanoclay. Nanoscale 2013, 5, 164-168). The probable movement of nanoclay particles, due to the change of nanocomposite morphology and structure, can be characterized by Confocal microscopy with the nanocomposite films in contact with various solvents under different temperatures.